AFFDL-TR-72-64
VOLUME I

DEVELOPMENT OF AN UNDERSTANDING OF THE FATIGUE PHENOMENA OF BONDED AND BOLTED JOINTS IN ADVANCED FILAMENTARY COMPOSITE MATERIALS

VOLUME I. ANALYSIS METHODS

J. N. Dickson, T. M. Hsu, and J. M. McKinney
Lockheed-Georgia Company
Marietta, Georgia

TECHNICAL REPORT AFFDL-TR-72-64, VOLUME I
June 1972

AIR FORCE FLIGHT DYNAMICS LABORATORY
AIR FORCE SYSTEMS COMMAND
WRIGHT-PATTERSON AIR FORCE BASE, OHIO

NOTICE

When Government drawings, specifications, or other data are used for any purpose other than in connection with a definitely related Government procurement operation, the United States Government thereby incurs no responsibility nor any obligation whatsoever; and the fact that the Government may have formulated, furnished, or in any way supplied the said drawings, specifications, or other data, is not to be regarded by implication or otherwise as in any manner licensing the holder or any other person or corporation, or conveying any rights or permission to manufacture, use, or sell any patented invention that may in any way be related thereto.

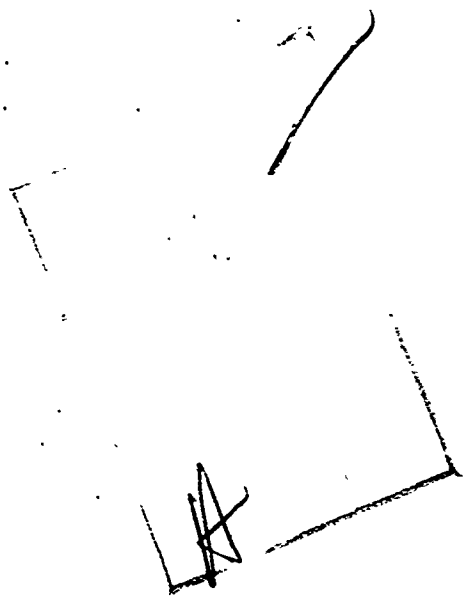

Copies of this report should not be returned unless return is required by security considerations, contractual obligations, or notice on a specific document.

UNCLASSIFIED

Security Classification

DOCUMENT CONTROL DATA - R & D

(Security classification of title, body of abstract and indexing annotation must be entered when the overall report is classified)

1 ORIGINATING ACTIVITY (Corporate author) Lockheed-Georgia Company A Division of Lockheed Aircraft Corporation Marietta, Georgia 30060	2a. REPORT SECURITY CLASSIFICATION Unclassified 2b GROUP

3 REPORT TITLE

DEVELOPMENT OF AN UNDERSTANDING OF THE FATIGUE PHENOMENA OF BONDED AND BOLTED JOINTS IN ADVANCED FILAMENTARY COMPOSITE MATERIALS

4 DESCRIPTIVE NOTES (Type of report and inclusive dates)
Final Technical Report August 1970 through April 1972

5 AUTHOR(S) (First name, middle initial, last name)
John N. Dickson, Teh-Min Hsu and James M. McKinney

6 REPORT DATE June 1972	7a. TOTAL NO OF PAGES	7b. NO OF REFS
8a CONTRACT OR GRANT NO F33615-70-C-1302 b PROJECT NO 4364 c. d	9a. ORIGINATOR'S REPORT NUMBER(S) AFFDL-TR-72-[illegible]-Vol I 9b. OTHER REPORT NO(S) (Any other numbers that may be assigned this report) ER-11319	

10 DISTRIBUTION STATEMENT

Approved for public release, distribution unlimited.

11 SUPPLEMENTARY NOTES Volume I, Analysis Methods	12 SPONSORING MILITARY ACTIVITY Air Force Flight Dynamics Laboratory Air Force Systems Command Wright-Patterson AFB, Ohio

13 ABSTRACT

This is Volume I of a final report presented in three volumes: Vol I - Analysis Methods; Vol II - Fabrication, Inspection and Testing; Volume III - Fatigue Analysis and Failure Mode Studies. This volume describes the analytical methods that were generated or used as part of this program. The main body of this volume is divided into three chapters as follows: Closed Form Analysis Methods, Finite Element Analysis, Photoelastic Stress Analysis. Emphasis was placed on the development of closed form analysis procedures for bonded joints in laminated composites. A comprehensive linear analysis method and associated computer program (BONJO I) has been developed. Numerical results obtained with this program are compared with finite element analyses, strain gage data and photoelastic results. A "Plastic Zone" approach was used to extend BONJO I to include joints with ideally elastic-plastic adhesive stress-strain behavior. The theoretical development of a rigorous non-linear analysis procedure for bonded joints has been presented, however, this method was not carried beyond the exploratory stage.

Finite element analyses used to evaluate the step lap bonded joints and bolted joints are presented and discussed. Photoelastic stress analysis procedures used in the program are described in the final chapter together with the results obtained.

DD FORM 1 NOV 68 1473

UNCLASSIFIED

Security Classification

14 KEY WORDS	LINK A		LINK B		LINK C	
	ROLE	WT	ROLE	WT	ROLE	WT
bonded joints						
mechanical joints						
joint analysis						
boron composite materials						
fatigue testing						
failure modes						
fatigue endurance						
fatigue analysis						
photoelastic stress analysis						
material properties						
joint fabrication						
non-destructive inspection						

DEVELOPMENT OF AN UNDERSTANDING OF THE FATIGUE PHENOMENA OF BONDED AND BOLTED JOINTS IN ADVANCED FILAMENTARY COMPOSITE MATERIALS

VOLUME I. ANALYSIS METHODS

J. N. Dickson, T. M. Hsu, and J. M. McKinney
Lockheed-Georgia Company
Marietta, Georgia

FOREWORD

This report summarizes the work accomplished under Contract F33615-70-C-1302, "Development of an Understanding of the Fatigue Phenomena of Bonded and Bolted Joints in Advanced Filamentary Composite Materials", and was prepared by the Lockheed-Georgia Company, a Division of Lockheed Aircraft Corporation. The work reported herein was sponsored by the Advanced Composite Branch, Air Force Flight Dynamics Laboratory, Air Force Systems Command, Wright-Patterson Air Force Base, Ohio 45433. Mr. Rodman Joblove, FBC, was the Air Force Project Engineer and Mr. A. C. Fehrle was the Lockheed-Georgia Program Manager.

The authors of Volume I are Mr. J. N. Dickson, Dr. T. M. Hsu, and Dr. J. M. McKinney. Mr. Dickson and Dr. Hsu are jointly responsible for the development of the closed form analysis procedures and the finite element analyses performed during the program. Dr. McKinney was responsible for the photoelastic analyses.

This technical report has been reviewed and is approved.

For internal control purposes, this report has been assigned Lockheed-Georgia Company Report Number ER-11319.

Philip A. Parmley
Chief, Advanced Composite Branch
Structures Division
Air Force Flight Dynamics Laboratory

ABSTRACT

This volume describes the analytical methods that were generated or used as part of this program. The main body of this volume is divided into three chapters, as follows:

- o Closed Form Analysis Methods
- o Finite Element Analyses
- o Photoelastic Stress Analysis

Emphasis was placed on the development of closed form analysis procedures for bonded joints in laminated composites. A comprehensive linear analysis method and associated computer program (BONJO I) has been developed. Numerical results obtained with this program are compared with finite element analyses, strain gage data, and photoelastic results. A "Plastic Zone" approach was used to extend BONJO I to include joints with ideally elastic-plastic adhesive stress-strain behavior. The theoretical development of a rigorous non-linear analysis procedure for bonded joints has been presented. However, this method was not carried beyond the exploratory stage.

Finite element analyses used to evaluate the step lap bonded joints and bolted joints are presented and discussed. Photoelastic stress analysis procedures used in the program are described in the final chapter together with the results obtained.

TABLE OF CONTENTS

TABLE OF CONTENTS (CONTD)

LIST OF ILLUSTRATIONS

LIST OF ILLUSTRATIONS (CONTD)

LIST OF ILLUSTRATIONS (CONTD)

1. INTRODUCTION

This program was undertaken to develop an understanding of the fatigue phenomena of structural joints in advanced filamentary composite materials and to develop analytical and testing methods to support proper fatigue design of advanced composite structural joints. The program included the evaluation of both bonded and bolted joints. Primary emphasis was placed on joints in boron-epoxy. However, a limited evaluation of bonded joints in graphite-epoxy and glass-epoxy was included. Although the sizes of the joints for this investigation were small (one to ten inches in width) all configurations evaluated are representative of typical structural joints currently utilized in advanced filamentary composite structures.

The program consisted of three major areas of investigation:

- o Analysis Methods
- o Fabrication, Inspection, and Testing
- o Fatigue Analysis and Failure Mode Studies

Analytical methods for determining joint stresses were divided into two major tasks: (1) analysis of bonded joints and (2) analysis of bolted joints. Primary emphasis was placed on the development of a closed form elastic analysis procedure for bonded joints. This analysis was used to evaluate a number of joint variables. A "plastic zone" approach was used to extend the closed form analysis procedure to include joints with inelastic adhesive stress-strain behavior. The results of the elastic closed form solution were verified with finite element analyses, photoelastic analysis and strain gage data. Finite element analyses were used to evaluate the step lap bonded joints and bolted joints.

The experimental program consisted of fabrication, inspection and testing of a large quantity of joint specimens. Fabrication and inspection methods were established which resulted in specimens being fabricated to close tolerances and of uniformly high quality. This provided specimens that would consistently develop stresses that were predicted by the

analytical methods. Developing testing techniques and actual specimen testing was a major portion of the program. Establishing proper specimen support was essential to obtaining repeatable joint strengths within a specimen configuration. Equally important was determining the proper cyclic rate for the different stress ratios and specimen configurations to preclude specimen heating and erratic fatigue lives.

Evaluation of the experimental results was divided into two separate but related tasks. These tasks were failure mode studies and fatigue analysis. The failure mode studies mentioned were photomicrographic analyses of the failure surfaces. This failure mode analysis does not replace but augments the gross failure modes generally defined within the experimental phases of a program. The photomicrographic analysis conducted within this program established failure modes related to specific joint designs, joint loading, and fatigue history. The fatigue analysis established relationships between specimen configurations, joint variables, material combinations, loading conditions and stress ratio effects for constant amplitude loading. The relationship between constant amplitude fatigue and spectrum fatigue (block and realistic) was also evaluated for specific joint configurations.

This report is divided into three separate volumes each containing the developments accomplished within a major area of investigation. Each volume is a self-contained document, complementing the other two volumes but not dependent upon them for coherence or continuity. The titles of the three volumes are:

Volume I - Analysis Methods

Volume II - Fabrication, Inspection and Testing

Volume III - Fatigue Analysis and Failure Mode Studies

Volume I is divided into three chapters, with primary emphasis being placed on the first chapter. This chapter, entitled "Closed Form Analysis Methods," contains sections on earlier methods and their short-comings; the development of the analysis procedure BONJO I; the plastic zone extension of BONJO I; and a section on numerical results. The second chapter is devoted to finite element analyses of the step lap bonded joints and mechanical joint specimens while the third chapter deals with photoelastic analysis methods.

II. GENERAL DISCUSSION

1.0 INTRODUCTORY REMARKS

The increasing utilization of advanced filamentary composites in the design of aircraft and space vehicles has necessitated the development of more sophisticated methods of analysis. Prior to the introduction of these new materials, the use of adhesive bonding was limited almost entirely to secondary structural applications. The design of bonded joints was based largely on experimental data. Theoretical methods such as those by Goland and Reissner (1), Volkerson (2), and Szepe (3) were used to obtain a more detailed knowledge of the distribution of adhesive shear and normal stresses in bonded lap joints and were generally considered as adequate for that purpose.

The determination of stresses in bonded joints with laminated composite adherends, however, is much more complex than in those with isotropic adherends. This increased complexity can be only partly attributed to the fact that composites are anisotropic and heterogeneous. A large part is caused by the necessity to account for the effects of inter-laminar shear and normal stresses in the analysis of composite joints. Numerical results that demonstrate the importance of the above effects are presented in this report.

Another factor that may be important in the analysis of composite joints is the presence of residual thermal stresses. These stresses are caused by bonding or curing at elevated temperatures and subsequent cooling to operating temperatures. Although thermal stresses are introduced in all multi-directional laminates, they become especially significant when bonding highly dissimilar materials such as boron and aluminum or graphite and aluminum.

It is within the capability of most large finite element programs in existence today to perform an analysis of virtually any degree of complexity; but such analyses are cumbersome and costly. In addition, the preparation of input data and interpretation of results is extremely time consuming. It is therefore preferable to use direct or closed form methods wherever possible.

Since the majority of specimens to be analyzed as part of this program were simple bonded lap joints of uniform geometry, it was decided to develop a closed form procedure for composite joints. Although it became necessary to develop a more comprehensive procedure than initially anticipated, for the reasons mentioned previously, the method turned out to be very efficient and offers tremendous cost and time savings as compared to the finite element method. Finite element analyses, however, were performed for some of the step lap joint and mechanical joint specimens and for the verification of the closed form procedure.

2.0 NOMENCLATURE

Symbols are defined in the text when they first appear. A list of the most important ones is given below for convenience.

A, B, D	Laminate Stiffness Matrices
E	Young's Modulus
G	Shear Modulus
L	Overlap Length
M_x, M_y, M_{xy}	Stress Couples
N_x, N_y, N_{xy}	Stress Resultants
V_x, V_y	Transverse Shear Forces
h_N	Distance from Reference Surface to Free Surface of Laminate
t	Thickness
u, v, w	Displacements in x, y, and z directions
x, y, z	Cartesian Coordinates

α_x, α_y	Thermal Expansion Coefficients
$\epsilon_x, \epsilon_y, \epsilon_{xy}$	In Plane Strains
$\epsilon_{xp}, \epsilon_{yp}, \epsilon_{xyp}$	In Plane Plastic Strains
ϵ_z	Normal Strain
ϵ_{zp}	Normal Plastic Strain
$\epsilon_{xz}, \epsilon_{yz}$	Transverse Shear Strains
$\bar{\sigma}$	Adhesive Effective Stress
$\sigma_x, \sigma_y, \sigma_{xy}$	In Plane Stresses
σ_z	Normal Stress
σ_{xz}, σ_{yz}	Transverse Shear Stresses
ν	Poisson's Ratio
u, L, a	Upper, Lower, Adhesive
Superscript	Reference Surface, k^{th} Lamina, Temperature

III. CLOSED FORM ANALYSIS METHODS

1.0 GENERAL

For the purpose of this report, theoretical methods other than finite element or finite difference procedures will be defined as closed form methods of analysis. This will include iterative as well as direct solutions based on the theory of elasticity. The assumptions of small deformations and uniform geometry are made throughout this section. Additional assumptions will be discussed as they are applied. Closed form solutions are developed for the two joint configurations shown in Figure 1. Because of assumed symmetry, only one half of the single lap joint and one quarter of the double lap joint need to be considered as shown by the heavy dashed line. The length of the joint is defined in Figure 1 as being in the plane of the paper and in the direction of the chosen x-axis. The width of the joint is the dimension perpendicular to the plane of the paper (parallel to the y-axis). The region $0 \leq x \leq L$ will be of primary interest and the governing differential equations to be developed will apply to this region only.

2.0 PRELIMINARY INVESTIGATIONS

After a thorough evaluation of available theoretical methods, it was decided early in the program to develop a procedure for the analysis of simple laminated composite lap joints based on the Goland-Reissner (1) differential equation approach. This procedure required the removal of the imposed symmetry restrictions in the Goland-Reissner analysis and the substitution of gross laminate properties in place of the isotropic elastic moduli. The Kirchhoff assumptions, however, were assumed to remain valid in this initial procedure.

For the case of single lap joints with relatively flexible bond layers and isotropic adherends, Goland and Reissner obtained the following uncoupled differential equations for the shear stress, σ^o_{xz}, and the normal stress, σ^o_z, in the adhesive:

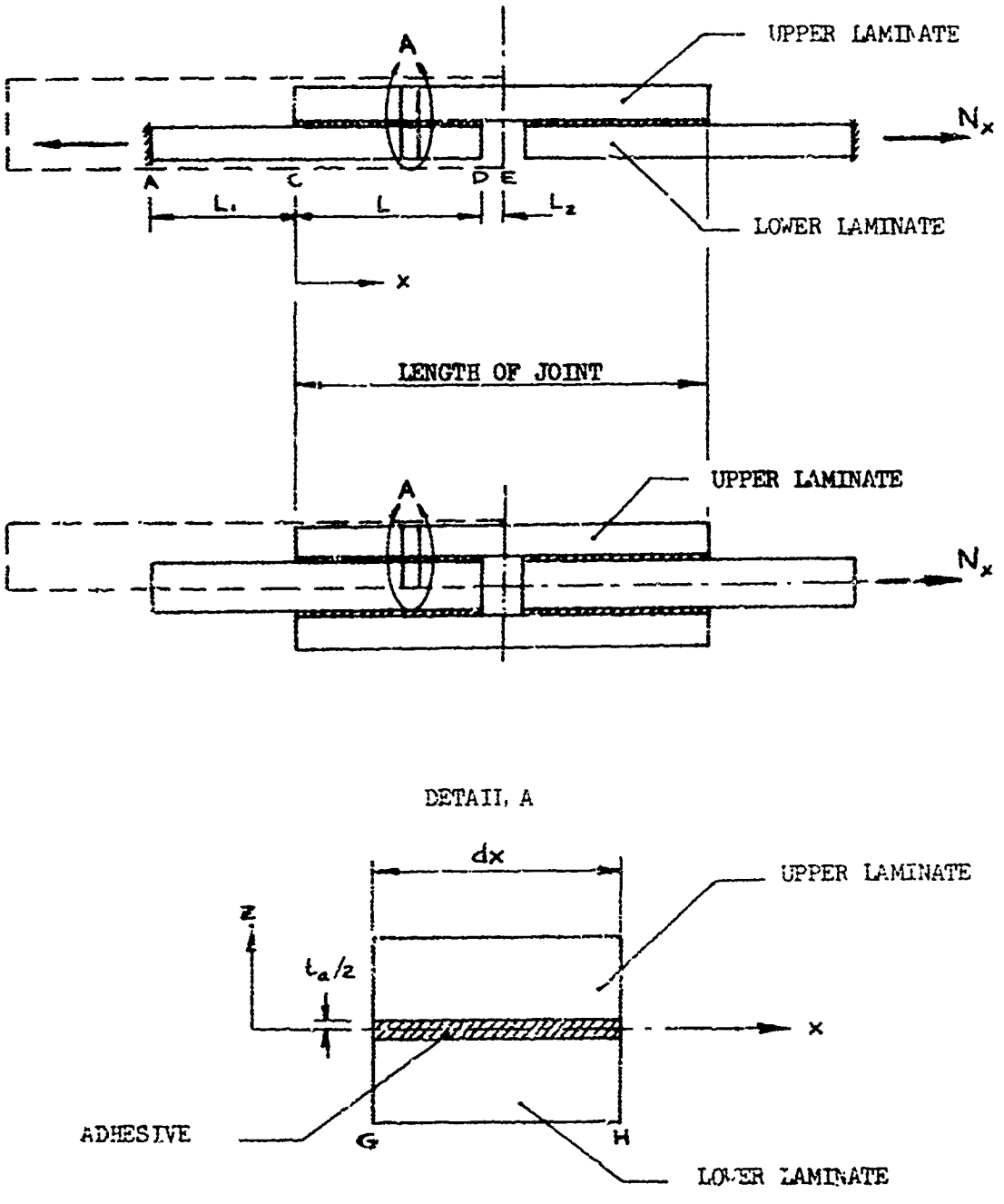

FIGURE 1 LAP JOINT CONFIGURATIONS

$$\frac{d^3\sigma^o_{xz}}{dx^3} - \frac{8\,G_a}{Et\,t_a}\cdot\frac{d\sigma^o_{xz}}{dx} = 0$$

$$\frac{d^4\sigma^o_z}{dx^4} + \frac{24(1-\nu^2)E_a}{Et^3\,t_a}\sigma^o_z = 0 \qquad (1)$$

It might be remarked that there is an inconsistency in equations (1). The first equation is based on plane stress considerations while the second one assumes a condition of plane strain.

The above equations are uncoupled as a result of the requirements that the thickness and material properties of the two adherends must be identical. If these restrictions are removed one may, by using essentially the same procedure, obtain the two coupled differential equations:

$$\frac{d^3\sigma^o_{xz}}{dx^3} - \frac{4G_a}{t_a}\left(\frac{1-\nu_u^2}{E_u t_u} + \frac{1-\nu_L^2}{E_L t_L}\right)\frac{d\sigma^o_{xz}}{dx} - \frac{6G_a}{t_a}\left(\frac{1-\nu_u^2}{E_u t_u^2} - \frac{1-\nu_L^2}{E_L t_L^2}\right)\sigma^o_z = 0$$

$$\frac{d^4\sigma^o_z}{dx^4} + \frac{12E_a}{t_a}\left(\frac{1-\nu_u^2}{E_u t_u^3} + \frac{1-\nu_L^2}{E_L t_L^3}\right)\sigma^o_z + \frac{6E_a}{t_a}\left(\frac{1-\nu_u^2}{E_u t_u^2} - \frac{1-\nu_L^2}{E_L t_L^2}\right)\frac{d\sigma^o_{xz}}{dx} = 0 \qquad (2)$$

These equations thus represent the governing differential equations for a single lap joint with unequal isotropic adherends in a state of plane strain (in the x-z plane). E_u and E_L are the elastic moduli, ν_u and ν_L are the Poisson's ratios, and t_u and t_L are the thicknesses of the upper and lower adherends, respectively. To obtain the relations for a plane stress condition, the Poisson's ratios are dropped from the above equations.

The normal stress, σ_z, may be found from the first of equations (2) and then substituted into the second one to yield the following sixth order differential equation in $(d\sigma^o_{xz}/dx)$:

$$\left(\frac{d^6}{dx^6} + C_1\frac{d^4}{dx^4} + C_2\frac{d^2}{dx^2} + C_3\right)\frac{d\sigma^o_{xz}}{dx} = 0 \qquad (3)$$

where:

$$C_1 = -\frac{4G_a}{t_a}\left(\frac{1-\nu_u^2}{E_u t_u}+\frac{1-\nu_L^2}{E_L t_L}\right)$$

$$C_2 = \frac{12E_a}{t_a}\left(\frac{1-\nu_u^2}{E_u t_u^3}+\frac{1-\nu_L^2}{E_L t_L^3}\right) \qquad (4a)$$

$$C_3 = C_1 C_2 + \frac{36 E_a G_a}{t_a^2}\left(\frac{1-\nu_u^2}{E_u t_u^2}-\frac{1-\nu_L^2}{E_L t_L^2}\right)^2$$

The solution of the differentiol equation (3) is in the form:

$$\sigma_{xz}^o = A_o + \sum_{i=1}^{6} A_i e^{\lambda_i x} \qquad (5)$$

where the λ_i's are the roots of the equation:

$$\lambda^6 + C_1\lambda^4 + C_2\lambda^2 + C_3 = 0 \qquad (6)$$

The constants A_i may be determined from the boundary conditions.

The analysis for a double lap joint configuration is similar to that of a single lap joint and differs only in the coefficients of equation (3) and the boundary conditions. The coefficients, C_i, for this case become:

$$C_1 = -\frac{4G_a}{t_a}\left(\frac{1-\nu_u^2}{E_u t_u}+\frac{1-\nu_L^2}{2E_L t_L}\right)$$

$$C_2 = \frac{12E_a}{t_a}\left(\frac{1-\nu_u^2}{E_u t_u^3}\right) \qquad (4b)$$

$$C_3 = C_1 C_2 + \frac{36 E_a G_a}{t_a^2}\left(\frac{1-\nu_u^2}{E_u t_u^2}\right)^2$$

In the above t_L represents the total thickness of the plates to be joined and t_U is the thickness of each splice plate.

The differential equation (3) applies to joints with laminated composite adherends; but the coefficients C_i will now involve the gross laminate stiffness properties. The stiffnesses may be obtained from laminated plate theory* without difficulty. The constitutive equations for a thin laminated plate are generally written in the form:

$$\{N\} = [A]\{\epsilon\} - [B]\{\kappa\}$$
$$\{M\} = [B]\{\epsilon\} - [D]\{\kappa\} \tag{7}$$

When the laminate is in a state of plane strain, one has, therefore:

$$N_x = A_{11}\epsilon_x^o - B_{11}\kappa_x$$
$$M_x = B_{11}\epsilon_x^o - D_{11}\kappa_x \tag{8}$$

where ϵ_x^o is the strain at the reference surface, which will for convenience be taken at the interface of the laminate and the bond layer. The gross laminate stiffnesses are given by:

$$A_{11} = \pm \sum_{k=1}^{N} C_{11}'^{(k)}(h_k - h_{k-1})$$
$$B_{11} = \pm \frac{i}{2} \sum_{k=1}^{N} C_{11}'^{(k)}(h_k^2 - h_{k-1}^2) \tag{9}$$
$$D_{11} = \pm \frac{1}{3} \sum_{k=1}^{N} C_{11}'^{(k)}(h_k^3 - h_{k-1}^3)$$
$$\bar{D}_{11} = D_{11} - B_{11}^2/A_{11}$$

*Note that at this point the Kirchhoff assumptions are still assumed to be valid.

In the above expressions, the positive sign refers to the upper laminate and the negative sign to the lower laminate; h_k is the distance from the upper surface of the k^{th} layer (lower surface for lower laminate) to the bond layer interface. For a single lap joint with composite adherends, one now obtains:

$$C_1 = -\frac{G_a}{t_a}\left(\frac{D_{11}^U}{A_{11}^U \bar{D}_{11}^U} + \frac{D_{11}^L}{A_{11}^L \bar{D}_{11}^L}\right)$$

$$C_2 = \frac{E_a}{t_a}\left(\frac{1}{\bar{D}_{11}^U} + \frac{1}{\bar{D}_{11}^L}\right) \tag{4c}$$

$$C_3 = C_1 C_2 + \frac{E_a G_a}{t_a^2}\left(\frac{B_{11}^U}{A_{11}^U \bar{D}_{11}^U} + \frac{B_{11}^L}{A_{11}^L \bar{D}_{11}^L}\right)^2$$

while for a double lap joint one finds

$$C_1 = -\frac{G_a}{t_a}\left(\frac{2}{A_{11}^L} + \frac{D_{11}^U}{A_{11}^U \bar{D}_{11}^U}\right)$$

$$C_2 = \frac{E_a}{t_a}\left(\frac{1}{\bar{D}_{11}^U}\right) \tag{4d}$$

$$C_3 = C_1 C_2 + \frac{E_a G_a}{t_a^2}\left(\frac{B_{11}^U}{A_{11}^U \bar{D}_{11}^U}\right)^2$$

When the laminates are in a state of plane stress (in x-z plane), i.e.

$$\sigma_y^{(k)} = \sigma_{xy}^{(k)} = \sigma_{yz}^{(k)} = 0$$

the gross laminate stiffness properties are obtained by replacing $C_{11}^{'(k)}$ by $1/S_{11}^{(k)}$ in equations (9). $C_{11}^{'}$ and $S_{11}^{'}$ are defined in reference 4 in terms of the elastic constants and lamina orientations.

After the coefficients, C_i, are determined, the roots, λ_i, can be calculated from equation (6). Seven boundary conditions are now required to obtain a solution and define the state of stress in the joint. None of the conditions that were used, however, pertained to the adhesive shear stress and as a result the peak shear stresses occurred at the ends of the joint, as was the case in the Goland-Reissner analysis. This cannot be correct, of course, and it will be shown later that in reality the peak stresses occur slightly inward from the edges.

The fact that the location of the peak shear stresses in the adhesive could not be accurately predicted was not considered a major argument against the use of the method described here, but studies were made which indicated that the magnitude of these stresses was considerably lower than calculated with this analysis. It was conjectured, and later substantiated, that because of the relatively low transverse shear stiffness and normal stiffness (through the thickness of the laminate) of most fibrous composites, adherence to the Kirchhoff assumptions could lead to unacceptable errors.

The above method of analysis was therefore discontinued and a more rigorous procedure developed in which the Kirchhoff assumptions were discarded. The theoretical development of this procedure is presented in the following sections.

3.0 GENERAL EQUATIONS FOR LAMINATED COMPOSITE JOINTS

3.1 Lamina Relations

The laminate is assumed to consist of orthotropic layers which may have arbitrary thickness and material properties. A Cartesian (x, y, z) coordinate system is used as the plate reference system in which the z-axis is normal to the plane of the plate. A small splice cut from the laminated plate is shown in Figure 2. The material symmetry axes (1, 2) of each lamina lie in a plane parallel to the x-y plane but may be rotated about the z-axis through an arbitrary angle θ. The thermal expansion coefficients are also assumed to be orthotropic and hence:

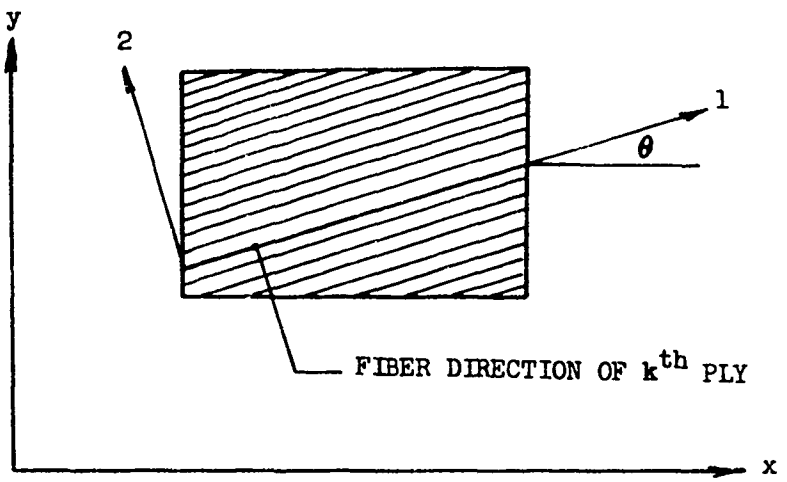

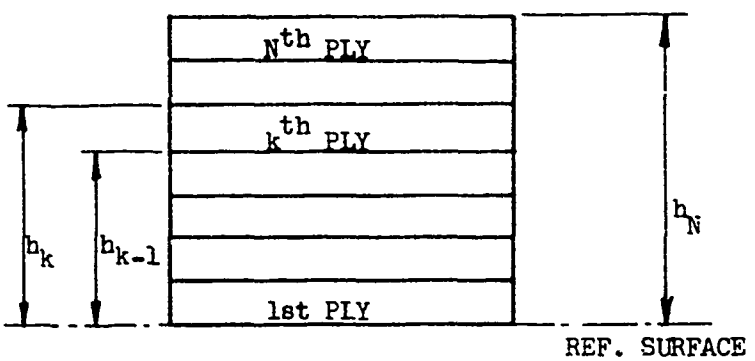

FIGURE 2 SMALL ELEMENT OF LAMINATED PLATE

$$\alpha_4 = \alpha_5 = \alpha_6 = 0$$

The linear strain-displacement relations for the k^{th} lamina may be written:

$$\begin{aligned} \epsilon_x^{(k)} &= u'^{(k)}_{,x} & \epsilon_{yz}^{(k)} &= v'^{(k)}_{,z} + w'^{(k)}_{,y} \\ \epsilon_y^{(k)} &= v'^{(k)}_{,y} & \epsilon_{xz}^{(k)} &= u'^{(k)}_{,z} + w'^{(k)}_{,x} \\ \epsilon_z^{(k)} &= w'^{(k)}_{,z} & \epsilon_{xy}^{(k)} &= u'^{(k)}_{,y} + v'^{(k)}_{,x} \end{aligned} \tag{10}$$

where a comma followed by a symbol means differentiation with respect to that symbol. The constitutive relations for the k^{th} lamina with respect to its own principal (1, 2, 3) axes may be expressed in matrix form by

$$\{\sigma\}^{(k)}_{1,2,3} = [C]^{(k)}_{1,2,3} \{\epsilon - \alpha T\}^{(k)}_{1,2,3} \tag{11}$$

T is the temperature change from some initial reference state (bonding or curing temperature, for instance). The non-zero coefficients of the stiffness matrix [C] are given in reference 4 in terms of the elastic constants of the material. The stress-strain equations with respect to the laminate reference (x,y,z) axes are:

$$\begin{Bmatrix} \bar{\sigma}_x \\ \bar{\sigma}_y \\ \bar{\sigma}_z \\ \bar{\sigma}_{yz} \\ \bar{\sigma}_{xz} \\ \bar{\sigma}_{xy} \end{Bmatrix}^{(k)} = \begin{bmatrix} Q_{11} & Q_{12} & Q_{13} & 0 & 0 & Q_{16} \\ & Q_{22} & Q_{23} & 0 & 0 & Q_{26} \\ & & Q_{33} & 0 & 0 & Q_{36} \\ & & & Q_{44} & Q_{45} & 0 \\ & & & & Q_{55} & 0 \\ & & & & & Q_{66} \end{bmatrix}^{(k)} \begin{Bmatrix} \epsilon_x \\ \epsilon_y \\ \epsilon_z \\ \epsilon_{yz} \\ \epsilon_{xz} \\ \epsilon_{xy} \end{Bmatrix}^{(k)} \tag{12}$$

Since the [Q] matrix is symmetric, only the upper half of the matrix is shown. The actual stress in the lamina is obtained from the relation

$$\{\sigma\}^{(k)}_{x,y,z} = \{\bar{\sigma}\}^{(k)}_{x,y,z} - \{\sigma^T\}^{(k)}_{x,y,z} = [Q]^{(k)} \{\epsilon\}^{(k)}_{x,y,z} - \{\sigma^T\}^{(k)}_{x,y,z} \tag{13}$$

where the equivalent thermal stresses are defined as follows

$$\sigma_x^T = [(C_{11}\alpha_1 + C_{12}\alpha_2 + C_{13}\alpha_3)m^2 + (C_{12}\alpha_1 + C_{22}\alpha_2 + C_{23}\alpha_3)n^2]T$$

$$\sigma_y^T = [(C_{11}\alpha_1 + C_{12}\alpha_2 + C_{13}\alpha_3)n^2 + (C_{12}\alpha_1 + C_{22}\alpha_2 + C_{23}\alpha_3)m^2]T$$

$$\sigma_z^T = (C_{13}\alpha_1 + C_{23}\alpha_2 + C_{33}\alpha_3)T \qquad (14)$$

$$\sigma_{yz}^T = \sigma_{xz}^T = 0$$

$$\sigma_{xy}^T = [C_{11}\alpha_1 + C_{12}(\alpha_2 - \alpha_1) - C_{22}\alpha_2 + (C_{13} - C_{23})\alpha_3]mnT$$

and $m = \cos\theta$, $n = \sin\theta$. The Q_{ij} are given by:

$$Q_{11} = m^4C_{11} + 2m^2n^2C_{12} + n^4C_{22} + 4m^2n^2C_{66}$$

$$Q_{12} = m^2n^2C_{11} + (m^4 + n^4)C_{12} + m^2n^2C_{22} - 4m^2n^2C_{66}$$

$$Q_{13} = m^2C_{13} + n^2C_{23}$$

$$Q_{16} = m^3nC_{11} - mn(m^2 - n^2)C_{12} - mn^3C_{22} - 2mn(m^2 - n^2)C_{66}$$

$$Q_{22} = n^4C_{11} + 2m^2n^2C_{12} + m^4C_{22} + 4m^2n^2C_{66}$$

$$Q_{23} = n^2C_{13} + m^2C_{23}$$

$$Q_{26} = mn^3C_{11} + mn(m^2 - n^2)C_{12} - m^3nC_{22} + 2mn(m^2 - n^2)C_{66}$$

$$Q_{33} = C_{33}$$

$$Q_{36} = mn(C_{13} - C_{23})$$

$$Q_{44} = m^2C_{44} + n^2C_{55}$$

$$Q_{45} = -mnC_{44} + mnC_{55}$$

$$Q_{55} = n^2C_{44} + m^2C_{55}$$

$$Q_{66} = m^2n^2C_{11} - 2m^2n^2C_{12} + m^2n^2C_{22} + (m^2 - n^2)^2 C_{66}$$

3.2 Effect of Transverse Shear

In lap joints made of conventional metallic materials the effect of transverse shear deformation on the stress distributions in the joint is generally found to be negligible and therefore an analysis based on the classical Kirchhoff assumptions is adequate in most cases. However, in laminated plates having relatively low transverse shear moduli, these assumptions are no longer permissible. The effect of transverse shear deformation on the bending of symmetrically laminated plates has been investigated by Whitney (5). His work has been extended for use in the present analysis.

The mid-surface of the adhesive layer has been taken as the reference surface for both laminated plates. The adhesive shear stresses at the reference surface are denoted by σ^o_{xz} and σ^o_{yz} and the transverse shear stresses in the k^{th} layer are assumed in the form:

$$\sigma^{(k)}_{xz} = \sigma^o_{xz}\left(1 - \frac{z}{h_N}\right) + [Q^{(k)}_{55}f(z) + b_{55}z + a^{(k)}_{55}]\varphi_x + [Q^{(k)}_{45}f(z) + b_{45}z + a^{(k)}_{45}]\varphi_y$$

$$\sigma^{(k)}_{yz} = \sigma^o_{yz}\left(1 - \frac{z}{h_N}\right) + [Q^{(k)}_{45}f(z) + b_{45}z + a^{(k)}_{45}]\varphi_x + [Q^{(k)}_{44}f(z) + b_{44}z + a^{(k)}_{44}]\varphi_y \qquad (15)$$

where φ_x and φ_y are functions of x and y only; z is measured from the reference surface; and hence will be negative for the lower laminate (see Figure 1). It must be noted that in this case h_N will also be a negative quantity. In an isotropic material the transverse shear stresses vary parabolically through its thickness. Whitney's assumption of a parabolic variation of shear stress within each layer therefore seems reasonable. With this assumption, f(z) is taken in the form:

$$f(z) = \frac{4}{h_N^2}(zh_N - z^2) \tag{16}$$

which is symmetric with respect to the middle surface of the laminated plate and goes to zero at the outside surfaces. The constants $a_{ij}^{(k)}$ are determined from the requirement that the shear stresses are continuous at the interfaces of adjacent layers, or

$$a_{ij}^{(k+1)} = a_{ij}^{(k)} + [Q_{ij}^{(k)} - Q_{ij}^{(k+1)}]\, f(h_k) \qquad i,j = 4,5 \qquad k = 1,2,\ldots(N-1) \tag{17}$$

It follows from equations (15) that:

$$a_{ij}^{(1)} = 0$$

and hence the remaining $a_{ij}^{(k)}$ can be calculated from equation (17). Since $f(0) = f(h_N) = 0$, one finds for the N^{th} lamina

$$a_{ij}^{(N)} = \sum_{k=1}^{N} Q_{ij}^{(k)}[f(h_k) - f(h_{k-1})]$$

The b_{ij} follow from the condition that the shear stresses are zero at the free surface ($z = h_N$) and therefore:

$$b_{ij} = -\frac{a_{ij}^{(N)}}{h_N} \tag{18}$$

For a laminate which is symmetrical with respect to its middle surface, $a_{ij}^{(N)}$ and therefore b_{ij} will be zero.

The transverse shear forces are obtained by integrating the shear stresses over the thickness of the laminate

$$\begin{aligned} \pm V_x &= \tfrac{1}{2}\sigma_{xz}^{o} h_N + A_{55}\varphi_x + A_{45}\varphi_y \\ \pm V_y &= \tfrac{1}{2}\sigma_{yz}^{o} h_N + A_{45}\varphi_x + A_{44}\varphi_y \end{aligned} \tag{19}$$

where:

$$A_{ij} = \frac{1}{2} b_{ij} h_N^2 + \sum_{k=1}^{N} \{Q_{ij}^{(k)}[F(h_k) - F(h_{k-1})] + a_{ij}^{(k)}(h_k - h_{k-1})\}$$

$$i,j = 4,5$$

and

$$F(z) = \int f(z)\, dz = \frac{2z}{3h_N^2}(3zh_N - 2z^2)$$

In equations (19), the positive sign refers to the upper laminate or splice plate while the negative sign refers to the lower laminate (negative z-axis). This convention will be maintained throughout the analysis. Solving for the shear functions φ_x and φ_y from equations (19) one obtains:

$$\varphi_x = \bar{A}_{55}\left(\pm V_x - \frac{1}{2} h_N \sigma_{xz}^o\right) + \bar{A}_{45}\left(\pm V_y - \frac{1}{2} h_N \sigma_{yz}^o\right)$$

$$\varphi_y = \bar{A}_{45}\left(\pm V_x - \frac{1}{2} h_N \sigma_{xz}^o\right) + \bar{A}_{44}\left(\pm V_y - \frac{1}{2} h_N \sigma_{yz}^o\right)$$

where:

$$\begin{bmatrix} \bar{A}_{44} & \bar{A}_{45} \\ \bar{A}_{45} & \bar{A}_{55} \end{bmatrix} = \begin{bmatrix} A_{44} & A_{45} \\ A_{45} & A_{55} \end{bmatrix}^{-1}$$

Substituting (20) into (15) yields for the transverse shear stresses in the k^{th} layer:

$$\sigma_{xz}^{(k)} = \bar{G}_1^{(k)} \sigma_{xz}^o + \bar{G}_2^{(k)} \sigma_{yz}^o \pm \bar{G}_3^{(k)} V_x \pm \bar{G}_4^{(k)} V_y$$

$$\sigma_{yz}^{(k)} = \bar{G}_5^{(k)} \sigma_{xz}^o + \bar{G}_6^{(k)} \sigma_{yz}^o \pm \bar{G}_7^{(k)} V_x \pm \bar{G}_8^{(k)} V_y \qquad (21)$$

in which the $G_i^{(k)}$'s are functions of z only. They are given by:

$$\bar{G}_1(z)^{(k)} = 1 - \frac{z}{h_N} - \frac{1}{2} h_N \bar{G}_3(z)^{(k)}$$

$$\bar{G}_2(z)^{(k)} = -\frac{1}{2} h_N \bar{G}_4(z)^{(k)}$$

$$\bar{G}_3(z)^{(k)} = \bar{A}_{55}[Q_{55}^{(k)} f(z) + b_{55} z + a_{55}^{(k)}] + \bar{A}_{45}[Q_{45}^{(k)} f(z) + b_{45} z + a_{45}^{(k)}]$$

$$\bar{G}_4(z)^{(k)} = \bar{A}_{44}[Q_{45}^{(k)} f(z) + b_{45} z + a_{45}^{(k)}] + \bar{A}_{45}[Q_{55}^{(k)} f(z) + b_{55} z + a_{55}^{(k)}]$$

$$\bar{G}_5(z)^{(k)} = -\frac{1}{2} h_N \bar{G}_7(z)^{(k)}$$

$$\bar{G}_6(z)^{(k)} = 1 - \frac{z}{h_N} - \frac{1}{2} h_N \bar{G}_8(z)^{(k)}$$

$$\bar{G}_7(z)^{(k)} = \bar{A}_{55}[Q_{45}^{(k)} f(z) + b_{45} z + a_{45}^{(k)}] + \bar{A}_{45}[Q_{44}^{(k)} f(z) + b_{44} z + a_{44}^{(k)}]$$

$$\bar{G}_8(z)^{(k)} = \bar{A}_{44}[Q_{44}^{(k)} f(z) + b_{44} z + a_{44}^{(k)}] + \bar{A}_{45}[Q_{45}^{(k)} f(z) + b_{45} z + a_{45}^{(k)}]$$

The transverse shear strains are obtained from equations (12):

$$\begin{Bmatrix} \epsilon_{yz} \\ \epsilon_{xz} \end{Bmatrix}^{(k)} = \begin{bmatrix} Q_{44} & Q_{45} \\ Q_{45} & Q_{55} \end{bmatrix}^{(k)^{-1}} \begin{Bmatrix} \sigma_{yz} \\ \sigma_{xz} \end{Bmatrix}^{(k)} = \begin{bmatrix} S_{44} & S_{45} \\ S_{45} & S_{55} \end{bmatrix}^{(k)} \begin{Bmatrix} \sigma_{yz} \\ \sigma_{xz} \end{Bmatrix}^{(k)} \tag{22}$$

and by substitution of equations (21) one has:

$$\begin{aligned} \epsilon_{xz}^{(k)} &= [S_{55}^{(k)} \bar{G}_1^{(k)} + S_{45}^{(k)} \bar{G}_5^{(k)}] \sigma_{xz}^{o} + [S_{55}^{(k)} \bar{G}_2^{(k)} + S_{45}^{(k)} \bar{G}_6^{(k)}] \sigma_{yz}^{o} \\ &\quad \pm [S_{55}^{(k)} \bar{G}_3^{(k)} + S_{45}^{(k)} \bar{G}_7^{(k)}] V_x \pm [S_{55}^{(k)} \bar{G}_4^{(k)} + S_{45}^{(k)} \bar{G}_8^{(k)}] V_y \\ \epsilon_{yz}^{(k)} &= [S_{45}^{(k)} \bar{G}_1^{(k)} + S_{44}^{(k)} \bar{G}_5^{(k)}] \sigma_{xz}^{o} + [S_{45}^{(k)} \bar{G}_2^{(k)} + S_{44}^{(k)} \bar{G}_6^{(k)}] \sigma_{yz}^{o} \\ &\quad \pm [S_{45}^{(k)} \bar{G}_3^{(k)} + S_{44}^{(k)} \bar{G}_7^{(k)}] V_x \pm [S_{45}^{(k)} \bar{G}_4^{(k)} + S_{44}^{(k)} \bar{G}_8^{(k)}] V_y \end{aligned} \tag{23}$$

The in-plane displacements may be obtained by integrating the shear strains with respect to z. From equations (10) and (23) one obtains, therefore:

$$u^{(k)} = u^o - \int_o^z w_{,x}\, d\eta + G_1^{(k)}\sigma_{xz}^o + G_2^{(k)}\sigma_{yz}^o \pm G_3^{(k)}V_x \pm G_4^{(k)}V_y$$

$$v^{(k)} = v^o - \int_o^z w_{,y}\, d\eta + G_5^{(k)}\sigma_{xz}^o + G_6^{(k)}\sigma_{yz}^o \pm G_7^{(k)}V_x \pm G_8^{(k)}V_y \qquad (24)$$

where:

$$G_i(z)^{(k)} = \int_o^z [S_{55}^{(k)}\bar{G}_i(\eta)^{(k)} + S_{45}^{(k)}\bar{G}_{i+4}(\eta)^{(k)}]d\eta + c_i^{(k)}$$

$$G_{i+4}(z)^{(k)} = \int_o^z [S_{45}^{(k)}\bar{G}_i(\eta)^{(k)} + S_{44}^{(k)}\bar{G}_{i+4}(\eta)^{(k)}]d\eta + c_{i+4}^{(k)} \qquad (25)$$

$$i = 1,2,3,4$$

Continuity of displacements at the interfaces of adjacent layers requires that:

$$G_i(h_k)^{(k)} = G_i(h_k)^{(k+1)} \qquad (26)$$

From equations (24) it can be seen that $G_i(0)^{(1)}$, and therefore $c_i^{(1)}$, is zero. The remaining constants of integration, $c_i^{(k)}$, may now be calculated from equation (26).

The in-plane strains are obtained from equations (10) by differentiation of the displacements (24). Hence

$$\varepsilon_x^{(k)} = \varepsilon_x^o - \int_o^z w_{,xx}\, d\eta + G_1^{(k)}\sigma_{xz,x}^o + G_2^{(k)}\sigma_{yz,x}^o \pm G_3^{(k)}V_{x,x} \pm G_4^{(k)}V_{y,x}$$

$$\varepsilon_y^{(k)} = \varepsilon_y^o - \int_o^z w_{,yy}\, d\eta + G_5^{(k)}\sigma_{xz,y}^o + G_6^{(k)}\sigma_{yz,y}^o \pm G_7^{(k)}V_{x,y} \pm G_8^{(k)}V_{y,y} \qquad (27)$$

$$\varepsilon_{xy}^{(k)} = \varepsilon_{xy}^{o} - 2\int_{o}^{z} w_{,xy}\, d\eta + G_5^{(k)}\sigma_{xz,x}^{o} + G_1^{(k)}\sigma_{xz,y}^{o} + G_6^{(k)}\sigma_{yz,x}^{o} \qquad (27)\ \text{(cont'd)}$$
$$+ G_2^{(k)}\sigma_{yz,y}^{o} \pm G_7^{(k)}V_{x,x} + G_3^{(k)}V_{x,y} \pm G_8^{(k)}V_{y,x} \pm G_9^{(k)}V_{y,y}$$

The functions $G_i(z)^{(k)}$ thus represent the effect of shear deformation in the laminate. If it is assumed that the normal displacement, w, does not vary through the thickness of the laminate, the integrals in equations (27) are replaced by $zw_{,xx}^{o}$; $zw_{,yy}^{o}$; and $2zw_{,xy}^{o}$; respectively. This assumption, however, is not necessary for the special cases considered in this report.

3.3 Laminate Stress Resultants and Stress Couples

It will be convenient to eliminate the normal strain from the lamina stress-strain relations and express the stresses in the plane of the k^{th} lamina in terms of the in-plane strains and the normal stress, $\sigma_z^{(k)}$. The normal strain follows from the third of equations (12):

$$\varepsilon_z^{(k)} = \frac{1}{Q_{33}^{(k)}}\left[\bar{\sigma}_z^{(k)} - Q_{13}^{(k)}\varepsilon_x^{(k)} - Q_{23}^{(k)}\varepsilon_y^{(k)} - Q_{36}^{(k)}\varepsilon_{xy}^{(k)}\right] \qquad (28)$$

After substitution of the above in the first, second, and sixth of equations (12), the in-plane stresses may be written in the form:

$$\begin{Bmatrix}\sigma_x\\ \sigma_y\\ \sigma_{xy}\end{Bmatrix}^{(k)} = \begin{bmatrix}\bar{Q}_{11} & \bar{Q}_{12} & \bar{Q}_{16}\\ \bar{Q}_{12} & \bar{Q}_{22} & \bar{Q}_{26}\\ \bar{Q}_{16} & \bar{Q}_{26} & \bar{Q}_{66}\end{bmatrix}^{(k)} \begin{Bmatrix}\varepsilon_x\\ \varepsilon_y\\ \varepsilon_{xy}\end{Bmatrix}^{(k)} + \begin{Bmatrix}\bar{Q}_{13}\\ \bar{Q}_{23}\\ \bar{Q}_{36}\end{Bmatrix}^{(k)} \sigma_z^{(k)} - \begin{Bmatrix}\sigma'_x\\ \sigma'_y\\ \sigma'_{xy}\end{Bmatrix}^{(k)} \qquad (29)$$

where

$$\begin{Bmatrix}\sigma'_x\\ \sigma'_y\\ \sigma'_{xy}\end{Bmatrix}^{(k)} = \begin{Bmatrix}\sigma_x^T\\ \sigma_y^T\\ \sigma_{xy}^T\end{Bmatrix}^{(k)} - \begin{Bmatrix}\bar{Q}_{13}\\ \bar{Q}_{23}\\ \bar{Q}_{36}\end{Bmatrix}^{(k)} \sigma_z^{T(k)}$$

and

$$\overline{Q}_{ij} = \overline{Q}_{ji} = Q_{ij} - \frac{Q_{i3}Q_{3j}}{Q_{33}} \qquad i = 1,2,6 \qquad j = 1,2,6$$

$$\overline{Q}_{ij} = \overline{Q}_{ji} = \frac{Q_{i3}}{Q_{33}} \qquad i = 1,2,6 \qquad j = 3$$

The stress resultants and stress couples are obtained by integrating the stresses over the thickness of each layer and summing the results for all layers, hence

$$\begin{Bmatrix} N_x \\ N_y \\ N_{xy} \end{Bmatrix} = \sum_{k=1}^{N} \int_{h_{k-1}}^{h_k} \begin{Bmatrix} \sigma_x \\ \sigma_y \\ \sigma_{xy} \end{Bmatrix}^{(k)} dz \tag{30}$$

$$\begin{Bmatrix} M_x \\ M_y \\ M_{xy} \end{Bmatrix} = \sum_{k=1}^{N} \int_{h_{k-1}}^{h_k} \begin{Bmatrix} \sigma_x \\ \sigma_y \\ \sigma_{xy} \end{Bmatrix}^{(k)} z\, dz \tag{31}$$

Equations (31) therefore represent the stress couples about the mid-surface of the adhesive layer.

3.4 Equilibrium Equations

Consider a thin slice cut from a double lap joint as shown in detail A of Figure 1. The surface GH for this case is not a free surface and therefore the normal stress will not be zero but equal to σ_z^c. The shear stress along GH, however, is zero because of symmetry. The forces and moments acting on the upper and lower laminate of such a slice are shown in Figure 3. Equilibrium of horizontal forces in the x- and y-directions yields

$$\begin{aligned} N_{xu,x} + N_{xyu,y} - \sigma_{xz}^o &= 0 \\ N_{xL,x} + N_{xyL,y} + \sigma_{xz}^o &= 0 \end{aligned} \tag{32}$$

and

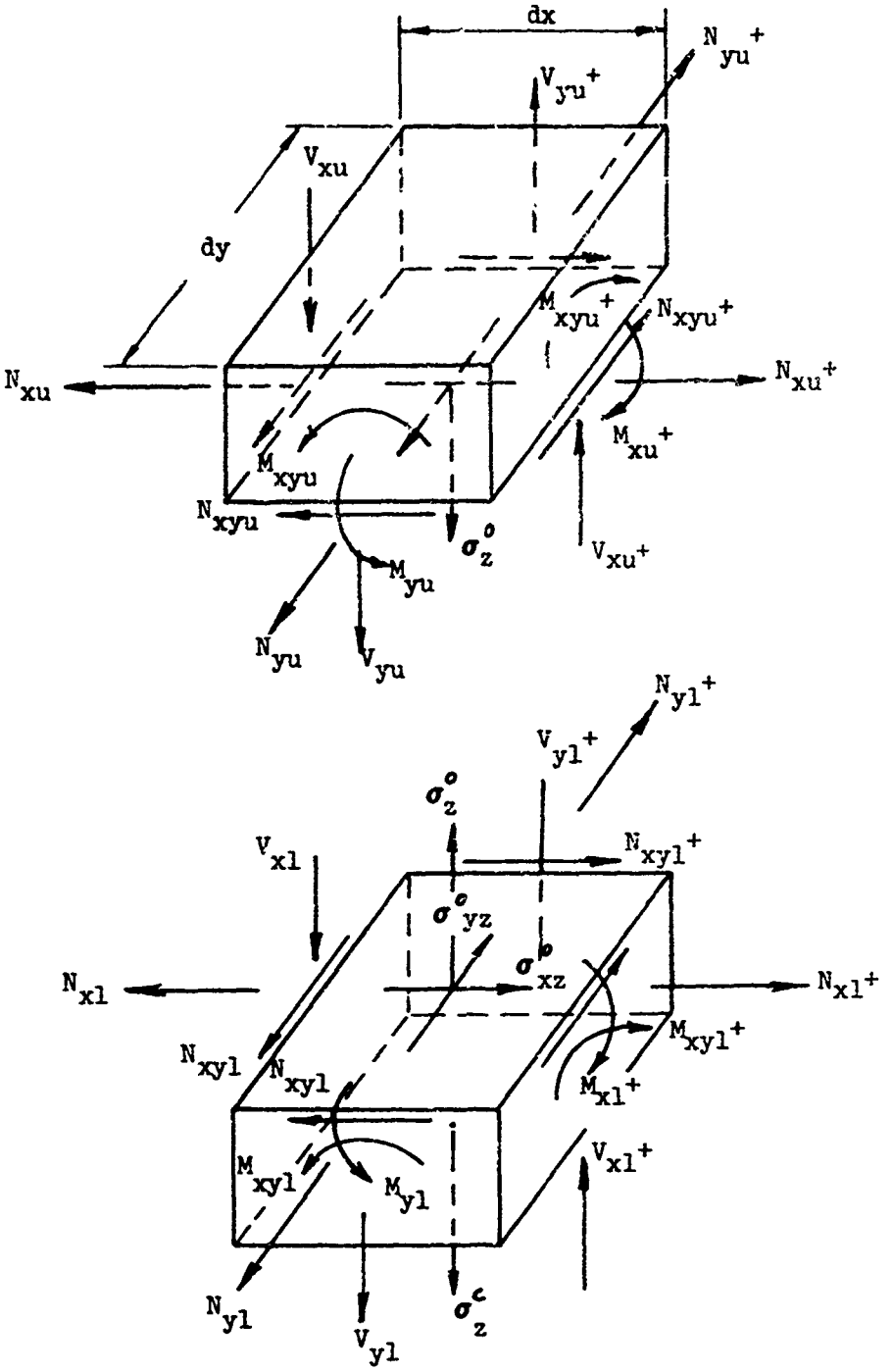

FIGURE 3 EQUILIBRIUM OF FORCES AND MOMENTS-DOUBLE LAP JOINT

$$N_{xyu,x} + N_{yu,y} - \sigma^{o}_{yz} = 0$$

$$N_{xyL,x} + N_{yL,y} + \sigma^{o}_{yz} = 0 \tag{33}$$

Summing vertical forces gives the relations between the transverse shear forces and the normal stresses at the mid-surface of the adhesive

$$V_{xu,x} + V_{yu,y} - \sigma^{o}_{z} = 0$$

$$V_{xL,x} + V_{yL,y} + \sigma^{o}_{z} - \sigma^{c}_{z} = 0 \tag{34}$$

Similarly equilibrium of moments in the x- and y-directions gives

$$M_{xu,x} + M_{xyu,y} - V_{xu} = 0$$

$$M_{xL,x} + M_{xyL,y} - V_{xL} = 0 \tag{35}$$

and

$$M_{xyu,x} + M_{yu,y} - V_{yu} = 0$$

$$M_{xyL,x} + M_{yL,y} - V_{yL} = 0 \tag{36}$$

Equations (32) through (36) are applicable to both double lap and single lap joints, but for the latter, σ^{c}_{z} in the second of equations will be zero. The sum of the stress resultants in the upper and lower laminate represent the total applied loading for the single lap joint and one half the applied loading for the double lap joint. All moments are again calculated with respect to the adhesive mid-surface. It must also be remembered that in a double lap joint the lower laminate represents only one half of the laminated plate and that the transverse shear forces and moments of the entire plate with respect to its middle surface are zero.

4.0 NARROW UNIAXIALLY LOADED JOINTS

4.1 General Remarks

Most of the joints tested as part of this contract were 1.0 inch wide uniaxially loaded specimens and therefore it appeared reasonable to assume the joints to be in a state of plane stress. This means the stresses σ_y, σ_{xy}, and σ_{yz} are assumed to be zero while the remaining stresses are constant along the width of the plate, i.e.

$$\sigma^{(k)}_{x,y} = \sigma^{(k)}_{xz,y} = \sigma^{(k)}_{z,y} = 0$$

The adhesive material will be assumed isotropic while the laminates are assumed to consist of orthotropic layers (Section 3.1). Half of the adhesive layer, that above the reference surface, will be considered as part of the upper laminate while the other half is taken as part of the lower laminate. The stacking arrangement of the laminated plates need not be symmetrical about the middle surface. The joint is assumed to be clamped at a distance L_1 from the splice plate. This assumption does not affect the derivation of the governing differential equations, of course, but will be used to establish the necessary boundary conditions.

4.2 Single Lap Joints

4.2.1 Effect of Transverse Shear

Because of the plane stress assumptions most of the expressions in Section 3.2 are simplified considerably. For a laminate consisting of a single layer, equations (15) may be written:

$$\begin{aligned} \sigma_{xz} &= \sigma^{o}_{xz}\left(1 - \frac{z}{h_N}\right) + [Q_{55}\varphi_x + Q_{45}\varphi_y]\, f(z) \\ \sigma_{yz} &= \sigma^{o}_{yz}\left(1 - \frac{z}{h_N}\right) + [Q_{45}\varphi_x + Q_{44}\varphi_y]\, f(z) \end{aligned} \qquad (37)$$

and since for plane stress $\sigma_{yz} = \sigma^{o}_{yz} = 0$, one obtains:

$$\sigma_{xz} = \sigma^{o}_{xz}\left(1 - \frac{z}{h_N}\right) + \frac{1}{S_{55}}\varphi_x f(z) \tag{38}$$

Equation (38) may be generalized for a multi-layer laminate by writing it in the form:

$$\sigma^{(k)}_{xz} = \sigma^{o}_{xz}\left(1 - \frac{z}{h_N}\right) + \left[\frac{1}{S^{(k)}_{55}} f(z) + bz + a^{(k)}\right]\varphi_x \tag{39}$$

Continuity of shear stress at the interfaces of adjacent layers gives:

$$a^{(k+1)} = a^{(k)} + \left[\frac{1}{S^{(k)}_{55}} - \frac{1}{S^{(k+1)}_{55}}\right] f(h_k) \tag{40}$$

and as before

$$a^{(1)} = 0$$

Since the shear stress vanishes at $z = h_N$, one finds:

$$b = -\frac{a^{(N)}}{h_N} \tag{41}$$

The transverse shear force, V_x, is obtained by integrating the shear stress over the thickness of the laminate, or:

$$\pm V_x = \frac{1}{2}\sigma^{o}_{xz} h_N + A_{55}\varphi_x \tag{42}$$

where:

$$A_{55} = \frac{1}{2} b h^2_N + \sum_{k=1}^{N}\left\{\frac{1}{S^{(k)}_{55}}[F(h_k) - F(h_{k-1})] + a^{(k)}(h_k - h_{k-1})\right\}$$

and F(z) is as defined in Section 3.2. Solving for φ_x from equation (42) and substituting into (39) yields:

$$\sigma^{(k)}_{xz} = \bar{G}^{(k)}_1 \sigma^{o}_{xz} \pm \bar{G}^{(k)}_2 V_x \tag{43}$$

in which:

$$\overline{G}_1(z)^{(k)} = 1 - \frac{z}{h_N} - \frac{1}{2} h_N \overline{G}_2(z)^{(k)}$$

$$\overline{G}_2(z)^{(k)} = \frac{1}{A_{55}} - \left[\frac{1}{S_{55}^{(k)}} f(z) + bz + a^{(k)} \right]$$

From the second of equations (22), setting $\sigma_{yz}^{(k)} = 0$ and substituting for $\sigma_{xz}^{(k)}$ from equation (43), one has for the transverse shear strain:

$$\epsilon_{xz}^{(k)} = S_{55}^{(k)} [\overline{G}_1^{(k)} \sigma_{xz}^{o} \pm \overline{G}_2^{(k)} V_x] \tag{44}$$

Substituting this into equation (10) and integrating with respect to z gives the displacement, u

$$u^{(k)} = u^{o} - \int_{o}^{z} w_{,x} \, d\eta + G_1^{(k)} \sigma_{xz}^{o} \pm G_2^{(k)} V_x \tag{45}$$

where

$$G_i(z)^{(k)} = S_{55}^{(k)} \int_{o}^{z} \overline{G}_i(\eta)^{(k)} d\eta + c_i^{(k)} \qquad i = 1,2 \tag{46}$$

It follows from (45) that the constant $c_i^{(1)}$ must be zero. Compatibility of displacement at the interfaces requires:

$$G_i(h_k)^{(k)} = G_i(h_k)^{(k+1)} \qquad i = 1,2 \tag{47}$$

and hence the remaining constants can be determined. Differentiating the displacement (45) with respect to x gives the longitudinal strain:

$$\epsilon_x^{(k)} = \epsilon_x^{o} - \int_{o}^{z} w_{,xx} \, d\eta + G_1^{(k)} \sigma_{xz,x}^{o} \pm G_2^{(k)} V_{x,x} \tag{48}$$

It must be noted that the shear functions, $\overline{G}_i^{(k)}$ and $G_i^{(k)}$, do not have the same meaning as in Section 3.2.

4.2.2 Variation of Normal Displacement

The integral in equation (48) will not be determined consistent with the assumed transverse shear deformation. The stress equilibrium equations for narrow uniaxially loaded plates reduce to:

$$\begin{aligned} \sigma^{(k)}_{x,x} + \sigma^{(k)}_{xz,z} &= 0 \\ \sigma^{(k)}_{z,z} + \sigma^{(k)}_{xz,x} &= 0 \end{aligned} \tag{49}$$

Integrating the last one with respect to z and substituting for $\sigma^{(k)}_{xz}$, gives the normal stress in the k^{th} layer:

$$\sigma^{(k)}_{z} = \sigma^{o}_{z} + P^{(k)}_{1}\sigma^{o}_{xz,x} \pm P^{(k)}_{2}V_{x,x} \tag{50}$$

where σ^{o}_{z} is the adhesive normal stress at the reference surface and the normal stress functions are given by:

$$P_1(z)^{(k)} = \frac{z^2}{2h_N} - z - \frac{1}{2}h_N\, P_2(z)^{(k)}$$

$$P_2(z)^{(k)} = -\frac{1}{A_{55}}\left[\frac{1}{S^{(k)}_{55}}F(z) + \frac{1}{2}bz^2 + a^{(k)}z + p^{(k)}_2\right]$$

Continuity of normal stress requires:

$$P_2(h_k)^{(k)} = P_2(h_k)^{(k+1)} \tag{51}$$

It follows from equation (50) that $p^{(1)}_2 = 0$. The remaining $p^{(k)}_2$ can be obtained from the above. Since the stresses $\sigma^{(k)}_y$ and $\sigma^{(k)}_{xy}$ are zero, one may write for the normal strain in the k^{th} layer:

$$\epsilon^{(k)}_z = w'^{(k)}_z = S^{(k)}_{13}\sigma^{(k)}_x + S^{(k)}_{33}\sigma^{(k)}_z \tag{52}$$

where:

$$[S] = [Q]^{-1}$$

Differentiating with respect to x and substituting the first of equations (49) gives:

$$w'^{(k)}_{xz} = - S^{(k)}_{13}\sigma^{(k)}_{xz,z} + S^{(k)}_{33}\sigma^{(k)}_{z,x} \tag{53}$$

Substituting equations (43) and (50) one obtains after integrating:

$$w'^{(k)}_{x} = w'^{o}_{x} + p^{(k)}_{3}\sigma^{o}_{xz} + p^{(k)}_{4}\sigma^{o}_{xz,xx} \pm p^{(k)}_{5}V_{x} \pm p^{(k)}_{6}V_{x,xx} \pm p^{(k)}_{7}\sigma^{o}_{z,x} \tag{54}$$

where:

$$P_3(z)^{(k)} = S^{(k)}_{13}\frac{z}{h_N} - \frac{1}{2}h_N P_5(z)^{(k)} + p^{(k)}_3$$

$$P_4(z)^{(k)} = S^{(k)}_{33}\int_o^z P_1(\eta)\,d\eta + p^{(k)}_4$$

$$P_5(z)^{(k)} = -\frac{S^{(k)}_{13}}{A_{55}}\left[\frac{1}{S^{(k)}_{55}}f(z) + bz\right] + p^{(k)}_5$$

$$P_6(z)^{(k)} = S^{(k)}_{33}\int_o^z P_2(\eta)\,d\eta + p^{(k)}_6$$

$$P_7(z)^{(k)} = S^{(k)}_{33}\,z + p^{(k)}_7$$

At the reference surface ($z = 0$), $w'^{(k)}_{x} = w'^{o}_{x}$; and hence:

$$p^{(1)}_i = 0 \qquad i = 3,4,\ldots 7$$

The remaining constants $p^{(k)}_i$ are determined from the condition that the slope must be equal for two adjacent laminae at their interface, or

$$P_i(h_k)^{(k)} = P_i(h_k)^{(k+1)} \tag{55}$$

Differentiating equation (54) with respect to x and integrating with respect to z gives:

$$\int_0^z w_{,xx}\, d\eta = z w^o_{,xx} + P_8^{(k)} \sigma^o_{xz,x} + P_9^{(k)} \sigma^o_{xz,xxx} \pm P_{10}^{(k)} V_{x,x} \pm P_{11}^{(k)} V_{x,xxx} \pm P_{12}^{(k)} \sigma^o_{z,xx} \tag{56}$$

where

$$P_{i+5}(z)^{(k)} = \int_{h_{k-1}}^{z} P_i(\eta)^{(k)}\, d\eta + \sum_{m=1}^{k-1} \int_{h_{m-1}}^{h_m} P_i(\eta)^{(m)} d\eta \qquad i = 3,4,\ldots 7$$

4.2.3 Laminate Stress Resultants and Couples

Since $\sigma_y^{(k)}$ and $\sigma_{xy}^{(k)}$ are assumed to be zero and only the longitudinal strain, $\epsilon_x^{(k)}$, is of interest here, one may solve for the in-plane strains from equations (29). This gives

$$\begin{Bmatrix} \epsilon_x \\ \epsilon_y \\ \epsilon_{xy} \end{Bmatrix}^{(k)} = \left|\bar{\bar{Q}}\right|^{(k)} \begin{Bmatrix} \sigma_x \\ \sigma_y \\ \sigma_{xy} \end{Bmatrix}^{(k)} - \begin{Bmatrix} Z_1 \\ Z_2 \\ Z_3 \end{Bmatrix}^{(k)} \sigma_z^{(k)} + \begin{Bmatrix} T_1 \\ T_2 \\ T_3 \end{Bmatrix}^{(k)} \tag{57}$$

where:

$$\left|\bar{\bar{Q}}\right| = \begin{bmatrix} \bar{Q}_{11} & \bar{Q}_{12} & \bar{Q}_{16} \\ \bar{Q}_{12} & \bar{Q}_{22} & \bar{Q}_{26} \\ Q_{16} & \bar{Q}_{26} & \bar{Q}_{66} \end{bmatrix}^{-1}$$

$$\begin{Bmatrix} Z_1 \\ Z_2 \\ Z_3 \end{Bmatrix} = \left|\bar{\bar{Q}}\right| \begin{Bmatrix} \bar{Q}_{13} \\ \bar{Q}_{23} \\ \bar{Q}_{36} \end{Bmatrix} \qquad \begin{Bmatrix} T_1 \\ T_2 \\ T_3 \end{Bmatrix} = \left|\bar{\bar{Q}}\right| \begin{Bmatrix} \sigma'_x \\ \sigma'_y \\ \sigma'_{xy} \end{Bmatrix}$$

From the first of equations (57) one finds:

$$\sigma_x^{(k)} = \frac{1}{\bar{\bar{Q}}_{11}^{(k)}} \left[\epsilon_x^{(k)} + Z_1^{(k)} \sigma_z^{(k)} - T_1^{(k)}\right]$$

and after substituting (48), (50), and (56), this becomes:

$$\sigma_x^{(k)} = \frac{1}{\bar{\bar{Q}}_{11}^{(k)}} [\varepsilon_x^o - z w_{,xx}^o - T_1^{(k)}] + R_1^{(k)} \sigma_{xz,x}^o + R_2^{(k)} \sigma_{xz,xxx}^o$$

$$+ R_3^{(k)} \sigma_z^o + R_4^{(k)} \sigma_{z,xx}^o \pm R_5^{(k)} V_{x,x} \pm R_6^{(k)} V_{x,xxx} \qquad (58)$$

where

$$R_1(z)^{(k)} = [G_1(z)^{(k)} - P_8(z)^{(k)} + Z_1^{(k)} P_1(z)^{(k)}] / \bar{\bar{Q}}_{11}^{(k)}$$

$$R_2(z)^{(k)} = - P_9(z)^{(k)} / \bar{\bar{Q}}_{11}^{(k)}$$

$$R_3(z)^{(k)} = Z_1^{(k)} / \bar{\bar{Q}}_{11}^{(k)}$$

$$R_4(z)^{(k)} = - P_{12}(z)^{(k)} / \bar{\bar{Q}}_{11}^{(k)}$$

$$R_5(z)^{(k)} = [G_2(z)^{(k)} - P_{10}(z)^{(k)} + Z_1^{(k)} P_2(z)^{(k)}] / \bar{\bar{Q}}_{11}^{(k)}$$

$$R_6(z)^{(k)} = - P_{11}(z)^{(k)} / \bar{\bar{Q}}_{11}^{(k)}$$

For the case under consideration the equilibrium equations (32) through (36) reduce to:

$$N_{xu,x} - \sigma_{xz}^o = 0$$
$$N_{xL,x} + \sigma_{xz}^o = 0 \qquad (59)$$

$$V_{xu,x} - \sigma_z^o = 0$$
$$V_{xL,x} + \sigma_z^o = 0 \qquad (60)$$

and

$$M_{xu,x} - V_{xu} = 0$$
$$M_{xL,x} - V_{xL} = 0 \qquad (61)$$

Adding the first and second of equations (59) and (60), one has:

$$N_{xu,x} + N_{xL,x} = 0$$
$$V_{xu,x} + V_{xL,x} = 0 \tag{62}$$

and therefore:

$$N_{xu} + N_{xL} = \text{Constant}$$
$$V_{xu} + V_{xL} = \text{Constant} \tag{63}$$

The first constant is, of course, equal to the applied axial load, N_x; while the second constant is zero from considerations of symmetry, so that:

$$V_{xL} = -V_{xu} \tag{64}$$

Also by adding equations (61) and substituting the above:

$$M_{xu,x} + M_{xL,x} = 0 \tag{65}$$

which means:

$$M_{xu} + M_{xL} = M_x = \text{Constant} \tag{66}$$

With the use of equations (60) and (64), the longitudinal stress (58) may be written in the general form:

$$\sigma_x^{(k)} = \frac{1}{\bar{\bar{Q}}_{11}^{(k)}}[\varepsilon_x^o - zw^o_{,xx} - T_1^{(k)}] + R_1^{(k)}\sigma^o_{xz,x} + R_2^{(k)}\sigma^o_{xz,xxx}$$
$$+ [R_3^{(k)} + R_5^{(k)}]V_{xu,x} + [R_4^{(k)} + R_6^{(k)}]V_{xu,xxx} \tag{67}$$

which is applicable to both upper and lower laminate. When the above is substituted into the first of equations (30) and (31), one obtains the stress resultants and stress couples on the laminates:

$$N_{xu} = A_{11}^u\varepsilon_x^o - B_{11}^u w^o_{,xx} + R_{11}^u\sigma^o_{xz,x} + R_{12}^u\sigma^o_{xz,xxx}$$
$$+ Z_{11}^u V_{xu,x} + Z_{12}^u V_{xu,xxx} - N'_{xu} \tag{68}$$

$$N_{xL} = A^L_{11}\varepsilon^o_x - B^L_{11}w^o_{,xx} + R^L_{11}\sigma^o_{xz,x} + R^L_{12}\sigma^o_{xz,xxx} + Z^L_{11}V_{xu,x} + Z^L_{12}V_{xu,xxx} - N'_{xL}$$

$$M_{xu} = B^u_{11}\varepsilon^o_x - D^u_{11}w^o_{,xx} + R^u_{21}\sigma^o_{xz,x} + R^u_{22}\sigma^o_{xz,xxx} + Z^u_{21}V_{xu,x} + Z^u_{22}V_{xu,xxx} - M'_{xu} \qquad (68 \text{ cont'd})$$

$$M_{xL} = B^L_{11}\varepsilon^o_x - D^L_{11}w^o_{,xx} + R^L_{21}\sigma^o_{xz,x} + R^L_{22}\sigma^o_{xz,xxx} + Z^L_{21}V_{xu,x} + Z^L_{22}V_{xu,xxx} - M'_{xL}$$

where

$$A_{11} = \pm \sum_{k=1}^{N} \frac{1}{\bar{\bar{Q}}^{(k)}_{11}} (h_k - h_{k-1})$$

$$B_{11} = \pm \frac{1}{2} \sum_{k=1}^{N} \frac{1}{\bar{\bar{Q}}^{(k)}_{11}} (h_k^2 - h_{k-1}^2)$$

$$D_{11} = \pm \frac{1}{3} \sum_{k=1}^{N} \frac{1}{\bar{\bar{Q}}^{(k)}_{11}} (h_k^3 - h_{k-1}^3)$$

$$R_{11} = \pm \sum_{k=1}^{N} \int_{h_{k-1}}^{h_k} R_1(z)^{(k)}\, dz$$

$$R_{12} = \pm \sum_{k=1}^{N} \int_{h_{k-1}}^{h_k} R_2(z)^{(k)}\, dz$$

$$R_{21} = \pm \sum_{k=1}^{N} \int_{h_{k-1}}^{h_k} R_1(z)^{(k)}\, z\, dz$$

$$R_{22} = \pm \sum_{k=1}^{N} \int_{h_{k-1}}^{h_k} R_2(z)^{(k)} \, z \, dz$$

$$N'_x = \pm \sum_{k=1}^{N} \frac{T_1^{(k)}}{\bar{Q}_{11}^{(k)}} (h_k - h_{k-1})$$

$$M'_x = \pm \frac{1}{2} \sum_{k=1}^{N} \frac{T_1^{(k)}}{\bar{Q}_{11}^{(k)}} (h_k^2 - h_{k-1}^2)$$

$$Z_{11} = \pm \sum_{k=1}^{N} \int_{h_{k-1}}^{h_k} [R_3(z)^{(k)} + R_5(z)^{(k)}] dz$$

$$Z_{12} = \pm \sum_{k=1}^{N} \int_{h_{k-1}}^{h_k} [R_4(z)^{(k)} + R_6(z)^{(k)}] dz$$

$$Z_{21} = \pm \sum_{k=1}^{N} \int_{h_{k-1}}^{h_k} [R_3(z)^{(k)} + R_5(z)^{(k)}] \, z \, dz$$

$$Z_{22} = \pm \sum_{k=1}^{N} \int_{h_{k-1}}^{h_k} [R_4(z)^{(k)} + R_6(z)^{(k)}] \, z \, dz$$

In the above, the superscripts u and L are omitted for convenience.

4.2.4 Governing Differential Equations

Differentiating equations (68) and substituting into the first of equations (62) and into equation (65), gives in matrix form.

$$\begin{bmatrix} A_{11} & B_{11} \\ B_{11} & D_{11} \end{bmatrix} \begin{Bmatrix} \varepsilon^{o}_{x,x} \\ -w^{o}_{,xxx} \end{Bmatrix} + \begin{bmatrix} R_{11} & R_{12} & Z_{11} & Z_{12} \\ R_{21} & R_{22} & Z_{21} & Z_{22} \end{bmatrix} \begin{Bmatrix} \sigma^{o}_{xz,xx} \\ \sigma^{o}_{xz,xxxx} \\ V_{xu,xx} \\ V_{xu,xxxx} \end{Bmatrix} = 0 \qquad (69)$$

where:

$$A_{11} = A^{u}_{11} + A^{L}_{11}$$

$$B_{11} = B^{u}_{11} + B^{L}_{11} \quad , \quad \text{etc.}$$

Solving for $\varepsilon^{o}_{x,x}$ and $w^{o}_{,xxx}$ from equation (69) yields:

$$\begin{Bmatrix} \varepsilon^{o}_{x,x} \\ -w^{o}_{,xxx} \end{Bmatrix} = \begin{bmatrix} \bar{R}_{11} & \bar{R}_{12} & \bar{Z}_{11} & \bar{Z}_{12} \\ \bar{R}_{21} & \bar{R}_{22} & \bar{Z}_{21} & \bar{Z}_{22} \end{bmatrix} \begin{Bmatrix} \sigma^{o}_{xz,xx} \\ \sigma^{o}_{xz,xxxx} \\ V_{xu,xx} \\ V_{xu,xxxx} \end{Bmatrix} \qquad (70)$$

in which:

$$\begin{bmatrix} \bar{R}_{11} & \bar{R}_{12} & \bar{Z}_{11} & \bar{Z}_{12} \\ \bar{R}_{21} & \bar{R}_{22} & \bar{Z}_{21} & \bar{Z}_{22} \end{bmatrix} = - \begin{bmatrix} A_{11} & B_{11} \\ B_{11} & D_{11} \end{bmatrix}^{-1} \begin{bmatrix} R_{11} & R_{12} & Z_{11} & Z_{12} \\ R_{21} & R_{22} & Z_{21} & Z_{22} \end{bmatrix}$$

Substituting the first and third of equations (68) into the first of equations (59) and (61), respectively, and using equations (70), one obtains the following two coupled differential equations:

$$\begin{aligned} &\sigma^{o}_{xz} + R^{*}_{11}\,\sigma^{o}_{xz,xx} + R^{*}_{12}\,\sigma^{o}_{xz,xxxx} + Z^{*}_{11}\,V_{xu,xx} + Z^{*}_{12}\,V_{xu,xxxx} = 0 \\ &R^{*}_{21}\,\sigma^{o}_{xz,xx} + R^{*}_{22}\,\sigma^{o}_{xz,xxxx} + V_{xu} + Z^{*}_{21}\,V_{xu,xx} + Z^{*}_{22}\,V_{xu,xxxx} = 0 \end{aligned} \qquad (71)$$

where:

$$R^*_{11} = -R^u_{11} - A^u_{11}\bar{R}_{11} - B^u_{11}\bar{R}_{21}$$

$$R^*_{12} = -R^u_{12} - A^u_{11}\bar{R}_{12} - B^u_{11}\bar{R}_{22}$$

$$R^*_{21} = -R^u_{21} - B^u_{11}\bar{R}_{11} - D^u_{11}\bar{R}_{21}$$

$$R^*_{22} = -R^u_{22} - B^u_{11}\bar{R}_{12} - D^u_{11}\bar{R}_{22}$$

$$Z^*_{11} = -Z^u_{11} - A^u_{11}\bar{Z}_{11} - B^u_{11}\bar{Z}_{21}$$

$$Z^*_{12} = -Z^u_{12} - A^u_{11}\bar{Z}_{12} - B^u_{11}\bar{Z}_{22}$$

$$Z^*_{21} = -Z^u_{21} - B^u_{11}\bar{Z}_{11} - D^u_{11}\bar{Z}_{21}$$

$$Z^*_{22} = -Z^u_{22} - B^u_{11}\bar{Z}_{12} - D^u_{11}\bar{Z}_{22}$$

Combining equations (71) to eliminate $V_{xu,xxxx}$, one has:

$$V_{xu,xx} = t_1 V_{xu} + t_2\sigma^o_{xz} + t_3\sigma^o_{xz,xx} + t_4\sigma^o_{xz,xxxx} \tag{72}$$

where

$$t_1 = Z^*_{12}/s_1$$

$$t_2 = -Z^*_{22}/s_1$$

$$t_3 = R^*_{21}\, t_1 + R^*_{11}\, t_2$$

$$s_1 = Z^*_{11}\, Z^*_{22} - Z^*_{12}\, Z^*_{21}$$

$$t_4 = R^*_{22}\, t_1 + R^*_{12}\, t_2$$

Differentiating (72) twice yields:

$$V_{xu,xxxx} = t_1 V_{xu,xx} + t_2\sigma^o_{xz,xx} + t_3\sigma^o_{xz,xxxx} + t_4\sigma^o_{xz,xxxxxx} \tag{73}$$

Substituting equations (72) and (73) into the second of (71) gives:

$$V_{xu} = t_5 \sigma^o_{xz} + t_6 \sigma^o_{xz,xx} + t_7 \sigma^o_{xz,xxxx} + t_8 \sigma^o_{xz,xxxxxx} \tag{74}$$

in which:

$$t_5 = - s_3 t_2 / s_2$$

$$t_6 = - (R^*_{21} + Z^*_{22} t_2 + s_3 t_3) / s_2$$

$$t_7 = - (R^*_{22} + Z^*_{22} t_3 + s_3 t_4) / s_2$$

$$s_2 = 1 + s_3 t_1$$

$$s_3 = Z^*_{21} + Z^*_{22} t_1$$

$$t_8 = - Z^*_{22} t_4 / s_2$$

Differentiating equation (74) twice and substituting it together with (73) into the first of equations (71), one obtains the following eighth order differential equation in σ^o_{xz}:

$$C_1 \sigma^o_{xz,xxxxxxxx} + C_2 \sigma^o_{xz,xxxxxx} + C_3 \sigma^o_{xz,xxxx} + C_4 \sigma^o_{xz,xx} + \sigma^o_{xz} = 0 \tag{75}$$

where

$$C_1 = s_4 t_8$$

$$C_2 = Z^*_{12} t_4 + s_4 t_7$$

$$C_3 = R^*_{12} + Z^*_{12} t_3 + s_4 t_6$$

$$C_4 = R^*_{11} + Z^*_{12} t_2 + s_4 t_5$$

$$s_4 = Z^*_{11} + Z^*_{12} t_1$$

The general solution to the differential equation (75) may be written in the form:

$$\sigma^o_{xz} = \sum_{j=1}^{8} A_j e^{\lambda_j x} \tag{76}$$

where λ_i are the roots of the equation:

$$C_1 \lambda^8 + C_2 \lambda^6 + C_3 \lambda^4 + C_4 \lambda^2 + 1 = 0 \tag{77}$$

By letting $\eta = \lambda^2$ and dividing through by C_1 this becomes

$$\eta^4 + \bar{C}_1 \eta^3 + \bar{C}_2 \eta^2 + \bar{C}_3 \eta + \bar{C}_4 = 0 \tag{78}$$

where

$$\bar{C}_i = \frac{C_{i+1}}{C_1} \qquad i = 1,2,3$$

$$\bar{C}_4 = \frac{1}{C_1}$$

In general the solution of equation (78) will yield a pair of complex conjugate, or imaginary roots, and hence the form in equation (76) does not lend itself for numerical computations. Considering, for example, the case in which equation (78) has two real roots, one of which is positive and the other negative, and a pair of complex conjugate roots, the solution, equation (76), may be written in the alternate form:

$$\sigma^o_{xz} = A_1 e^{\alpha_1 x} + A_2 e^{-\alpha_1 x} + A_3 \cos\beta_3 x + A_4 \sin\beta_3 x$$
$$+ e^{\alpha_5 x}(A_5 \cos\beta_5 x + A_6 \sin\beta_5 x)$$
$$+ e^{-\alpha_5 x}(A_7 \cos\beta_5 x + A_8 \sin\beta_5 x) \tag{79}$$

where α_i is the real part and β_i the imaginary part of the complex root:

$$\lambda_i = \alpha_i + i\beta_i$$

In general one may write equation (76) in the form

$$\sigma^o_{xz} = \sum_{i=1}^{8} A_i \varphi_i(x) \tag{80}$$

where each function φ_i has one of the following five forms:

$$e^{\alpha_i x}$$

$$\cos\beta_i x$$

$$\sin\beta_i x$$

$$e^{\alpha_i x}\cos\beta_i x$$

$$e^{\alpha_i x}\sin\beta_i x$$

For the case when the joint configuration is symmetrical with respect to the middle surface of the adhesive layer, i.e.

$$A_{11}^{U} = A_{11}^{L}$$

$$B_{11}^{U} = -B_{11}^{L}$$

$$D_{11}^{U} = D_{11}^{L}$$

it can be shown that Z_{11}^{*}, Z_{12}^{*}, R_{21}^{*}, and R_{22}^{*} are zero and the two differential equations (71) become uncoupled. Instead of equations (80), one now has:

$$\sigma_{xz}^{o} = \sum_{i=1}^{4} A_i \varphi_i(x)$$

$$V_{xu} = \sum_{i=5}^{8} A_i \varphi_i(x) \qquad (81)$$

In addition, one finds for the symmetrical case:

$$\bar{R}_{11} = \bar{R}_{12} = \bar{Z}_{21} = \bar{Z}_{22} = 0$$

4.2.5 Boundary Conditions and Solution

The eight constants, A_i in equations (80) or (81), must be determined from the boundary conditions of the problem. The first four boundary conditions are as follows:

$$\begin{aligned} \sigma^{oo}_{xz} &= \sigma^{o}_{xz}(0) = 0 \\ \sigma^{oL}_{xz} &= \sigma^{o}_{xz}(L) = 0 \\ V^{o}_{xu} &= V_{xu}(0) = 0 \\ V^{L}_{xu} &= V_{xu}(L) = 0 \end{aligned} \tag{82}$$

In other words, the adhesive shear stress and the transverse shear forces vanish at $x = 0$ and $x = L$. In the Goland-Reissner analysis, the adhesive shear stress would have its maximum value at these points, which is, of course, a violation of the boundary conditions.

The loads and moments at the ends will provide the remaining boundary conditions. It will be necessary, however, to determine the strain and curvature at the reference surface first. From equations (70), after integrating:

$$\begin{aligned} \varepsilon_x &= \bar{R}_{11}\,\sigma^{o}_{xz,x} + \bar{R}_{12}\,\sigma^{o}_{xz,xxx} + \bar{Z}_{11}\,V_{xu,x} + \bar{Z}_{12}\,V_{xu,xxx} + A_9 \\ -w_{,xx} &= \bar{R}_{21}\,\sigma^{o}_{xz,x} + \bar{R}_{22}\,\sigma^{o}_{xz,xxx} + \bar{Z}_{21}\,V_{xu,x} + \bar{Z}_{22}\,V_{xu,xxx} + A_{10} \end{aligned} \tag{83}$$

Substituting this into equations (68), one obtains:

$$\begin{aligned} N_{xu} &= -R^{*}_{11}\,\sigma^{o}_{xz,x} - R^{*}_{12}\,\sigma^{o}_{xz,xxx} - Z^{*}_{11}\,V_{xu,x} - Z^{*}_{12}\,V_{xu,xxx} \\ &\quad + A^{u}_{11}\,A_9 + B^{u}_{11}\,A_{10} - N'_{xu} \\ N_{xL} &= R^{**}_{11}\,\sigma^{o}_{xz,x} + R^{**}_{12}\,\sigma^{o}_{xz,xxx} + Z^{**}_{11}\,V_{xu,x} + Z^{**}_{12}\,V_{xu,xxx} \\ &\quad + A^{L}_{11}\,A_9 + B^{L}_{11}\,A_{10} - N'_{xL} \end{aligned} \tag{84}$$

$$M_{xu} = -R^{*}_{21}\,\sigma^{o}_{xz,x} - R^{*}_{22}\,\sigma^{o}_{xz,xxx} - Z^{*}_{21}\,V_{xu,x} - Z^{*}_{22}\,V_{xu,xxx}$$
$$+B^{u}_{11}\,A_9 + D^{u}_{11}\,A_{10} - M'_{xu}$$

$$M_{xL} = R^{**}_{21}\,\sigma^{o}_{xz,x} + R^{**}_{22}\,\sigma^{o}_{xz,xxx} + Z^{**}_{21}\,V_{xu,x} + Z^{**}_{22}\,V_{xu,xxx}$$
$$+B^{L}_{11}\,A_9 + D^{L}_{11}\,A_{10} - M'_{xL}$$

where the R^{*}_{ij} and Z^{*}_{ij} are as defined previously, and:

$$R^{**}_{11} = R^{L}_{11} + A^{L}_{11}\,\bar{R}_{11} + B^{L}_{11}\,\bar{R}_{21}$$

$$R^{**}_{12} = R^{L}_{12} + A^{L}_{11}\,\bar{R}_{12} + B^{L}_{11}\,\bar{R}_{22}$$

$$R^{**}_{21} = R^{L}_{21} + B^{L}_{11}\,\bar{R}_{11} + D^{L}_{11}\,\bar{R}_{21}$$

$$R^{**}_{22} = R^{L}_{22} + B^{L}_{11}\,\bar{R}_{12} + D^{L}_{11}\,\bar{R}_{22}$$

$$Z^{**}_{11} = Z^{L}_{11} + A^{L}_{11}\,\bar{Z}_{11} + B^{L}_{11}\,\bar{Z}_{21}$$

$$Z^{**}_{12} = Z^{L}_{12} + A^{L}_{11}\,\bar{Z}_{12} + B^{L}_{11}\,\bar{Z}_{22}$$

$$Z^{**}_{21} = Z^{L}_{21} + B^{L}_{11}\,\bar{Z}_{11} + D^{L}_{11}\,\bar{Z}_{21}$$

$$Z^{**}_{22} = Z^{L}_{22} + B^{L}_{11}\,\bar{Z}_{12} + D^{L}_{11}\,\bar{Z}_{22}$$

With the additional two integration constants, A_9 and A_{10}, there are ten undetermined coefficients and therefore six more conditions are required for a solution. Although it appears that eight more boundary conditions (two loads and two moments at each end) are available, only six of them are independent. Because the first of equations (62) and equation (65) were used in the derivation of the governing differential equations (71), only three load and three moment conditions can be specified. As shown previously:

$$M_{xu} + M_{xL} = M_x$$

$$N_{xu} + N_{xL} = N_x$$

where N_x is equal to the applied load and therefore a known quantity. M_x represents the total moment about the reference surface and can be determined from the condition that the slope is zero at the ends and at the center of the joint.

In the region AC of the lower laminate (Figure 1), the strain and curvature will be assumed constant and equal to $\bar{\epsilon}^o_x$ and $\bar{w}^o_{,xx}$, respectively. The slope at C now becomes:

$$\bar{w}^o_{,x} = L_1 \bar{w}^o_{,xx} \tag{85}$$

The load and moment will be constant also, and are given by:

$$\begin{aligned} N^o_{xL} = N_x &= A^L_{11} \bar{\epsilon}^o_x - B^L_{11} \bar{w}^o_{,xx} - N'_{xL} \\ M^o_{xL} = M_x &= B^L_{11} \bar{\epsilon}^o_x - D^L_{11} \bar{w}^o_{,xx} - M'_{xL} \end{aligned} \tag{86}$$

By eliminating $\bar{\epsilon}^o_x$ from equations (86) and substituting (85), one obtains the relation:

$$M_x + M'_{xL} - \frac{B^L_{11}}{A^L_{11}} (N_x + N'_{xL}) = - \bar{D}^L_{11} \bar{w}^o_{,xx} = \frac{\bar{D}^L_{11}}{L_1} \bar{w}^o_{,x} \tag{87}$$

where:

$$\bar{D}_{11} = D_{11} - \frac{B^2_{11}}{A_{11}}$$

In a similar manner one finds for region DE:

$$\bar{w}^L_{,x} = - L_2 \bar{w}^L_{,xx} \tag{88}$$

and:

$$M_x + M'_{xu} - \frac{B^u_{11}}{A^u_{11}}(N_x + N'_{xu}) = \frac{\bar{D}^u_{11}}{L_2} \bar{w}^L_{,x} \tag{89}$$

An expression for the slope in region CD is obtained by integrating the second of equations (83) with respect to x:

$$w^o_{,x} = -\bar{R}_{21}\sigma^o_{xz,x} - \bar{R}_{22}\sigma^o_{xz,xxx} - \bar{Z}_{21}V_{xu,x} - \bar{Z}_{22}V_{xu,xxx} - A_{10}x + A'_{11} \tag{90}$$

Before matching slopes on both sides of points C and D, an inconsistency of minor importance must be pointed out. According to equation (54), the slope varies through the thickness of the laminate in region CD. However, beam theory was used in region AC of the lower laminate and in region DE of the upper laminate to derive equations (87) and (89). It would therefore be better to use the average slopes of the laminates at the ends of region CD. These average slopes follow from equations (54), (60), (64), (82), and (90), hence:

$$\begin{aligned}
\bar{w}^o_{,x} &= (P^L_{4AV} - \bar{R}_{22})\sigma^{oo}_{xz,xx} + (P^L_{6AV} - \bar{Z}_{22})V^o_{xu,xx} + A'_{11} \\
\bar{w}^L_{,x} &= (P^u_{4AV} - \bar{R}_{22})\sigma^{oo}_{xz,xx} + (P^u_{6AV} - \bar{Z}_{22})V^L_{xu,xx} - A_{10}L + A'_{11}
\end{aligned} \tag{91}$$

where:

$$P_{4AV} = \frac{1}{2}\left[P_4(h_1)^{(1)} + P_4(h_N)^{(N)}\right]$$

$$P_{6AV} = \frac{1}{2}\left[P_6(h_1)^{(1)} + P_6(h_N)^{(N)} + P_7(h_1)^{(1)} + P_7(h_N)^{(N)}\right]$$

Substituting the above into equations (87) and (89), one obtains, after rearranging:

$$(P^L_{4AV} - \bar{R}_{22})\sigma^{oo}_{xz,xx} + (P^L_{6AV} - \bar{Z}_{22})V^o_{xu,xx} + A'_{11} + \frac{L_1}{\bar{D}^L_{11}}M_x =$$

$$-\frac{L_1}{\bar{D}^L_{11}}\left[M'_{xL} - \frac{B^L_{11}}{A^L_{11}}(N_x + N'_{xL})\right] \tag{92}$$

and:

$$(P^{U}_{4AV} - \bar{R}_{22})\sigma^{oL}_{xz,xx} + (P^{U}_{6AV} - \bar{Z}_{22})V^{L}_{xu,xx} - A_{10}{}^{L} + A'_{11} -$$

$$\frac{L_2}{\bar{D}^{U}_{11}} M_x = \frac{L_2}{\bar{D}^{U}_{11}} \left[M'_{xu} - \frac{B^{U}_{11}}{A^{U}_{11}} (N_x + N'_{xu}) \right] \tag{93}$$

Equations (92) and (93) provide the conditions necessary for the determination of the total moment and the integration constant A'_{11}. Six independent load and moment boundary conditions are given by:

$$\begin{aligned} N_{xu}(0) &= 0 \\ N_{xu}(L) &= N_x \\ N_{xu}(x) + N_{xL}(x) &= N_x \\ M_{xu}(0) &= 0 \\ M_{xu}(L) &= M_x \\ M_{xu}(x) + M_{xL}(x) &= M_x \end{aligned} \tag{94}$$

Equation (82), (92), (93), and (94) represent a system of twelve conditions with twelve unknowns. In matrix form one may write:

$$
\begin{Bmatrix}
\sigma^{o}_{xz}(0) \\
\sigma^{o}_{xz}(L) \\
V_{xu}(0) \\
V_{xu}(L) \\
\bar{N}_{xu}(0) \\
\bar{N}_{xu}(L) \\
\bar{N}_{xu} + \bar{N}_{xL} \\
\bar{M}_{xu}(0) \\
\bar{M}_{xu}(L) \\
\text{eq. (93)} \\
\text{eq. (92)} \\
\bar{M}_{xu} + \bar{M}_{xL}
\end{Bmatrix}
=
\begin{bmatrix}
H_{1,1} & H_{1,2} & \cdots & H_{1,12} \\
H_{2,1} & H_{2,2} & & H_{2,12} \\
- & - & & - \\
- & - & & - \\
- & - & & - \\
- & - & & - \\
- & - & & - \\
- & - & & - \\
- & - & & - \\
- & - & & - \\
- & - & & - \\
H_{12,1} & H_{12,2} & \cdots & H_{12,12}
\end{bmatrix}
\begin{Bmatrix}
A_1 \\ A_2 \\ A_3 \\ A_4 \\ A_5 \\ A_6 \\ A_7 \\ A_8 \\ M_x \\ A_9 \\ A_{10} \\ A_{11}
\end{Bmatrix}
\tag{95}
$$

The conditions involving the transverse shear force are obtained from (74) and those involving the stress resultants and couples are given by equations (84). Equations (95) may be written in the compact form:

$$[H]\{A^*\} = \{C^*\} \tag{96}$$

where the coefficients of [H] are given by:

$$H_{1,i} = \varphi_i(0)$$

$$H_{2,i} = \varphi_i(L)$$

$$H_{3,i} = \psi_i(0)$$

$$H_{4,i} = \psi_i(L)$$

$$H_{5,i} = \mu_i(0)$$

$$H_{6,i} = \mu_i(L)$$

$$H_{7,i} = 0$$

$$H_{8,i} = \rho_i(0)$$

$$H_{9,i} = \rho_i(L)$$

$$H_{10,i} = (P^U_{4AV} - \bar{R}_{22})\varphi_i''(L) + (P^U_{6AV} - \bar{Z}_{22})\psi_i''(L)$$

$$H_{11,i} = (P^L_{4AV} - \bar{R}_{22})\varphi_i''(0) + (P^L_{6AV} - \bar{Z}_{22})\psi_i''(0)$$

$$H_{12,i} = 0$$

$$\dot{\psi}_i = t_5\varphi_i + t_6\varphi_i'' + t_7\varphi_i^{iv} + t_8\varphi_i^{vi}$$

$$\mu_i = -R^*_{11}\varphi_i' - R^*_{12}\varphi_i''' - Z^*_{11}\psi_i' - Z^*_{12}\psi_i'''$$

$$\rho_i = -R^*_{21}\varphi_i' - R^*_{22}\varphi_i''' - Z^*_{21}\psi_i' - Z^*_{22}\psi_i''' \qquad i = 1,2,\ldots 8$$

$$H_{i,i} = C \qquad i = 1,2,3,4 \qquad i = 9,10,11,12$$

$$H_{i,9} = H_{i,12} = C \qquad i = 5,6,7,8$$

$$H_{5,10} = H_{6,10} = A^U_{11}$$

$$H_{5,11} = H_{6,11} = B^U_{11}$$

$$H_{7,10} = A_{11}$$

$$H_{7,11} = B_{11}$$

$$H_{8,10} = H_{9,10} = B^U_{11}$$

$$H_{8,11} = H_{9,11} = D^U_{11}$$

$$H_{9,9} = -1$$

$$H_{9,12} = 0$$

$$H_{10,9} = \frac{-L_2}{\bar{D}^U_{11}}$$

$$H_{10,10} = 0$$

$$H_{10,11} = -L$$

$$H_{10,12} = 1$$

$$H_{11,9} = \frac{L_1}{\bar{D}^L_{11}}$$

$$H_{11,10} = 0$$

$$H_{11,11} = 0$$

$$H_{11,12} = 1$$

$$H_{12,9} = -1$$

$$H_{12,10} = B_{11}$$

$$H_{12,11} = D_{11}$$

$$H_{12,12} = 0$$

and the coefficients of the column matrix {C*}:

$$C^*_i = 0 \qquad i = 1,2,3,4$$

$$C^*_5 = N'_{xu}$$

$$C^*_6 = N_x + N'_{xu}$$

$$C^*_7 = N_x + N'_{xu} + N'_{xL}$$

$$C_8^* = C_9^* = M'_{xU}$$

$$C_{10}^* = \frac{L_2}{\bar{D}_{11}^U}\left[M'_{xU} - \frac{B_{11}^U}{A_{11}^U}(N_x + N'_{xU})\right]$$

$$C_{11}^* = -\frac{L_1}{\bar{D}_{11}^L}\left[M'_{xL} - \frac{B_{11}^L}{A_{11}^L}(N_x + N'_{xL})\right]$$

$$C_{12}^* = M'_{xU} + M'_{xL}$$

Solving the set of simultaneous equations (96) yields the unknown coefficients A_i^* and therefore A_i and M_x.

$$\{A^*\} = [H]^{-1}\{C^*\} \tag{97}$$

After determination of the coefficients A_i, the shear and normal stresses in the adhesive may be calculated from equations (80) and (60), or in the symmetrical case from equations (81) and (60). The interlaminar shear and normal stresses in the adherends may be obtained from equations (43) and (50), and the longitudinal stresses in the laminate are given by equation (67).

4.3 Double Lap Joints

For the upper laminate, the analysis is identical to that for the single lap joint, but some minor modifications are required with respect to the lower laminate. As a result of symmetry, the laminated plate as a whole will not incur any bending and therefore it will be reasonable to assume the shear function, ω_x, to be zero for the lower laminate. With this assumption, the transverse shear stress will vary linearly through the laminate according to the relation:

$$\sigma_{xz}^{(k)} = \sigma_{xz}^{o}\left(1 - \frac{z}{h_N}\right) \tag{98}$$

while the shear strain $\varepsilon_{xz}^{(k)}$ becomes:

$$\varepsilon_{xz}^{(k)} = S_{55}^{(k)} \left(1 - \frac{z}{h_N}\right) \sigma_{xz}^{o} \tag{99}$$

Substituting this into equation (10) and integrating with respect to z yields for the longitudinal displacement:

$$u^{(k)} = u^{o} - \int_{o}^{z} w_{,x}\, d\eta + G_1^{(k)} \sigma_{xz}^{o} \tag{100}$$

where

$$G_1(z)^{(k)} = S_{55}^{(k)} \left(z - \frac{z^2}{2h_N}\right) + c_1^{(k)}$$

The longitudinal strain is obtained by differentiating the displacement (100) with respect to x. Hence:

$$\varepsilon_x^{(k)} = \varepsilon_x^{o} - \int_{o}^{z} w_{,xx}\, d\eta + G_1^{(k)} \sigma_{xz,x}^{o} \tag{101}$$

The shear force acting on the lower laminate becomes:

$$V_{xL} = -\frac{1}{2} \sigma_{xz}^{o} h_N \tag{102}$$

The normal stress in the k^{th} layer is found by integrating the second of equations (49) with respect to z and substituting (98):

$$\sigma_z^{(k)} = \sigma_z^{o} + \sigma_{xz,x}^{o} \left(-z + \frac{z^2}{2h_N}\right) \tag{103}$$

Equation (53) is valid. By substituting the expressions (98) and (103) and integrating the result with respect to z, one has for the slope:

$$w_{,x}^{(k)} = w_{,x}^{o} + P_3^{(k)} \sigma_{xz}^{o} + P_4^{(k)} \sigma_{xz,xx}^{o} + P_7^{(k)} \sigma_{z,x}^{o} \tag{104}$$

where

$$P_3(z)^{(k)} = S_{13}^{(k)} \frac{z}{h_N} + p_3^{(k)}$$

$$P_4(z)^{(k)} = S_{33}^{(k)}\left(-\frac{z^2}{2} + \frac{z^3}{6h_N}\right) + p_4^{(k)}$$

$$P_7(z)^{(k)} = S_{33}^{(k)}\, z + p_7^{(k)}$$

The constants $p_3^{(k)}$, $p_4^{(k)}$, and $p_7^{(k)}$ are determined from conditions of slope compatibility of adjacent layers at their interfaces. From the above one obtains:

$$\int_o^z w_{,xx}\, d\eta = z w^o_{,xx} + P_8^{(k)}\sigma^o_{xz,x} + P_9^{(k)}\sigma^o_{xz,xxx} + P_{12}^{(k)}\sigma^o_{z,xx} \tag{105}$$

in which, as before:

$$P_{i+5}(z)^{(k)} = \int_{h_{k-1}}^{z} P_i(\eta)^{(k)} d\eta + \sum_{m=1}^{k-1} \int_{h_{m-1}}^{h_m} P_i(\eta)^{(m)} d\eta$$

$$i = 3,4,7$$

The equilibrium equations for the double lap joint are the same as those for the single lap joint except that in place of the second of equations (60), one has:

$$V_{xL,x} + \sigma_z^o - \sigma_z^c = 0 \tag{106}$$

The longitudinal stress for the lower laminate may now be written:

$$\sigma_x^{(k)} = \frac{1}{\bar{\bar{Q}}_{11}^{(k)}}\left|\varepsilon_x^{(k)} - z w^o_{,xx} - T_1^{(k)}\right| + R_1^{(k)}\sigma^o_{xz,x} + R_2^{(k)}\sigma^o_{xz,xxx}$$

$$+ R_3^{(k)} V_{xu,x} + R_4^{(k)} V_{xu,xxx} \tag{107}$$

which is identical to equation (67), if the quantities $P_2^{(k)}$, $R_5^{(k)}$, and $R_6^{(k)}$ in that equation are set equal to zero. Equations (64) and (65) are no longer valid but the first of equations (62) still applies and hence:

$$N_{xu} + N_{xL} = N_x \tag{108}$$

As mentioned previously, however, N_x in this case represents only half of the applied load. The expressions for the stress resultants and stress couples given by equations (68) remain valid, but the coefficients, R^L_{ij} and Z^L_{ij}, must be modified in accordance with (107). Since the slope of the lower laminate is zero for $z = h_N$, one has from (104), and the first of equations (60):

$$w^o_{,x} = - P^L_3(h_N)^{(N)}\sigma^o_{xz} - P^L_4(h_N)^{(N)}\sigma^o_{xz,xx} - P^L_7(h_N)^{(N)}V_{xu,xx} \tag{109}$$

Differentiating the above, substituting into the first and second of equations (68), and using (108) yields:

$$A_{11}\varepsilon^o_x + \left[R_{11} + B_{11}P^L_3(h_N)^{(N)}\right]\sigma^o_{xz,x} + \left[R_{12} + B_{11}P^L_4(h_N)^{(N)}\right]\sigma^o_{xz,xxx}$$
$$+ Z_{11}V_{xu,x} + \left[Z_{12} + B_{11}P_7(h_N)^{(N)}\right]V_{xu,xxx} = N_x + N'_{xu} + N'_{xL}$$

and hence:

$$\varepsilon^o_x = \bar{R}_{11}\sigma^o_{xz,x} + \bar{R}_{12}\sigma^o_{xz,xxx} + \bar{Z}_{11}V_{xu,x} + \bar{Z}_{12}V_{xu,xxx}$$
$$+ \frac{1}{A_{11}}(N_x + N'_{xu} + N'_{xL}) \tag{110}$$

where

$$\bar{R}_{11} = - \left[R_{11} + B_{11}P^L_3(h_N)^{(N)}\right] / A_{11}$$

$$\bar{R}_{12} = - \left[R_{12} + B_{11}P^L_4(h_N)^{(N)}\right] / A_{11}$$

$$\bar{Z}_{11} = - Z_{11}/A_{11}$$

$$\bar{Z}_{12} = - \left[Z_{12} + B_{11}P^L_7(h_N)^{(N)}\right] / A_{11}$$

After substituting (109) and (110) into the first and third of equations (68), and using the equilibrium equations (59) and (61), one obtains two fourth order differential equations identical to (71). The coefficients R^*_{ij} and Z^*_{ij} for this case are given by:

$$R^*_{11} = -R^U_{11} - A^U_{11}\,\bar{R}_{11} - B^U_{11}\,P^L_3(h_N)^{(N)}$$

$$R^*_{12} = -R^U_{12} - A^U_{11}\,\bar{R}_{12} - B^U_{11}\,P^L_4(h_N)^{(N)}$$

$$R^*_{21} = -R^U_{21} - B^U_{11}\,\bar{R}_{11} - D^U_{11}\,P^L_3(h_N)^{(N)}$$

$$R^*_{22} = -R^U_{22} - B^U_{11}\,\bar{R}_{12} - D^U_{11}\,P^L_4(h_N)^{(N)}$$

$$Z^*_{11} = -Z^U_{11} - A^U_{11}\,\bar{Z}_{11} - B^U_{11}\,P^L_7(h_N)^{(N)}$$

$$Z^*_{12} = -Z^U_{12} - A^U_{11}\,\bar{Z}_{12}$$

$$Z^*_{21} = -Z^U_{21} - B^U_{11}\,\bar{Z}_{11} - D^U_{11}\,P^L_7(h_N)^{(N)}$$

$$Z^*_{22} = -Z^U_{22} - B^U_{11}\,\bar{Z}_{12}$$

The governing differential equation (75) remains unchanged but the modified definitions for R^*_{ij} and Z^*_{ij} must be used to determine the coefficients C_1 through C_4. The solution is then again given by equation (80).

Equations (90) and (109) represent the slope at the reference surface for the single and double lap joint, respectively. The two expressions become identical by setting:

$$\bar{R}_{21} = P^L_3(h_N)^{(N)}$$

$$\bar{R}_{22} = P^L_4(h_N)^{(N)}$$

$$\bar{Z}_{22} = P^L_7(h_N)^{(N)}$$

$$\bar{Z}_{21} = A_{10} = A'_{11} = 0$$

for the double lap joint. Similarly, by letting:

$$\frac{1}{A_{11}}\left(N_x + N'_{xu} + N'_{xl}\right) = A_9 \qquad (111)$$

in equation (110), the expression for the strain ϵ_x^o becomes identical to that given by (83) for the single lap joint. The correctness of (111) can easily be verified by substituting $A_{10} = 0$ in the seventh of equations (95). Since equation (66) is not applicable and the condition of zero slope at the ends of the joint (point A) is satisfied automatically, the last two of equations (95) are discarded for the double lap joint. By dropping the last two columns of the coefficient matrix [H] (those corresponding to A_{10} and A_{11}') a system of ten equations with ten unknowns remains; the solution of which is given by (97).

4.4 Numerical Results

A number of runs were made with the computer program BONJO I in order to verify the numerical results and to study the effect of certain parameters. No experimental data could be found that provided information with regard to the stress distributions within a joint as virtually all such data deals with overall joint strength or average shear stresses. Comparisons were made, however, with the Goland-Reissner analysis and with finite element analyses performed at Lockheed. The results are presented and discussed below.

4.4.1 Adhesive Shear and Normal Stresses

Adhesive shear and normal stresses were calculated for a single lap joint with aluminum adherends, using the Goland-Reissner procedure for joints with relatively inflexible cement layers as reported in reference 1. The same joint was then analyzed in detail with BONJO I (symmetrical version) in order to make a direct comparison between the two procedures and study the effects of transverse shear and normal stresses in the adherends on the adhesive stress distributions. These effects are ignored in reference 1. Curves (1) and (2) in Figures 4 and 5 show a direct comparison of the adhesive shear and normal stresses between the Goland-Reissner procedure and BONJO I.

It can be seen from Figure 4 that the peak shear stresses do not occur at the ends of the joint and that the magnitude of these stresses is considerably lower than those calculated with the Goland-Reissner approach. This is attributed to the fact that the transverse shear

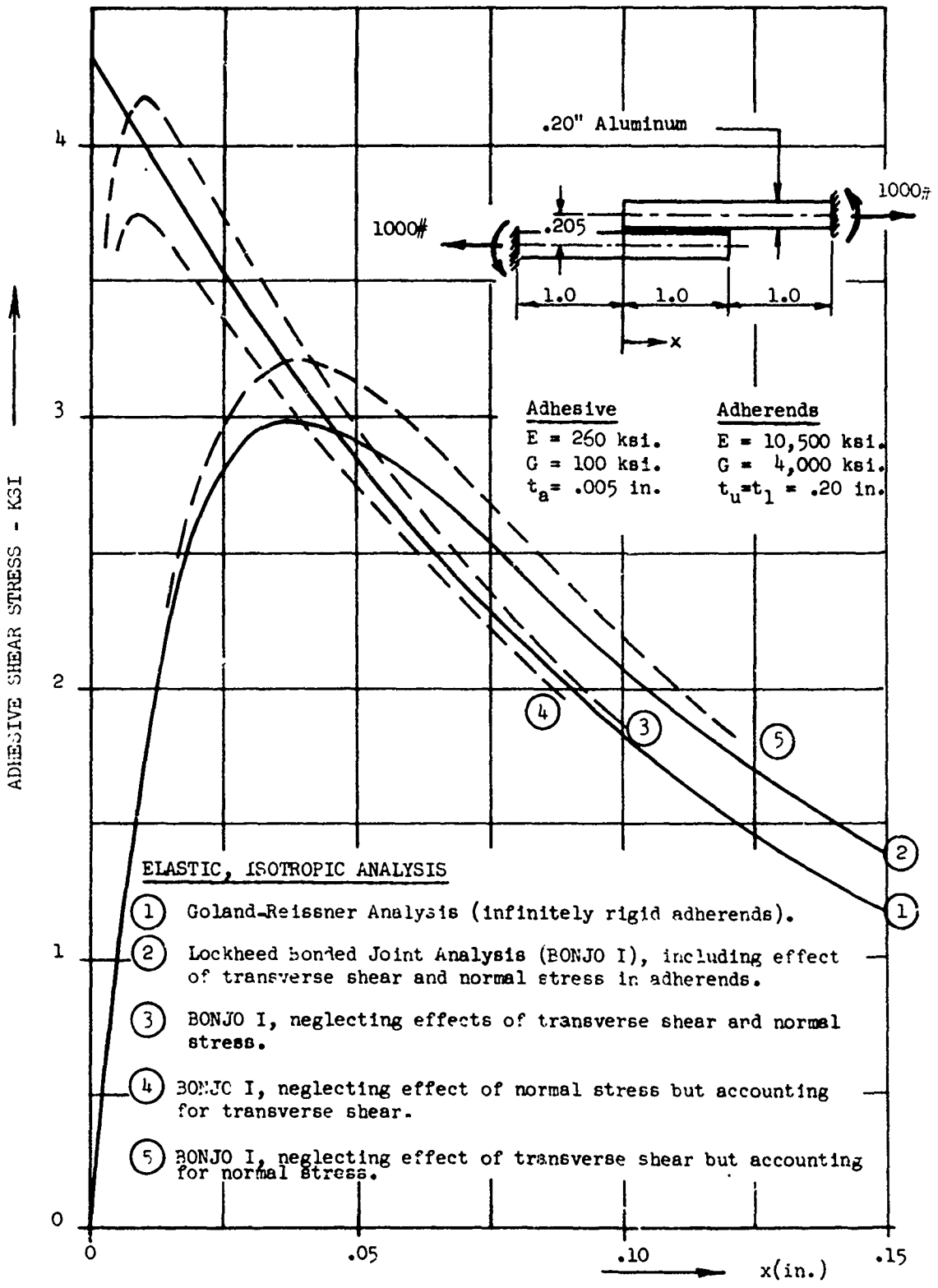

FIGURE 4 ADHESIVE SHEAR STRESS DISTRIBUTION IN SINGLE LAP JOINT, COMPARISON WITH GOLAND-REISSNER ANALYSIS

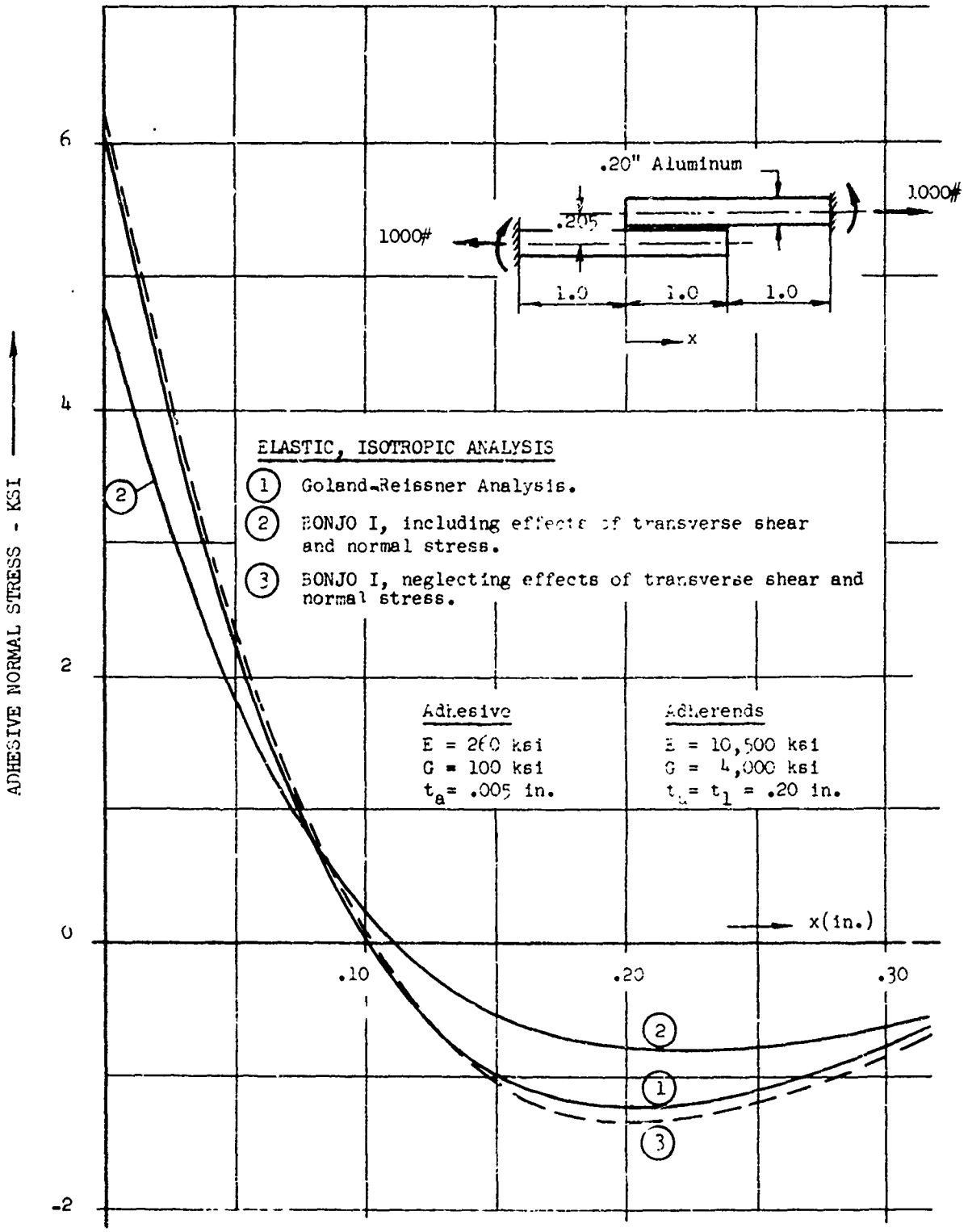

FIGURE 5 ADHESIVE NORMAL STRESS DISTRIBUTION IN SINGLE LAP JOINT, COMPARISON WITH GOLAND-REISSNER ANALYSIS

moduli as well as the elastic moduli through the thickness of the joint have finite values in the Lockheed analysis. Curve (3) shows the adhesive shear stresses obtained with BONJO I if both the transverse shear modulus and the modulus of elasticity of the adherends in the direction normal to the plane of the joint are made very large and it is shown that the stresses in this case agree much closer with those of reference 1. Curve (4) represents the case when only the effect of transverse shear is accounted for, while curve (5) takes only the normal stress into account. A somewhat surprising result is that the larger part of the difference between the two procedures lies in the fact that, in the Goland-Reissner analysis, the adherends are assumed to be incompressible in the direction normal to the plane of the joint. A comparison between the two methods with regard to the adhesive normal stresses (peel stresses) is shown in Figure 5. Again, most of the difference is caused by assuming that the adherends are incompressible normal to the plane of loading.

The effects of transverse shear and normal stresses in the adherends on the adhesive shear stresses have also been investigated for an aluminum double lap joint. The joint was first analyzed by using the actual isotropic material properties of aluminum. The resulting shear stresses are shown in Curves (2) of Figures 6 and 7. These curves therefore represent the actual shear stresses for the joint under consideration. In order to determine the effect of transverse shear, the same joint was analyzed again after arbitrarily decreasing and increasing the transverse shear modulus G' by a factor of 10. This is shown in Figure 6 by Curves (1) and (3), respectively. No appreciable change in shear stresses resulted when the modulus was increased but when the modulus was decreased from 4.0×10^6 to 4.0×10^5 psi the peak shear stresses were reduced significantly. The effect of the normal stresses in the adherends on the adhesive shear stresses was determined in the same manner and the results are shown in Figure 7.

The effect of using finite values for the transverse shear and normal stiffnesses in the adherends on the adhesive shear stress distribution in a composite double lap joint is shown in Figure 8. In this case BONJO I is compared with the modified Goland-Reissner method described in Chapter 2.0. The magnitude of the peak shear stresses computed with the latter method was more than 50 percent greater than those calculated with BONJO I.

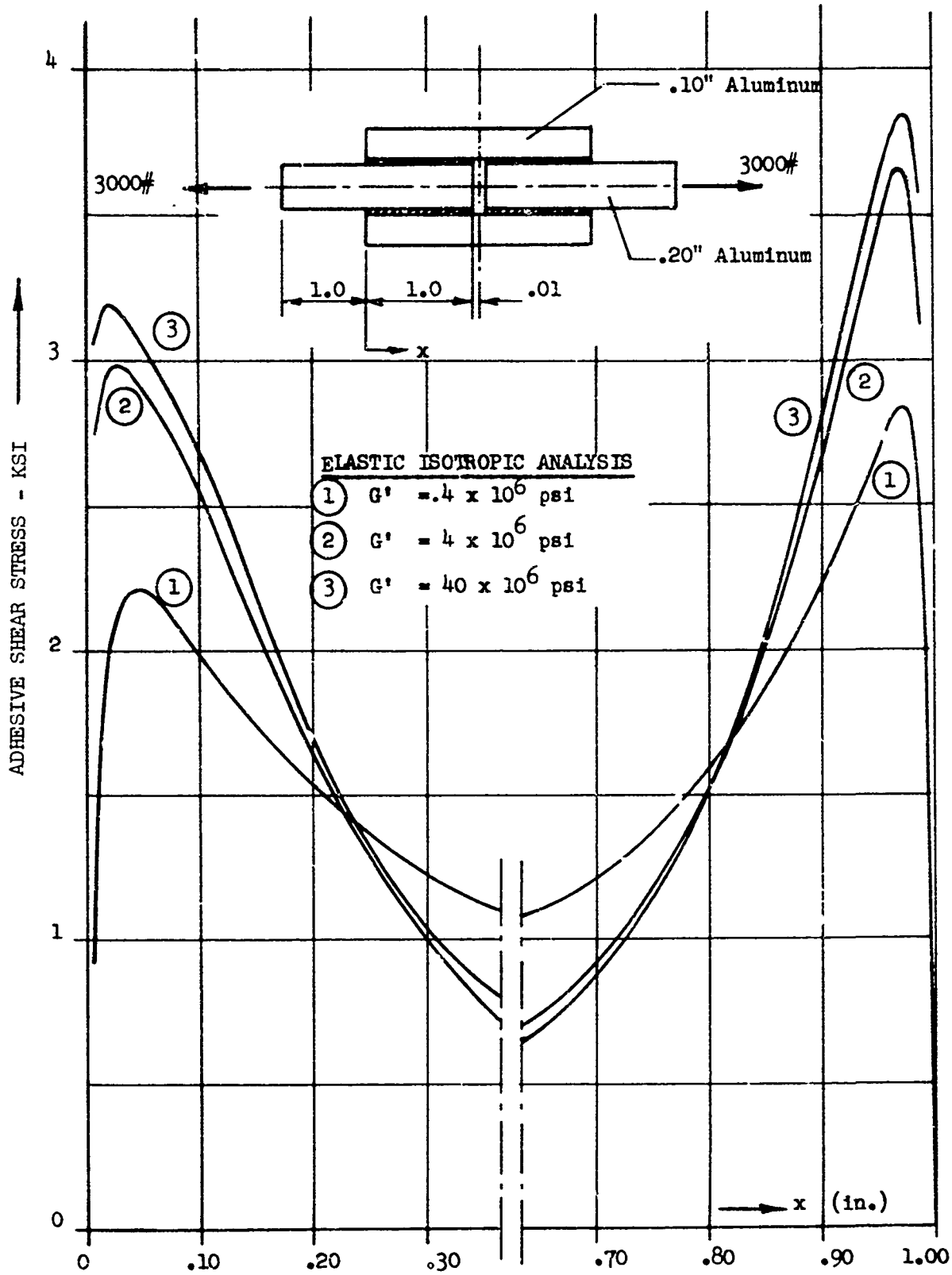

FIGURE 6 ADHESIVE SHEAR STRESS DISTRIBUTION IN DOUBLE LAP JOINT, EFFECT OF TRANSVERSE SHEAR MODULUS

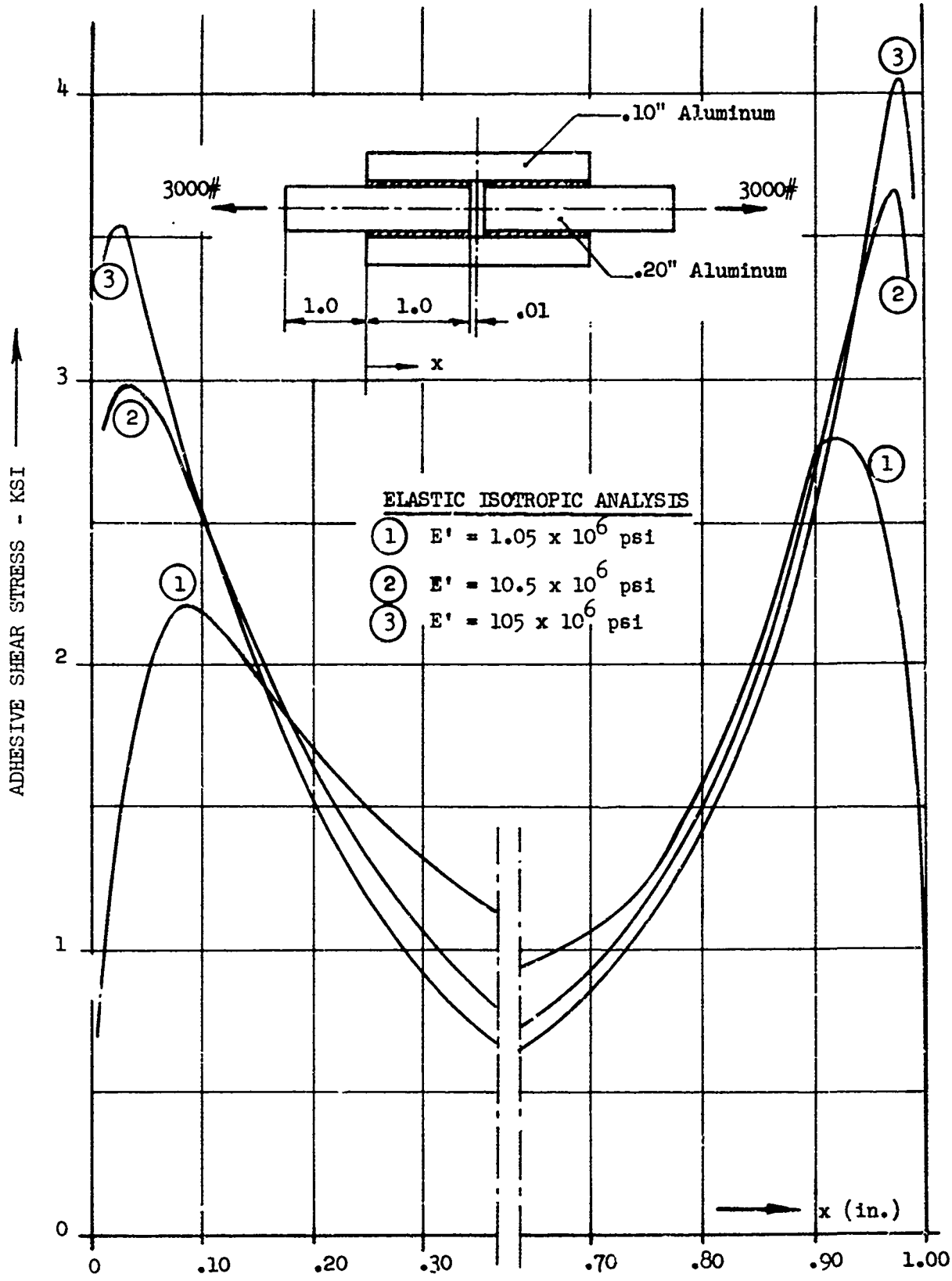

FIGURE 7 ADHESIVE SHEAR STRESS DISTRIBUTION IN DOUBLE LAP JOINT-
EFFECT OF MODULUS OF ELASTICITY NORMAL TO PLANE OF JOINT

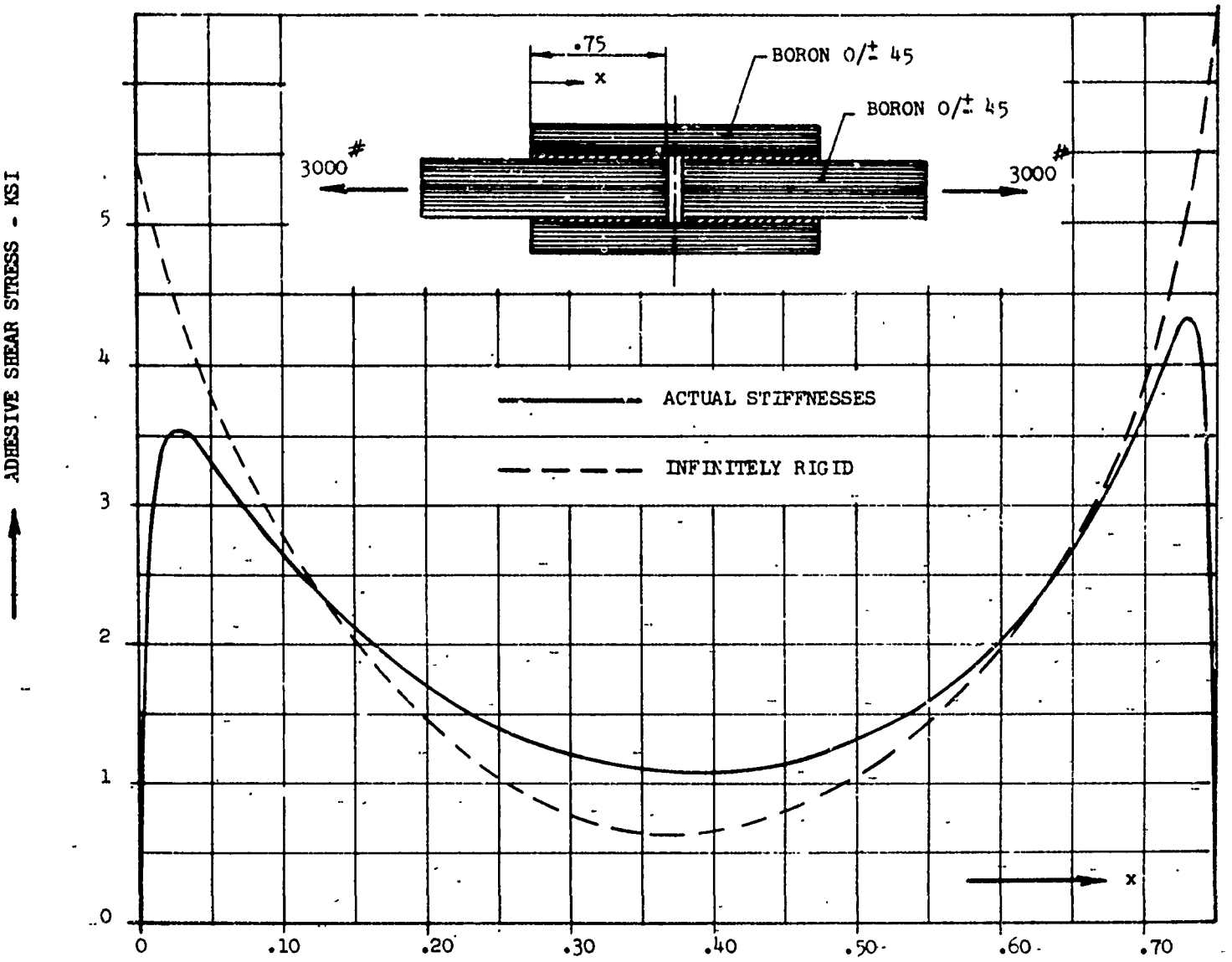

FIGURE 8 EFFECT OF TRANSVERSE SHEAR AND NORMAL STRESS-COMPOSITE DOUBLE LAP JOINT

These results substantiate the statement made earlier that an analysis based on the Kirchhoff assumptions could lead to unacceptable errors.

The presence of residual thermal stresses may become important in the analysis of composite joints. These stresses are caused by bonding at elevated temperature and subsequent cooling to operating temperature. The adhesive shear and normal stresses in a boron/aluminum double lap joint caused by a temperature differential of $-175^{\circ}F$ is shown in Figure 9. Since the thermal shear stresses are positive on one side of the joint and negative on the other, they will usually cause an increase of the maximum adhesive shear stress in a loaded joint. This is illustrated in Figure 10, which shows the joint subjected to a load of 2250 lbs. The adhesive shear stresses due this load are compared with those resulting from the same load plus a temperature differential of $-175^{\circ}F$. The maximum adhesive shear stress was increased from 3550 to 5400 psi as a result of thermal effects.

Comparisons with finite element analyses (FAMAS*) were made for a few lap joint configurations and good agreement with BONJO I was obtained in all cases. One of these cases will be presented here. The joint configuration and the material properties used are given in Figure 11. The joint was modeled with triangular anisotropic constant stress elements in the x-z plane as shown in Figure 12. Element stiffness properties corresponding to a plane stress condition ($\sigma_y = \sigma_{xy} = \sigma_{yz} = 0$) were used in the program. A comparison of the adhesive shear and normal stresses obtained with the two methods is given in Figure 13. Agreement between the two procedures was extremely good except in the immediate vicinity of the joint edges where, as expected, it was not possible to approach a zero shear stress condition with the finite element analysis.

4.4.2 Adherend Stresses

Axial stresses in the boron laminate and the titanium splice plate for the joint configuration shown in Figure 11 were calculated with BONJO I and FAMAS for the purpose of comparing results. The titanium was divided into four equal slices and the stresses were

---

*Flutter And Matrix Algebra System; Lockheed developed analysis programs.

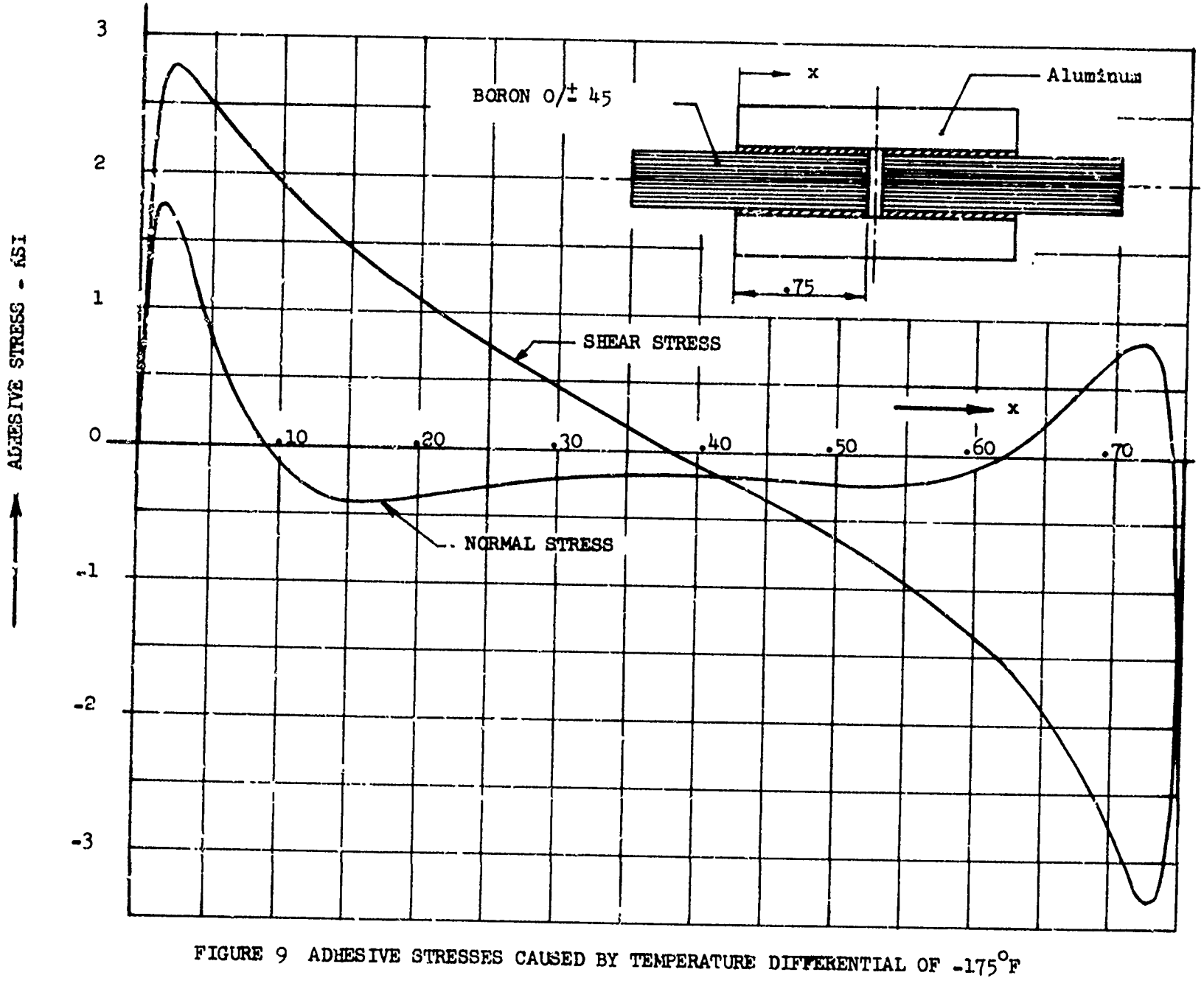

FIGURE 9 ADHESIVE STRESSES CAUSED BY TEMPERATURE DIFFERENTIAL OF -175°F

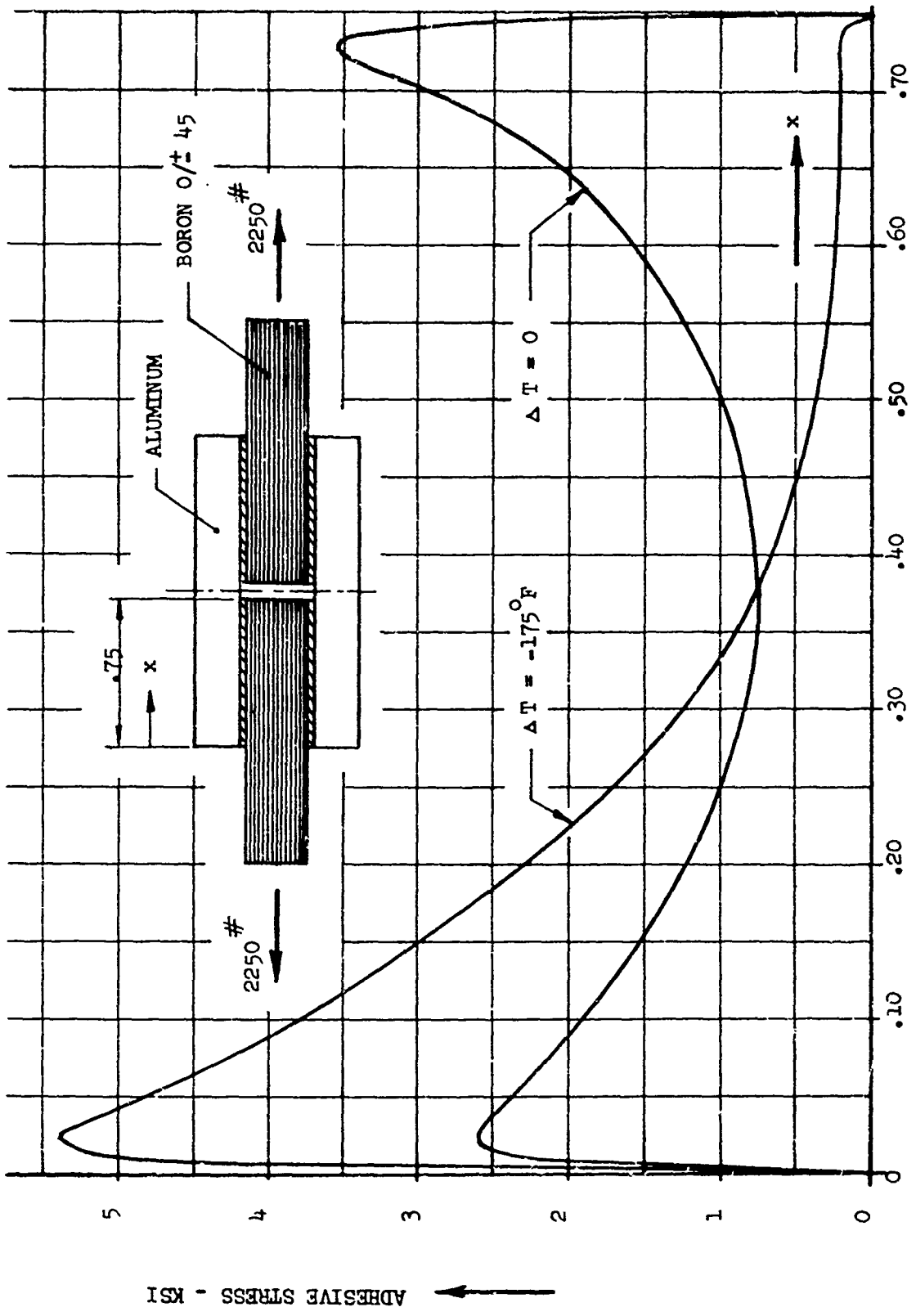

FIGURE 10 EFFECT OF TEMPERATURE DIFFERENTIAL

BORON PROPERTIES:

$E_1 = 3.16 \times 10^7$ psi

$E_2 = E_3 = 3.13 \times 10^6$ psi

$G_{12} = G_{13} = 6.50 \times 10^5$ psi

$G_{23} = 4.20 \times 10^5$ psi

$\nu_{12} = \nu_{13} = 0.21$

$\nu_{23} = 0.021$

TITANIUM PROPERTIES

$E = 1.6 \times 10^7$ psi

$G = 6.2 \times 10^6$ psi

$\nu = 0.29$

ADHESIVE PROPERTIES

$E = 2.6 \times 10^5$ psi

$G = 1.0 \times 10^5$ psi

$\nu = 0.30$

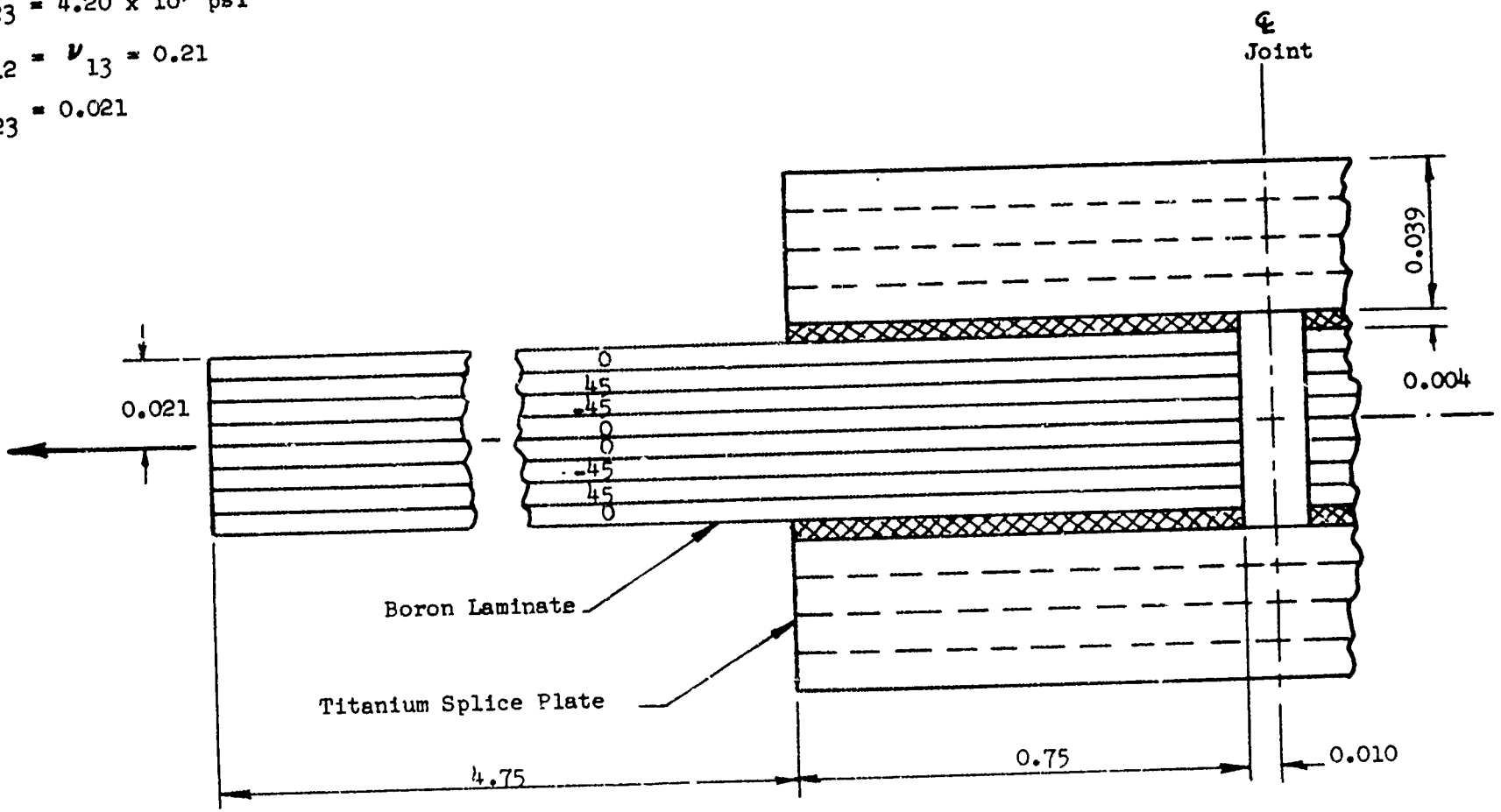

FIGURE 11 COMPOSITE DOUBLE LAP JOINT

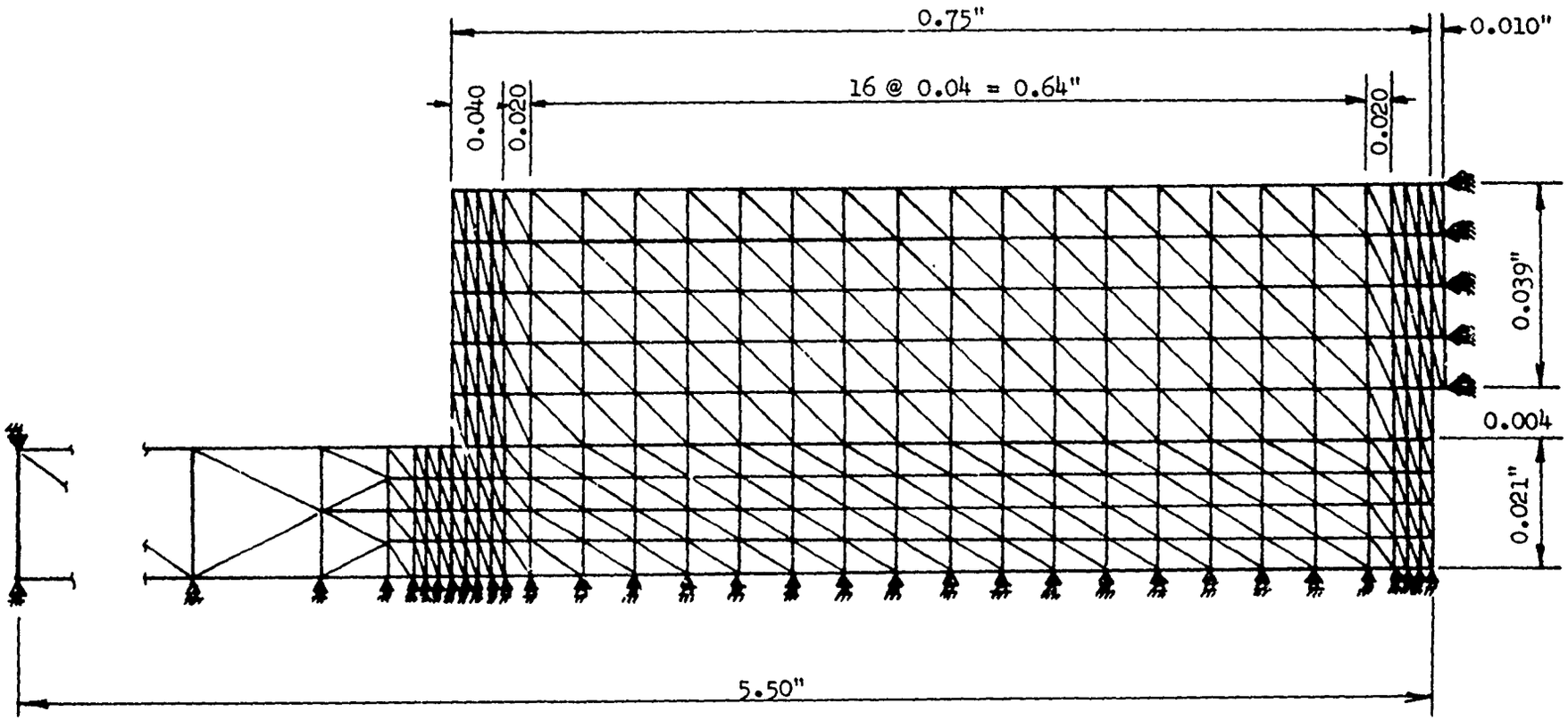

FIGURE 12 FINITE ELEMENT MODEL - DOUBLE LAP JOINT

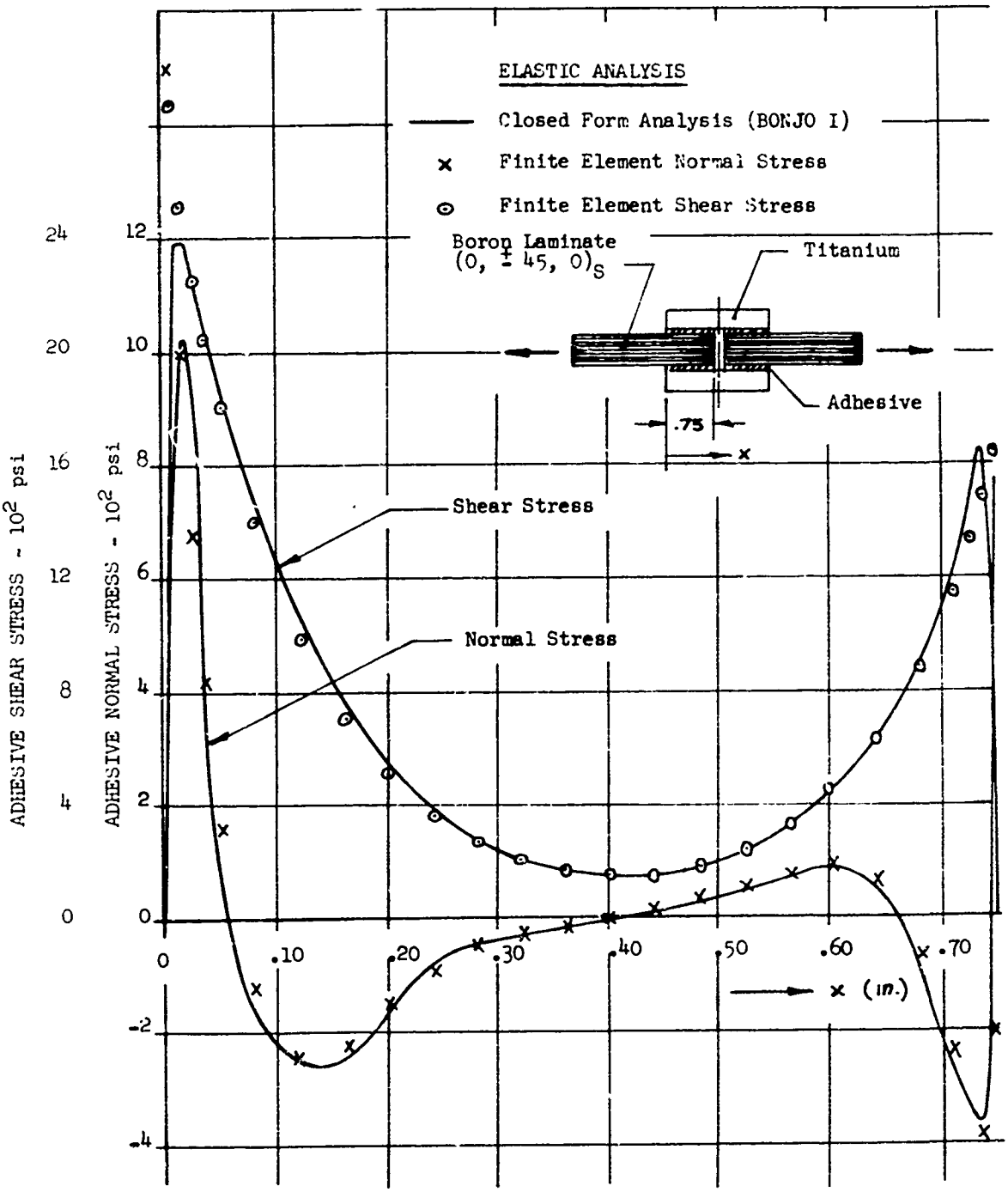

FIGURE 13 SHEAR AND NORMAL STRESS DISTRIBUTION AT CENTER LINE OF ADHESIVE IN COMPOSITE DOUBLE LAP JOINT

calculated at the five locations shown in Figure 14. Finite element results are shown at the outer surface, the midsurface and at the titanium/adhesive interface. The stresses across the thickness of the splice plate are essentially uniform for a large portion of the joint. In areas of appreciable bending BONJO I shows generally higher gradients than FAMAS, but it appears that this is a result of the fact that the FAMAS model was not detailed enough in these areas. Axial stresses in the boron laminate were calculated and plotted in Figure 15 for the three locations shown. Good agreement with the finite element analysis was obtained. Finally Figure 16 shows a plot of the transverse shear stress and normal stress at the joint cross section x = 0.025" which is near the point of maximum adhesive shear stress. Finite element results are not shown here but agreement with FAMAS results was excellent.

4.5 Joints with Non-Linear Adhesive Stress-Strain Behavior

4.5.1 General

A major drawback of the method of analysis described in Sections 4.2 and 4.3 is the fact that it is based on the assumption that all stresses in the joint remain in the elastic range. This assumption may usually be justified with regard to the stresses in the adherend materials, but the joint configuration is generally such that the adhesive stresses will reach the proportional limit of the material at an early stage of loading. For this reason it became necessary to extend the linear analysis, to permit non-linear stress-strain behavior in the adhesive material. Several iterative type methods were investigated to solve this complex problem. Some of these are discussed below.

4.5.2 Secant Modulus Approach

The portion of the joint defined by $0 \leq x \leq L$ (see Figure 1) was divided into regions and secant moduli were calculated for the adhesive material based on the average stresses in each region. These secant moduli were then used in place of the elastic moduli of the adhesive to obtain the coefficients of the governing differential equations for each region. Conditions of continuity and compatibility were satisfied between adjacent regions, which together with the boundary conditions at the ends of the joint were necessary to obtain a solution. This procedure was used to establish basic joint design parameters early in the

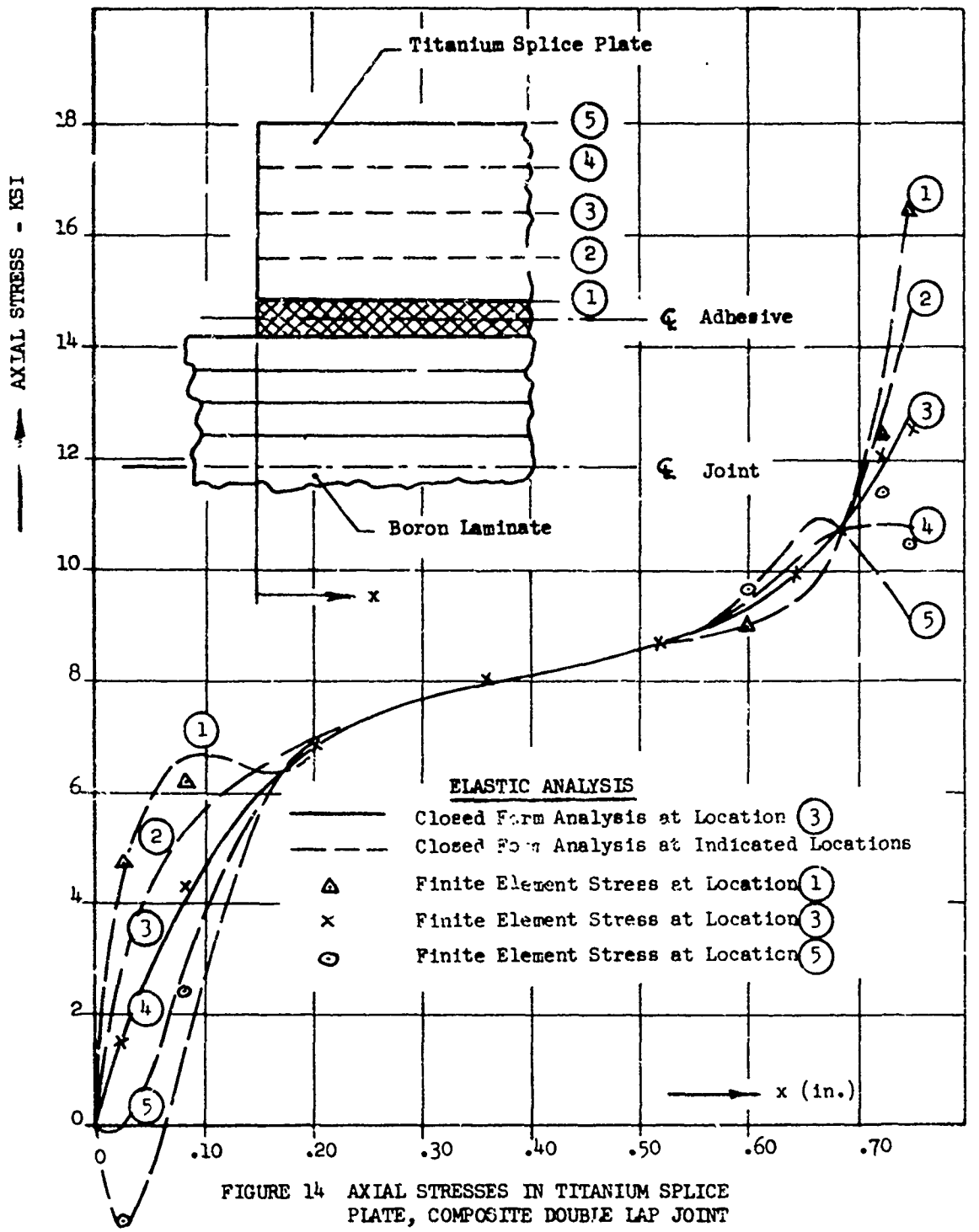

FIGURE 14 AXIAL STRESSES IN TITANIUM SPLICE PLATE, COMPOSITE DOUBLE LAP JOINT

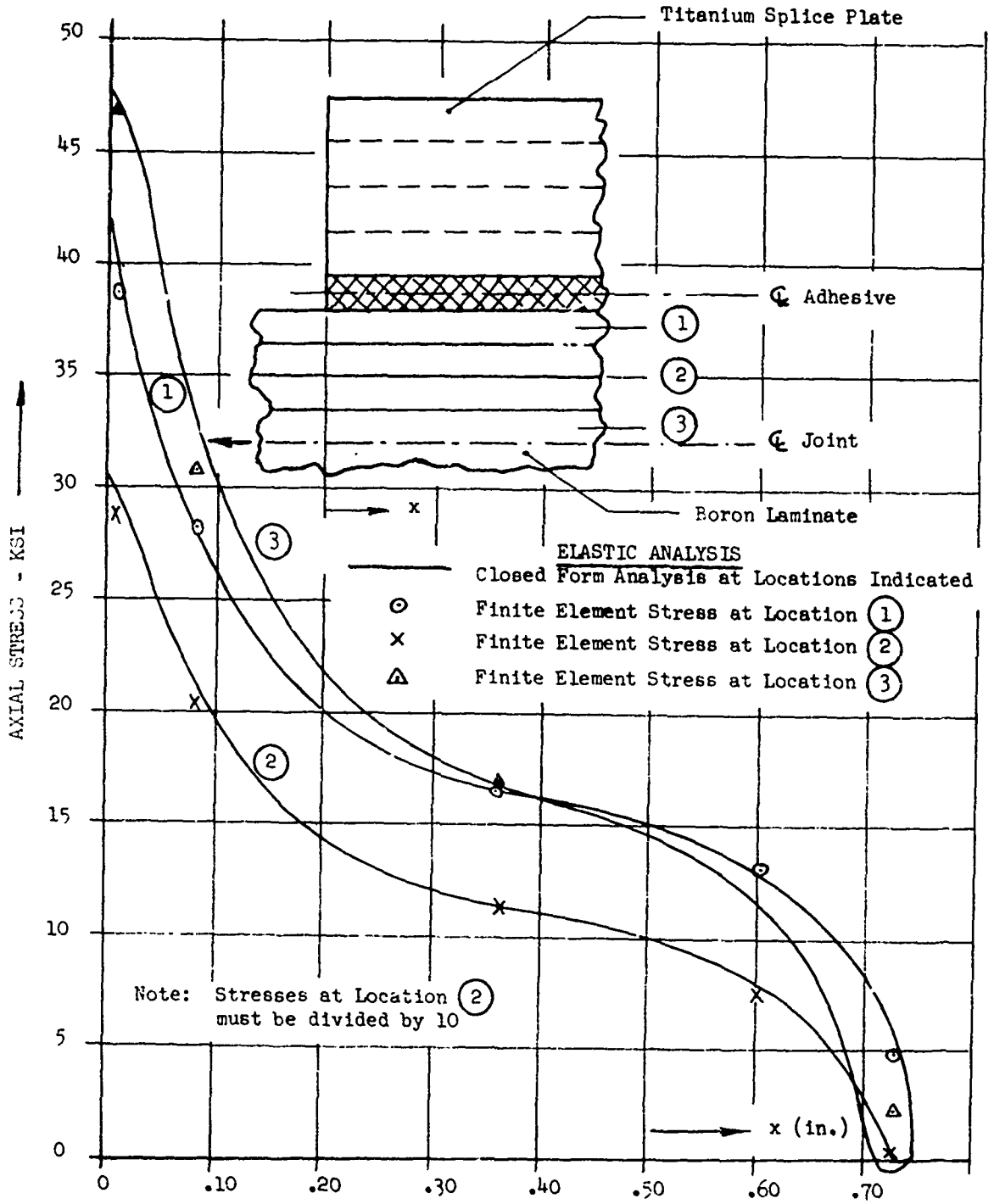

FIGURE 15 AXIAL STRESSES IN BORON LAMINATE, COMPOSITE DOUBLE LAP JOINT

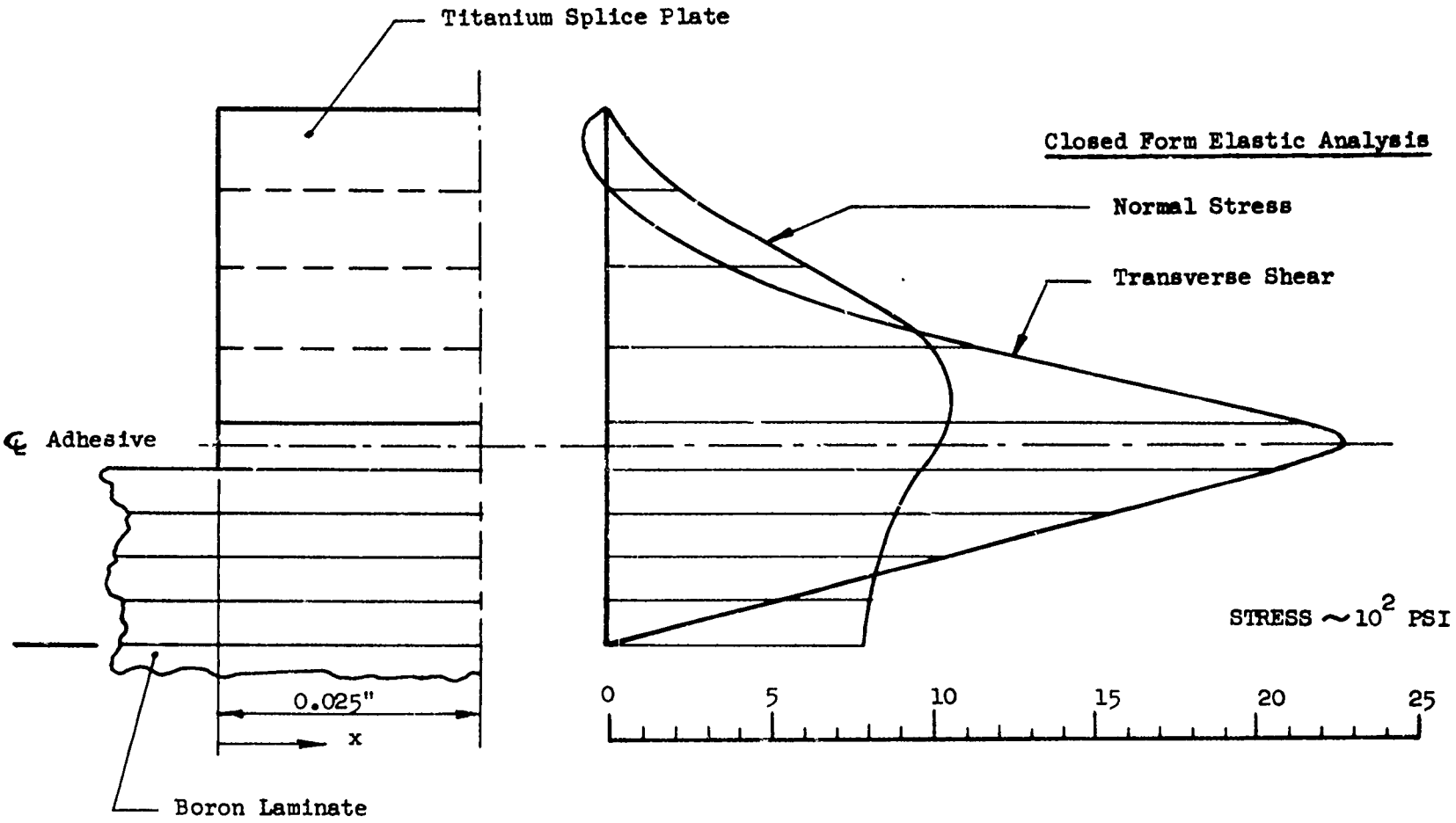

FIGURE 16 TRANSVERSE SHEAR AND NORMAL STRESS AT x = 0.025", COMPOSITE DOUBLE LAP JOINT

program but it turned out to be unsatisfactory for joints in which a relatively large portion of the bond layer is in the plastic range. Computational difficulties arise when matching boundary conditions between adjacent regions because of the discontinuous nature of the analysis. For this reason development work using this approach was discontinued.

4.5.3 Analysis Based on Deformation Theory of Plasticity

The theoretical work for this procedure has been completed and is described below.

Assuming that the only non-zero stresses in the adhesive are the shear stress, σ^o_{xz}, and the normal stress, σ^o_z, one may write the stress-strain relations in the adhesive as:

$$\begin{aligned} \epsilon_x &= -\frac{\nu}{E}\sigma^o_z + \epsilon_{xp} \\ \epsilon_y &= -\frac{\nu}{E}\sigma^o_z + \epsilon_{yp} \\ \epsilon_z &= \frac{1}{E}\sigma^o_z + \epsilon_{zp} \\ \epsilon_{xz} &= \frac{\sigma^o_{xz}}{G} + \epsilon_{xzp} \end{aligned} \tag{112}$$

where ϵ_{xp}, ϵ_{yp}, ϵ_{zp}, and ϵ_{xzp} are the plastic strain components. The equivalent stress, equivalent total strain and total plastic strain are defined by the expressions:

$$\begin{aligned} \bar{\sigma} &= \sqrt{\sigma_z^{o\,2} + 3\sigma_{xz}^{o\,2}} \\ \bar{\epsilon} &= \frac{1}{3}\sqrt{2\left[(\epsilon_x - \epsilon_y)^2 + (\epsilon_y - \epsilon_z)^2 + (\epsilon_x - \epsilon_z)^2 + \frac{3}{2}\epsilon_{xz}^2\right]} \\ \bar{\epsilon}_p &= \frac{1}{3}\sqrt{2\left[(\epsilon_{xp} - \epsilon_{yp})^2 + (\epsilon_{yp} - \epsilon_{zp})^2 + (\epsilon_{xp} - \epsilon_{zp})^2 + \frac{3}{2}\epsilon_{xzp}^2\right]} \end{aligned} \tag{113}$$

which are related by the equation:

$$\bar{\epsilon} = \frac{2(1+\nu)}{3}\frac{\bar{\sigma}}{E} + \bar{\epsilon}_p = \frac{\bar{\sigma}}{3G} + \bar{\epsilon}_p \tag{114}$$

With the assumption that the volume remains constant in the plastic range one obtains:

$$\bar{\epsilon}_p = 2\sqrt{\frac{1}{3}\left[\epsilon_{xp}^2 + \epsilon_{zp}^2 - \frac{1}{3}\epsilon_{xp}\epsilon_{zp} + \frac{1}{4}\epsilon_{xzp}^2\right]} \tag{115}$$

It can be shown that the individual plastic strain components are given by:

$$\begin{aligned}
\epsilon_{xp} &= -\frac{\bar{\epsilon}_p}{2\bar{\sigma}}\sigma_z^o \\
\epsilon_{zp} &= \frac{\bar{\epsilon}_p}{\bar{\sigma}}\sigma_z^o \\
\epsilon_{xzp} &= \frac{3\bar{\epsilon}_p}{\bar{\sigma}}\sigma_{xz}^o
\end{aligned} \tag{116}$$

By using a Ramberg-Osgood representation of the stress-strain curve in the yield region one has

$$\frac{\bar{\epsilon}_p}{\bar{\sigma}} = \frac{1}{7G}\left(\frac{\bar{\sigma}}{\sigma_{0.7}}\right)^{n-1} \tag{117}$$

and since n and $\sigma_{0.7}$ are constants for a given material, the plastic strain components (116) may be determined if the stresses σ_z^o and σ_{xz}^o are known.

If in the linear analysis procedure, the elastic stress-strain relations are replaced by equations (112) and if the plastic strains are assumed constant through the thickness of the adhesive, the two governing differential equations are no longer homogeneous but in the form:

$$\begin{aligned}
&\sigma_{xz}^o + R_{11}^* \sigma_{xz,xx}^o + R_{12}^* \sigma_{xz,xxxx}^o + Z_{11}^* V_{xu,xx} + Z_{12}^* V_{xu,xxxx} = \\
&\qquad \eta_1 \epsilon_{xzp,xx} - \eta_2 \epsilon_{zp,xxx} \\
&R_{21}^* \sigma_{xz,xx}^o + R_{22}^* \sigma_{xz,xxxx}^o + V_{xu} + Z_{21}^* V_{xu,xx} + Z_{22}^* V_{xu,xxxx} = \\
&\qquad \eta_3 \epsilon_{xzp,xx} - \eta_4 \epsilon_{zp,xxx}
\end{aligned} \tag{118}$$

where

$$\eta_1 = \frac{1}{2} t_a \left[A_{11}^u (1 + \Delta a_1) + B_{11}^u \Delta a_2 \right]$$

$$\eta_2 = \frac{1}{2} t_a \left[A_{11}^u \Delta b_1 + B_{11}^u (1 + \Delta b_2) \right]$$

$$\eta_3 = \frac{1}{2} t_a \left[B_{11}^u (1 + \Delta a_1) + D_{11}^u \Delta a_2 \right]$$

$$\eta_4 = \frac{1}{2} t_a \left[B_{11}^u \Delta b_1 + D_{11}^u (1 + \Delta b_2) \right]$$

$$\Delta a_1 = \frac{1}{\bar{D}_{11} A_{11}} \left[B_{11} (B_{11}^u - B_{11}^L) - D_{11} (A_{11}^u - A_{11}^L) \right]$$

$$\Delta a_2 = \frac{1}{\bar{D}_{11} A_{11}} \left[B_{11} (A_{11}^u - A_{11}^L) - A_{11} (B_{11}^u - B_{11}^L) \right]$$

$$\Delta b_1 = \frac{1}{\bar{D}_{11} A_{11}} \left[B_{11} (D_{11}^u - D_{11}^L) - D_{11} (B_{11}^u - B_{11}^L) \right]$$

$$\Delta b_2 = \frac{1}{\bar{D}_{11} A_{11}} \left[B_{11} (B_{11}^u - B_{11}^L) - A_{11} (D_{11}^u - D_{11}^L) \right]$$

As was done in the linear procedure, the two differential equations (118) may be combined into a single eighth order differential equation:

$$C_1 \sigma^o_{xz,xxxxxxxx} + C_2 \sigma^o_{xz,xxxxxx} + C_3 \sigma^o_{xz,xxxx} + C_4 \sigma^o_{xz,xx} + \sigma^o_{xz} = \sum_{i=2}^{7} \frac{d^i \bar{P}_i}{dx^i} \tag{119}$$

where

$$\bar{P}_2 = \eta_1 \epsilon_{xzp}$$

$$\bar{P}_3 = -\eta_2 \epsilon_{zp}$$

$$\bar{P}_4 = (Z^*_{21} \eta_1 - Z^*_{11} \eta_3) \epsilon_{xzp}$$

$$\bar{P}_5 = -(Z^*_{21} \eta_2 - Z^*_{11} \eta_4) \epsilon_{zp}$$

$$\bar{P}_6 = (Z^*_{22}\eta_1 - Z^*_{12}\eta_3)\epsilon_{xzp}$$

$$\bar{P}_7 = -(Z^*_{22}\eta_2 - Z^*_{12}\eta_4)\epsilon_{zp}$$

In deriving the differential equation (119), the following expression was obtained for the transverse shear force in place of (74)

$$V_{xu} = t_5\sigma^o_{xz} + t_6\sigma^o_{xz,xx} + t_7\sigma^o_{xz,xxxx} + t_8\sigma_{xz,xxxxx}$$

$$\eta_5\epsilon_{xzp,xx} + \eta_6\epsilon_{zp,xxx} + \eta_7\epsilon_{xzp,xxxx} + \eta_8\epsilon_{zp,xxxxx} \qquad (120)$$

where

$$\eta_5 = -\frac{s_3}{s_4}\eta_1 + \eta_3$$

$$\eta_6 = \frac{s_3}{s_4}\eta_2 - \eta_4$$

$$\eta_7 = -\frac{1}{s_4}(\eta_1 Z^*_{22} - \eta_3 Z^*_{12})$$

$$\eta_8 = \frac{1}{s_4}(\eta_2 Z^*_{22} - \eta_4 Z^*_{12})$$

and s_3 and s_4 are as defined in Section 4.2.4.

Since a direct solution of equations (120) is not possible, an iterative procedure must be used so that the plastic strains and their derivatives will be treated not as unknowns, but as known quantities obtained from the previous iteration. Attempts to represent the plastic strains by continuous functions such as truncated Fourier series or power series were unsuccessful because of the extremely high gradients that exist near the edges of the joint. Other possibilities were investigated, the most promising of which appeared to be the use of Green's functions coupled with a numerical integration procedure. Using the latter approach, one may write the solution of the differential equation (119) in the form:

$$\sigma^o_{xz} = \sum_{i=1}^{8} A_i\varphi_i(x) + \int_o^x \sum_{i=2}^{7} \bar{P}_i(\xi)\frac{d^iG(x-\xi)}{dx^i}\,d\xi \qquad (121)$$

where $G(x-\xi)$ is the Green's function ot the differential operator:

$$L(\cdot) = C_1 \frac{d^8}{dx^8} + C_2 \frac{d^6}{dx^6} + C_3 \frac{d^4}{dx^4} + C_4 \frac{d^2}{dx^2} + 1$$

The first summation in equation (121) represents the elastic solution to the problem. The form of the Green's function is dependent on the type of roots resulting from the linear solution. In general, one has:

$$G(x-\xi) = \sum_{n=1}^{4} K_n \varphi_n^*(x-\xi) \tag{122}$$

in which each of the functions φ_n^* has one of the following forms:

1) $\sinh\alpha(x-\xi)$

2) $\sin\alpha(x-\xi)$

3) $\sinh\alpha(x-\xi)\cos\beta(x-\xi)$

4) $\cosh\alpha(x-\xi)\sin\beta(x-\xi)$

corresponding to a real positive, a real negative, and a pair of complex conjugate (or imaginary) roots of equations (78), respectively. For convenience it will be assumed that the Green's function contains one of each of these forms, hence:

$$G(x-\xi) = K_1 \sinh\alpha_1(x-\xi) + K_2 \sin\beta_3(x-\xi) + K_3 \sinh\alpha_5(x-\xi)\cos\beta_5(x-\xi) + K_4 \cosh\alpha_5(x-\xi)\sin\beta_5(x-\xi) \tag{123}$$

The constants K_n are determined from the conditions:

$$\frac{dG(0)}{dx} = \frac{d^3G(0)}{dx^3} = \frac{d^5G(0)}{dx^5} = 0$$

$$\frac{d^7G(0)}{dx^7} = \frac{1}{C_1} \tag{124}$$

Higher derivatives of the Green's function are given by:

$$\frac{d^n G(x-\xi)}{dx^n} = K_1 \alpha_1^n \cosh\alpha_1(x-\xi) + (-1)^{\frac{n-1}{2}} K_2 \beta_3^n \cos\beta_3(x-\xi)$$
$$+ (a_n K_3 + b_n K_4) \cosh\alpha_5(x-\xi) \cos\beta_5(x-\xi)$$
$$+ (a_n K_4 - b_n K_3) \sinh\alpha_5(x-\xi) \sin\beta_5(x-\xi)$$

$$\frac{d^m G(x-\xi)}{dx^m} = K_1 \alpha_1^m \sinh\alpha_1(x-\xi) + (-1)^{\frac{m}{2}} K_2 \beta_3^m \sin\beta_3(x-\xi) \qquad (125)$$
$$+ (a_m K_3 + b_m K_4) \cosh\alpha_5(x-\xi) \sin\beta_5(x-\xi)$$
$$+ (b_m K_3 - a_m K_4) \sinh\alpha_5(x-\xi) \cos\beta_5(x-\xi)$$

where m is an even and n is an odd number, and:

$$a_o = 0$$

$$a_n = \beta_5 a_{n-1} + \alpha_5 b_{n-1}$$

$$a_m = -(\beta_5 a_{m-1} + \alpha_5 b_{m-1})$$

$$b_o = 1$$

$$b_n = \beta_5 b_{n-1} - \alpha_5 a_{n-1}$$

$$b_m = \alpha_5 a_{m-1} - \beta_5 b_{m-1}$$

Equations (125) may be written in alternate form:

$$\frac{d^n G(x-\xi)}{dx^n} = g_{1n}(\xi) e^{\alpha_5 x} \cos\beta_5 x + g_{2n}(\xi) e^{\alpha_5 x} \sin\beta_5 x$$
$$+ g_{3n}(\xi) e^{-\alpha_5 x} \cos\beta_5 x + g_{4n}(\xi) e^{-\alpha_5 x} \sin\beta_5 x$$
$$+ g_{5n}(\xi) \cos\beta_3 x + g_{6n}(\xi) \sin\beta_3 x$$
$$+ g_{7n}(\xi) e^{\alpha_1 x} + g_{8n}(\xi) e^{-\alpha_1 x} =$$
$$\sum_{i=1}^{8} g_{in}(\xi) \varphi_i(x) \qquad (126)$$

and similarly:

$$\frac{d^m G(x-\xi)}{dx^m} = \sum_{i=1}^{8} g_{im}(\xi)\varphi_i(x)$$

where:

$$g_{1n}(\xi) = e^{-\alpha_5\xi}(\bar{K}_1 \cos\beta_5\xi - \bar{K}_2 \sin\beta_5\xi)$$

$$g_{2n}(\xi) = e^{-\alpha_5\xi}(\bar{K}_1 \sin\beta_5\xi + \bar{K}_2 \cos\beta_5\xi)$$

$$g_{3n}(\xi) = e^{\alpha_5\xi}(\bar{K}_1 \cos\beta_5\xi + \bar{K}_2 \sin\beta_5\xi)$$

$$g_{4n}(\xi) = e^{\alpha_5\xi}(\bar{K}_1 \sin\beta_5\xi - \bar{K}_2 \cos\beta_5\xi)$$

$$g_{5n}(\xi) = (-1)^{\frac{n-1}{2}} K_2 \beta_3^n \cos\beta_3\xi$$

$$g_{6n}(\xi) = (-1)^{\frac{n-1}{2}} K_3 \beta_3^n \sin\beta_3\xi$$

$$g_{7n}(\xi) = \frac{1}{2}\alpha_1^n K_1 e^{-\alpha_1\xi}$$

$$g_{8n}(\xi) = \frac{1}{2}\alpha_1^n K_1 e^{\alpha_1\xi}$$

and:

$$g_{1m}(\xi) = e^{-\alpha_5\xi}(-\bar{K}_3 \sin\beta_5\xi - \bar{K}_4 \cos\beta_5\xi)$$

$$g_{2m}(\xi) = e^{-\alpha_5\xi}(\bar{K}_3 \cos\beta_5\xi - \bar{K}_4 \sin\beta_5\xi)$$

$$g_{3m}(\xi) = e^{\alpha_5\xi}(-\bar{K}_3 \sin\beta_5\xi + \bar{K}_4 \cos\beta_5\xi)$$

$$g_{4m}(\xi) = e^{\alpha_5\xi}(\bar{K}_3 \cos\beta_5\xi + \bar{K}_4 \sin\beta_5\xi)$$

$$g_{5m}(\xi) = -(-1)^{\frac{m}{2}} K_2 \beta_3^m \sin\beta_3\xi$$

$$g_{6m}(\xi) = (-1)^{\frac{m}{2}} K_2 \beta_3^m \cos\beta_3\xi$$

$$g_{7m}(\xi) = \frac{1}{2}\alpha_1^m K_1 e^{-\alpha_1\xi}$$

$$g_{8m}(\xi) = -\frac{1}{2}\alpha_1^m K_1 e^{\alpha_1\xi}$$

$$\bar{K}_1 = \frac{1}{2}(a_n K_3 + b_n K_4)$$

$$\bar{K}_2 = \frac{1}{2}(a_n K_4 - b_n K_3)$$

$$\bar{K}_3 = \frac{1}{2}(a_m K_3 + b_m K_4)$$

$$\bar{K}_4 = \frac{1}{2}(a_m K_4 - b_m K_3)$$

In addition to (124) the following conditions must be satisfied:

$$\frac{d^i}{dx^i} L(G) = 0 \qquad i = 2,3,\ldots \tag{127}$$

where L is the differential operator defined earlier. Equations (127) lead to the expressions:

$$\frac{d^9 G(0)}{dx^9} = -\frac{C_2}{C_1^2}$$

$$\frac{d^{11} G(0)}{dx^{11}} = \frac{1}{C_1^3}(C_2^2 - C_1 C_3) \tag{128}$$

$$\frac{d^{13} G(0)}{dx^{13}} = \frac{1}{C_1^4}(2C_1 C_2 C_3 - C_1^2 C_4 - C_2^3)$$

The solution (121) may be written in the form:

$$\sigma_{xz}^o = \sum_{j=1}^{8} [A_j + \bar{A}_j(x)]\, \varphi_j(x) \tag{129}$$

where:

$$\bar{A}_i(x) = \sum_{k=2}^{7} \int_o^x \bar{P}_k(\xi)\, g_{ik}(\xi)\, d\xi$$

It can be shown that the transverse shear force, V_{xu}, the stress resultant, N_{xu}, and the stress couple, M_{xu}, can be expressed as:

$$V_{xu} = \sum_{i=1}^{8} [A_i + \bar{A}_i(x)]\psi_i(x)$$

$$N_{xu} = \sum_{i=1}^{8} [A_i + \bar{A}_i(x)]\mu_i(x) + A_{11}^u A_9 + B_{11}^u A_{10} - N'_{xu} \qquad (130)$$

$$M_{xu} = \sum_{i=1}^{8} [A_i + \bar{A}_i(x)]\rho_i(x) + B_{11}^u A_9 + D_{11}^u A_{10} - M'_{xu}$$

where the functions $\psi_i(x)$, $\mu_i(x)$, and $\rho_i(x)$ have been defined as part of equations (96).

The average slope of the lower laminate at $x = 0$ and the average slope of the upper laminate at $x = L$ are given by:

$$\bar{w}^o_{,x} = \sum_{i=1}^{8} \left| (P^L_{4AV} - \bar{R}_{22})\varphi_i''(0) + (P^L_{6AV} - \bar{Z}_{22})\psi_i''(0) \right| A_i$$

$$+ A'_{11} + \left\{ \frac{1}{C_1} \left| (\bar{R}_{22} - P^L_{4AV})(Z^*_{22}\eta_2 - Z^*_{12}\eta_4) + \right.\right.$$

$$\left.\left. (P^L_{6AV} - \bar{Z}_{22})(R^*_{22}\eta_2 - R^*_{12}\eta_4) \right| - \frac{1}{2} t_a (1 - \Delta b_2) \right\} \epsilon^o_{zp,x} \qquad (131)$$

$$\bar{w}'^{L}_{,x} = \sum_{j=1}^{8} \left[(P^{U}_{4AV} - \bar{R}_{22})\varphi_i''(L) + (P^{U}_{6AV} - \bar{Z}_{22})\psi_i''(L)\right]\left[A_i + \bar{A}_i(L)\right]$$

$$+ A_{10}L + A'_{11} + \left| \frac{1}{C_1} \left[(\bar{R}_{22} - P^{U}_{4AV})(Z^*_{22}\eta_2 - Z^*_{12}\eta_4)\right.\right.$$

$$\left.\left. + (P^{U}_{6AV} - \bar{Z}_{22})(R^*_{22}\eta_2 - k^*_{12}\eta_4)\right] + \frac{1}{2} t_a(1 + \Delta b_2) \right| \varepsilon^{L}_{zp,x} \qquad (132)$$

where P^{L}_{4AV}, P^{U}_{4AV}, P^{L}_{6AV}, and P^{U}_{6AV} are as given in equation (91). Instead of equation (96) one has for the non-linear problem:

$$[H]\{A^*\} = \{C^*\} + \{\Delta_p\} \qquad (133)$$

which differs from the linear case only in the addition of the column matrix $\{\Delta_p\}$. This matrix contains all the plastic strain terms. The non-zero coefficients of $\{\Delta_p\}$ may be obtained by using equations (129), (130), (131), and (132) in place of the corresponding elastic relations, in the formulation of the boundary conditions. They are given by:

$$\Delta_p(2) = -\sum_{j=1}^{8} \bar{A}_i(L)\varphi_i(L)$$

$$\Delta_p(4) = -\sum_{j=1}^{8} \bar{A}_i(L)\psi_i(L)$$

$$\Delta_p(6) = -\sum_{j=1}^{8} \bar{A}_i(L)\mu_i(L)$$

$$\Delta_p(9) = -\sum_{j=1}^{8} \bar{A}_i(L)\rho_i(L)$$

$$\Delta_p(10) = \sum_{i=1}^{8} \bar{A}_i(L) \left| (\bar{R}_{22} - P^U_{4AV})\varphi_i''(L) + (\bar{Z}_{22} - P^U_{6AV})\psi_i''(L) \right|$$

$$- \left\{ \frac{1}{C_1} \left| (\bar{R}_{22} - P^U_{4AV})(Z^*_{22}\eta_2 - Z^*_{12}\eta_4) - (\bar{Z}_{22} - P^U_{6AV})(R^*_{22}\eta_2 - R^*_{12}\eta_4) \right| \right.$$

$$\left. + \frac{1}{2} t_a (1 + \Delta b_2) \right\} \epsilon^L_{zp,x}$$

$$\Delta_p(11) = - \left\{ \frac{1}{C_1} \left| (\bar{R}_{22} - P^L_{4AV})(Z^*_{22}\eta_2 - Z^*_{12}\eta_4) - (\bar{Z}_{22} - P^L_{6AV})(R^*_{22}\eta_2 - R^*_{12}\eta_4) \right| \right.$$

$$\left. - \frac{1}{2} t_a (1 - \Delta b_2) \right\} \epsilon^o_{zp,x}$$

In order to determine the coefficients, A^*_i, in equations (133), the coefficients, Δ_p, must be known. This in turn requires a knowledge of the plastic strain distributions in the bond-layer. The solution to this problem may be obtained by successive approximations, starting with the assumption that the plastic strains, and hence the coefficients of $\{\Delta_p\}$, are zero. Initial values for the plastic strains are therefore obtained based on elastic adhesive stresses. The plastic strains are computed at a number of stations along the length of the joint, so that a numerical integration procedure may be used to evaluate the integrals necessary to determine the coefficients $\bar{A}_i(x)$, defined in equation (129). After calculating the coefficients of $\{\Delta_p\}$, new values for A^*_i may be obtained by solution of equations (133). This leads to a new set of adhesive stresses and plastic strains. The above process is repeated until the desired convergence is obtained.

Although the procedure described above appears sound, a number of computational problems dealing with accuracy and convergence are anticipated. Since the development of a non-linear analysis program of this complexity is outside the scope of the present contract, it was decided to develop an approximate but far less complex approach as an interim method of analysis.

4.5.4 Plastic Zone Approach

An analysis procedure and associated computer program was developed for bonded joints with non-linear adhesive stress-strain behavior. The analysis uses a "plastic zone" approach together with a two-stage, elasto-plastic, effective stress-strain curve. The assumption that plastic zones develop at the ends of the over-lap when the adhesive stresses reach a certain (maximum) value, and then spread inwardly toward the center of the overlap when the load on the joint increases, was reported by Douglas Aircraft Company, Inc. (reference 6). The Douglas analysis, however, ignores the presence of normal stresses in the bond-layer and assumes that the shear stresses are constant inside the plastic zones. In practice neither the shear stress nor the effective stress will be constant for any appreciable distance along the bond-layer. Nevertheless, it was felt that integrating the "plastic zone" concept with the linear bonded joint analysis (BONJO I) would provide a good approximation for the analysis of bonded joints in which the adhesive was stressed above its yield strength.

The effective stress is defined accoring to the Von Mises condition as:

$$\bar{\sigma} = \sqrt{\sigma_z^{o\,2} + 3\sigma_{xz}^{o\,2}}$$

which is identical to the first of equations (113). The effective stress inside the plastic zones is assumed constant and equal to the maximum stress obtained from a unidirectional stress-strain curve. The stress-strain behavior of the adhesive between the plastic zones is assumed to be linear elastic; hence, the slope of the effective stress-strain curve in this region will be equal to 3G. As illustrated in Figure 17, the two-stage stress-strain curve used in this procedure is obtained by extending the elastic region until the ultimate stress is reached, at which point the strain increases without further increase in stress. Determining the length of the plastic zones is a quickly convergent iterative process. Initially an elastic solution is performed and adhesive shear and normal stresses are calculated at 76 locations as indicated in Figure 18. The initial lengths of the plastic zones are selected so that the effective stresses are below the maximum stress level at all locations situated between the two zones. After the plastic zone lengths are obtained, the shear and normal stresses within those zones are reduced proportionally so that the resulting

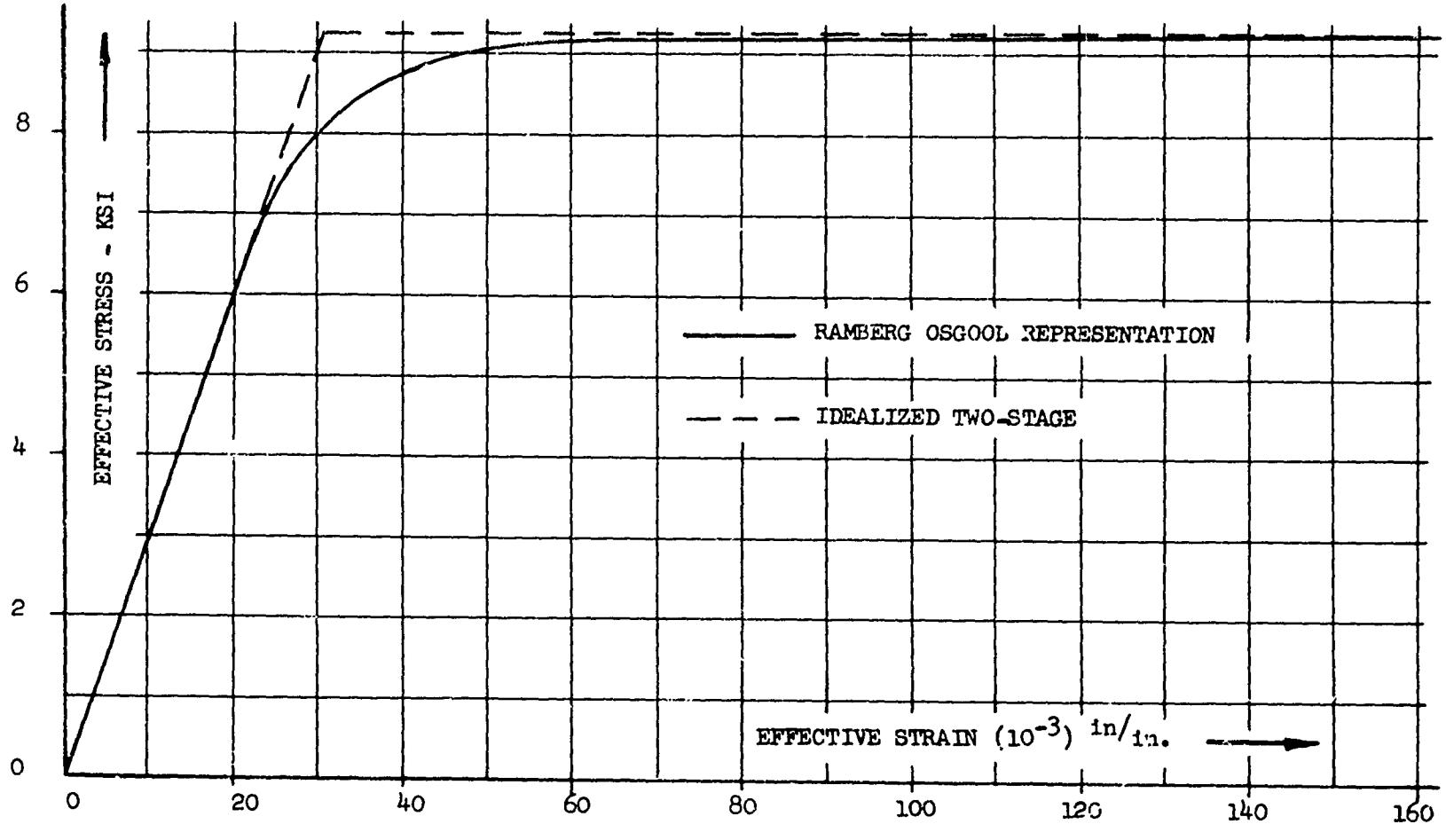

FIGURE 17 EFFECTIVE STRESS-STRAIN CURVE EPON 9601

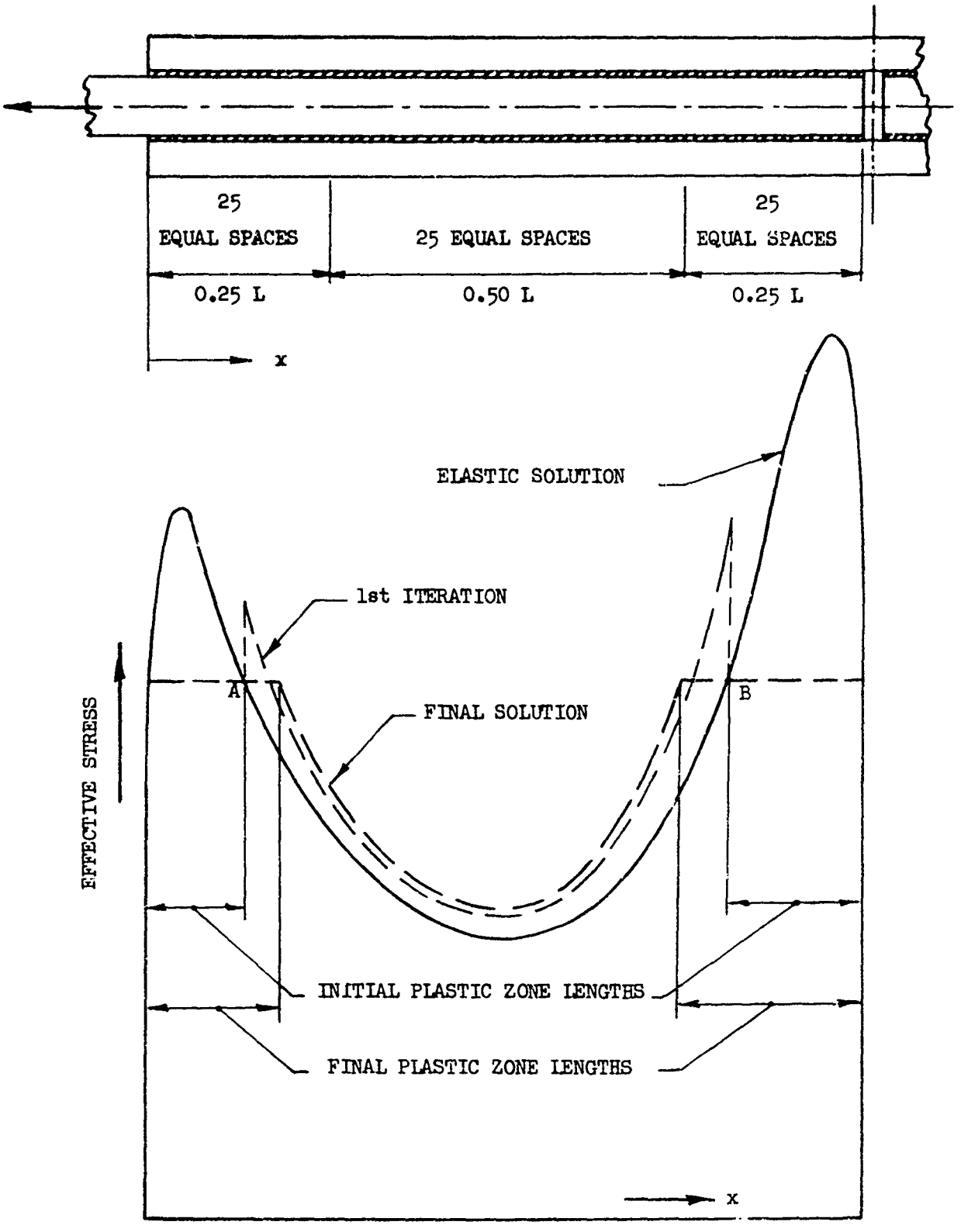

FIGURE 18 EFFECTIVE STRESSES - PLASTIC ZONE APPROACH

effective stress becomes equal to its maximum value, or:

$$\sigma^{o}_{xzp} = \frac{\bar{\sigma}_{max}}{\bar{\sigma}} \sigma^{o}_{xz} \qquad \sigma^{o}_{zp} = \frac{\bar{\sigma}_{max}}{\bar{\sigma}} \sigma^{o}_{z} \tag{134}$$

In the next step, an elastic analysis is performed for that portion ot the joint which is between the two plastic zones. Although the analysis itself is identical to that discussed in Sections 4.2 and 4.3, new boundary conditions must be established for this problem, which may be obtained from the known shear and normal stresses inside the plastic zones. Denoting the length of the plastic zone near the end of the splice plate ($x = 0$) by x_1 and that near tne center of the splice plate by x_2, the following boundary conditions are defined for the center portion of the joint:

$$\sigma^{oo}_{xz} = \sigma^{o}_{xzp}(x_1)$$

$$\sigma^{oL}_{xz} = \sigma^{o}_{xzp}(L - x_2)$$

$$V^{o}_{xu} = \int_{o}^{x_1} \sigma^{o}_{zp}\, dx$$

$$V^{L}_{xu} = -\int_{L-x_2}^{L} \sigma^{o}_{zp}\, dx$$

$$N^{o}_{xu} = \int_{o}^{x_1} \sigma^{o}_{xzp}\, dx \tag{135}$$

$$N^{L}_{xu} = N_x - \int_{L-x_2}^{L} \sigma^{o}_{xzp}\, dx$$

$$N^{o}_{xL} = N_x - N^{o}_{xu}$$

$$M^{o}_{xu} = \int_{o}^{x_1} \int \sigma^{o}_{zp}\, dx\, dx$$

$$M_{xu}^{L} = M_x - \int_{L-x_2}^{L}\int \sigma_{zp}^{o}\, dx\, dx \qquad \text{(135 cont'd)}$$

For a single lap joint, the condition

$$M_{xu}(x) + M_{xL}(x) = M_x \qquad (136)$$

is also needed in order to obtain a solution. The total moment, M_x, may be determined from the condition that the slope is zero at the ends and at the center of the joint. All integrations in equations (135) are performed numerically in the program.

The effective stresses resulting from the above analysis are generally as shown by the dashed line in Figure 18. Since the effective stresses at points A and B exceed the maximum stress level, the plastic zone lengths are increased and the entire process is repeated until the difference between the plastic zone lengths of successive iterations becomes negligible.

Figure 19 shows the peak adhesive shear stresses and the final plastic zone length at each side of the joint as a function of the total applied load, for the configuration D specimen.

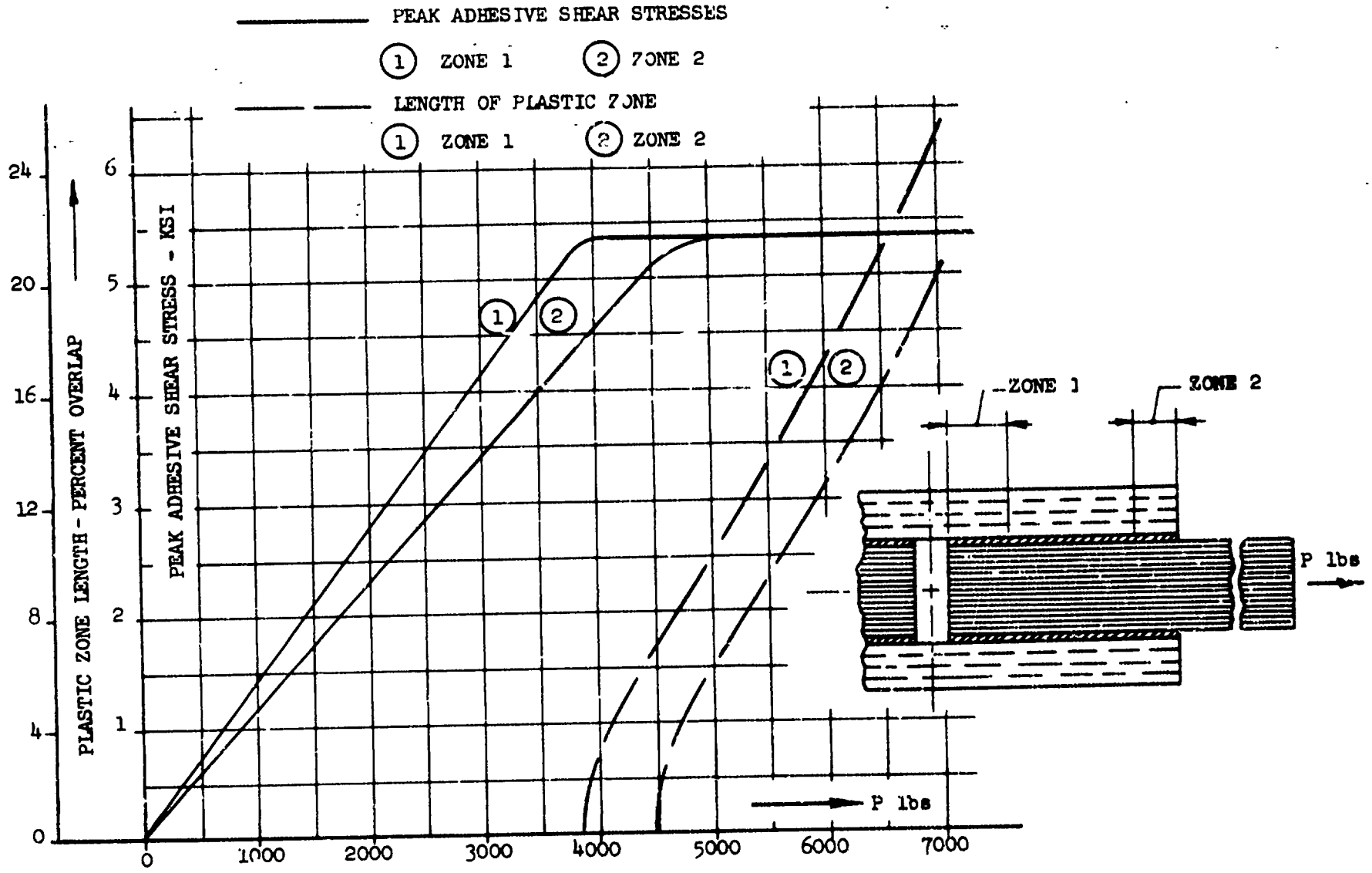

FIGURE 19 PEAK ADHESIVE SHEAR STRESSES AND PLASTIC ZONE LENGTHS
NON-LINEAR BONDED JOINT ANALYSIS

IV. FINITE ELEMENT ANALYSIS

1.0 GENERAL

Finite element analyses were performed as part of this contract for the purpose of evaluating the numerical results obtained with the closed form analysis program, BONJO I. These results were presented and discussed in Chapter III, Section 4.4. In addition, finite element analyses were made for some of the step joint and mechanical joint specimens, which will be described in this chapter.

Lockheed FAMAS Program #97 was used to perform the numerical calculations. This program employs the direct-stiffness displacement method to perform a linear structural analysis for deflections and internal loads of statically loaded structures. Formulation and decomposition of the structural-stiffness matrix are done in double precision. Anisotropic triangular constant stress elements were incorporated in this program. Several options are available to input the material properties so that either a plane stress or plane strain analysis can be made. A capability to determine thermally induced stresses or strains in anisotropic structures has recently been added to the program.

2.0 STEP LAP JOINT ANALYSES

Analyses were made of two different step lap joints of the Configuration 'B' small scale specimens. Detailed dimensions and material specifications are given on Drawing No. 7226-130213 in Appendix C of Volume II. The first joint analyzed utilizes a 16-ply boron laminate (-13 specimen) consisting of 8 plies at 0° and 8 plies at $\pm 45^{\circ}$. The laminate is bonded to an aluminum adherend in three steps of 0.50 inch overlap each. The adhesive thickness was taken as 0.0042 inch, which was the approximate average thickness of all test specimens. The pertinent part of the finite element model used for the analysis is shown in Figure 20. A finer grid is used near the ends of each step since higher gradients exist in these areas. Figures 21 and 22 show the adhesive shear and normal stresses, respectively, along the length of the joint. Both types of stresses peak at the ends of each step and

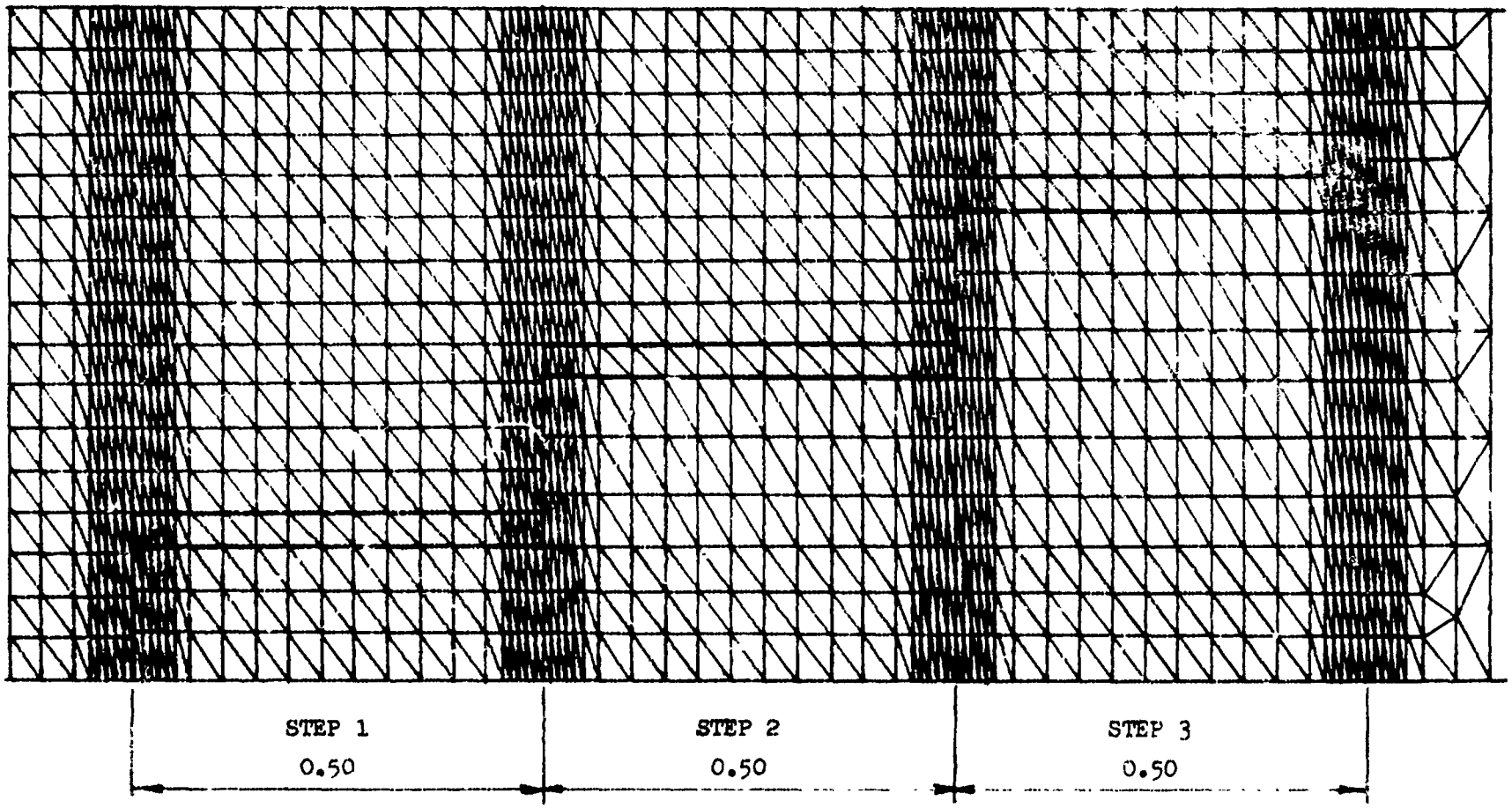

FIGURE 20 FINITE ELEMENT MODEL-STEP JOINT

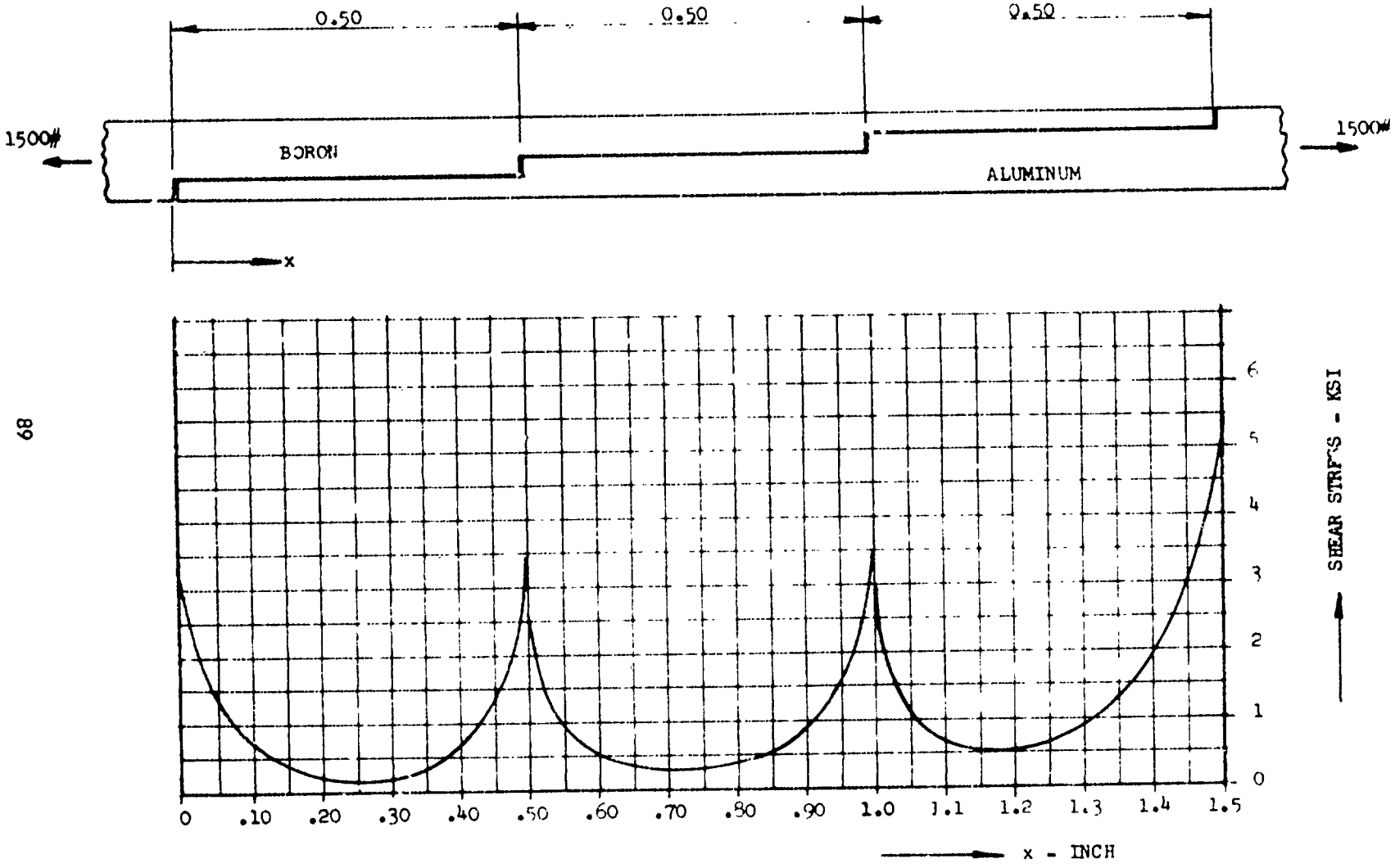

FIGURE 21 ADHESIVE SHEAR STRESS DISTRIBUTION - STEP JOINT

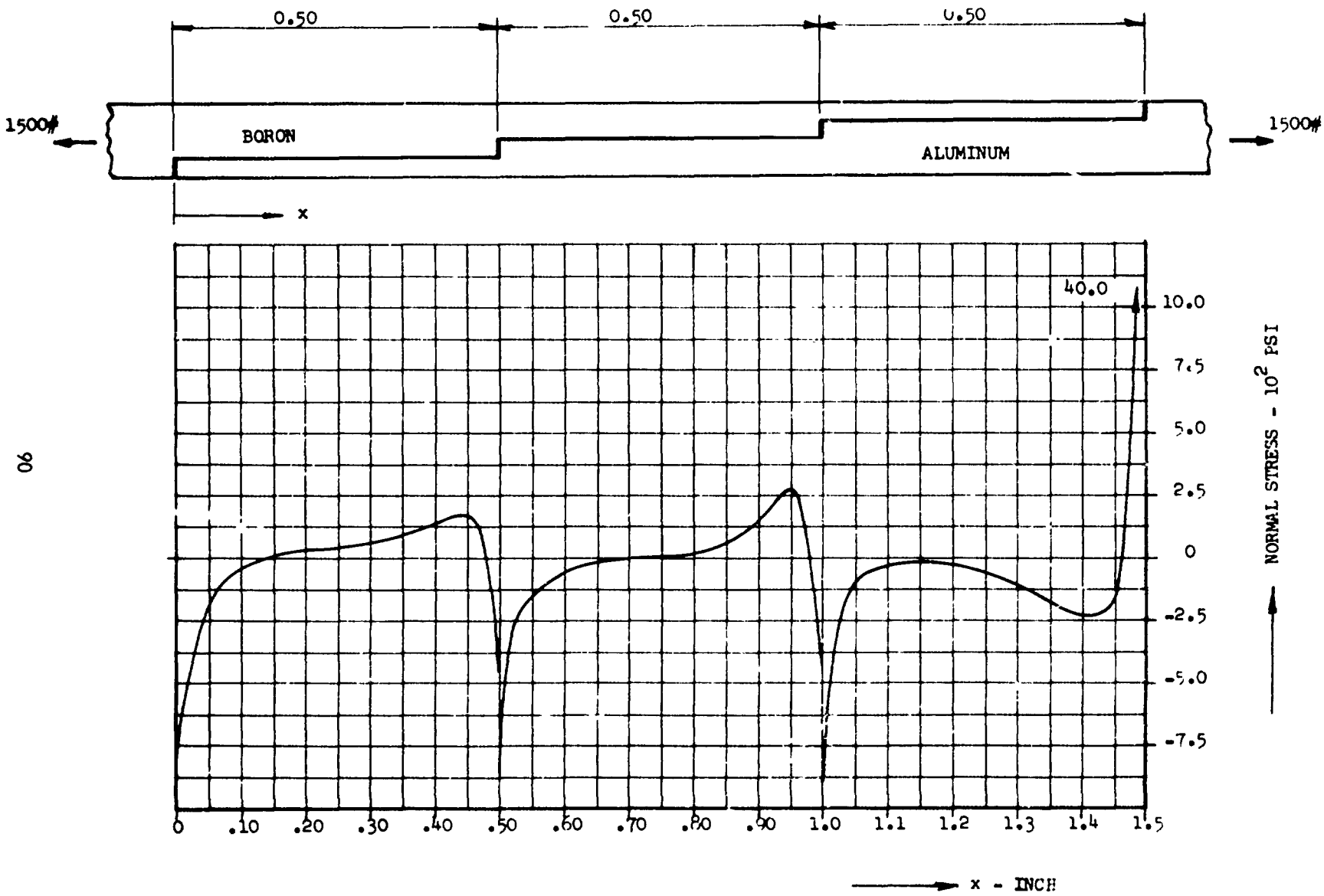

FIGURE 22 ADHESIVE NORMAL STRESS - STEP JOINT

have their maximum values at the end of the last step where the aluminum to boron thickness ratio is largest. The longitudinal stresses in the aluminum adherend along three parallel surfaces are presented in Figures 23. These surfaces are situated so that each one represents the mid-plane of a row of elements adjacent to the bond-layer of one of the steps. The stresses along a given surface adjacent to the bond-layer build up rapidly toward the end of the step and then drop sharply at the beginning of the next step when the adherend thickness is increased. The longitudinal stresses in the boron laminate are presented in a similar manner in Figure 24.

A modified analysis was performed to investigate the effect of recognizing the tension ties between the adherends and between the adhesive and adherends at the ends of each step. The resulting adhesive shear stress distribution is plotted in Figure 25. For comparison, the adhesive shear stress distribution obtained in the original analysis (without tension ties) is shown also. It can be seen that the peak shear stresses at the ends of the steps are reduced significantly as a result of recognizing the tension ties and that the maximum adhesive shear stress in the joint was cut by 30 percent. Because of the fact that part of the applies load is reacted by tensile forces between the adherends, the total area under the shear curve no longer represents the applied load for the modified analysis. A detail, showing how the joint was modeled at the ends of each step, is presented in Figure 25. The tensile stresses in the shaded elements range from 2000 to 3000 psi, while the shear stresses in these elements are almost negligible.

The second joint analyzed was identical to the first one except that titanium was substituted for aluminum for one of the adherends. The finite element model shown in Figure 20 therefore remains applicable. Tension ties were assumed to exist at the ends of each step. The adhesive shear stress distribution for this case is shown in Figure 26. The corresponding stresses for the case with aluminum adherends are given by the dashed line, for comparison. The boron/titanium joint yields considerably lower shear stresses at the end of the last step than the boron/aluminum one, but generally the stresses differ only slightly.

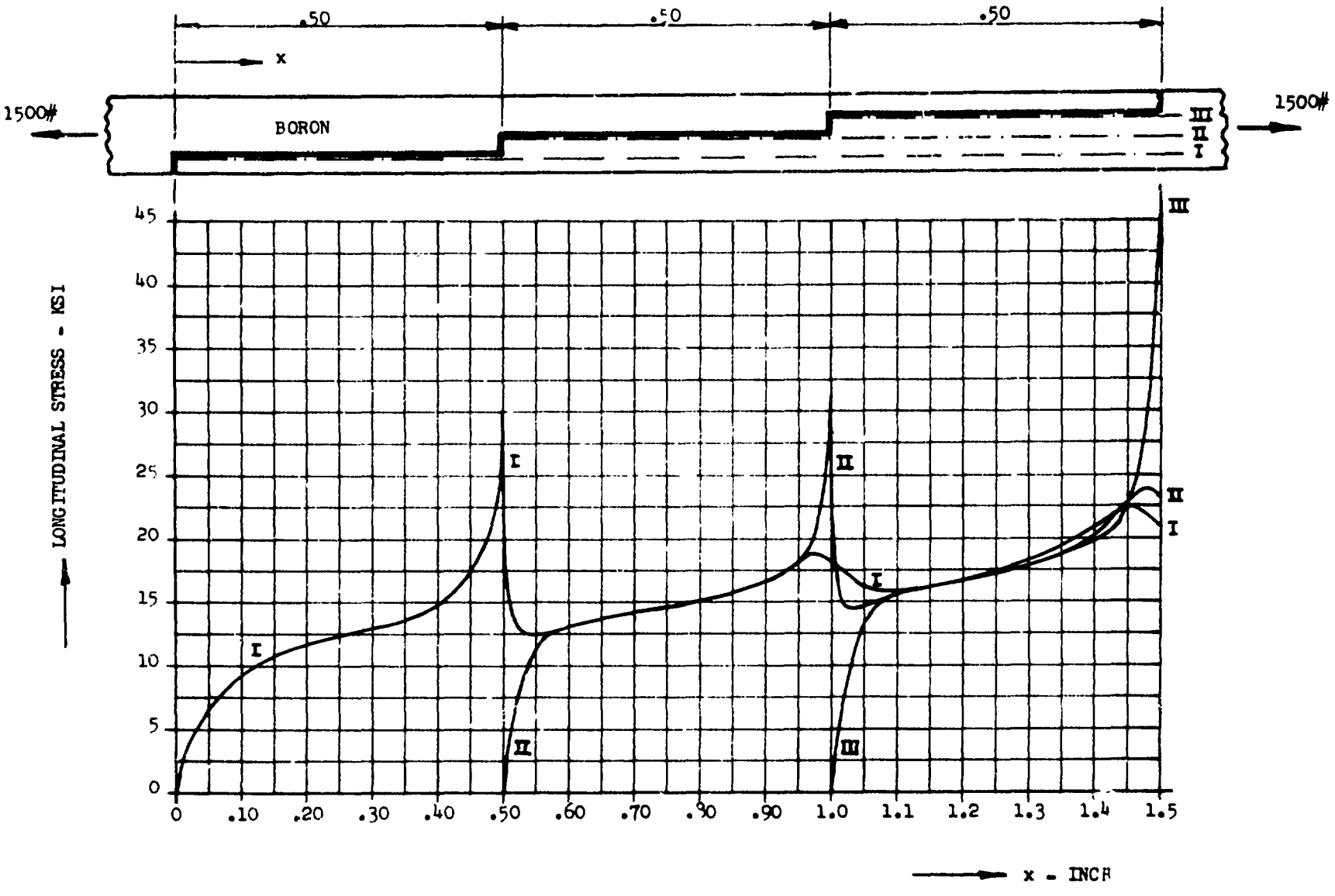

FIGURE 23 LONGITUDINAL STRESSES IN ALUMINUM ADHEREND

FIGURE 24 LONGITUDINAL STRESSES IN BORON LAMINATE

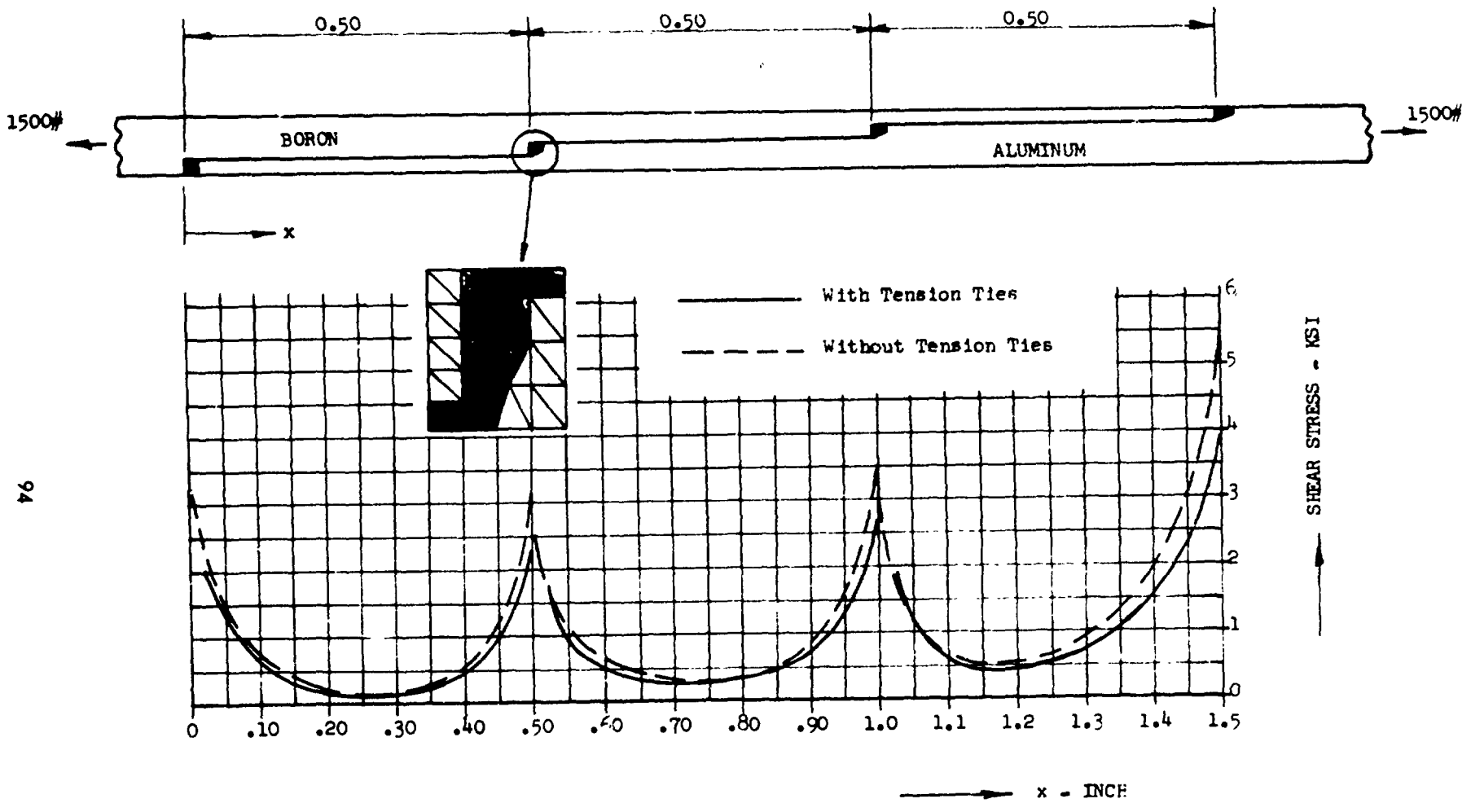

FIGURE 25 ADHESIVE SHEAR STRESS DISTRIBUTION - STEP JOINT
EFFECT OF TENSION TIES

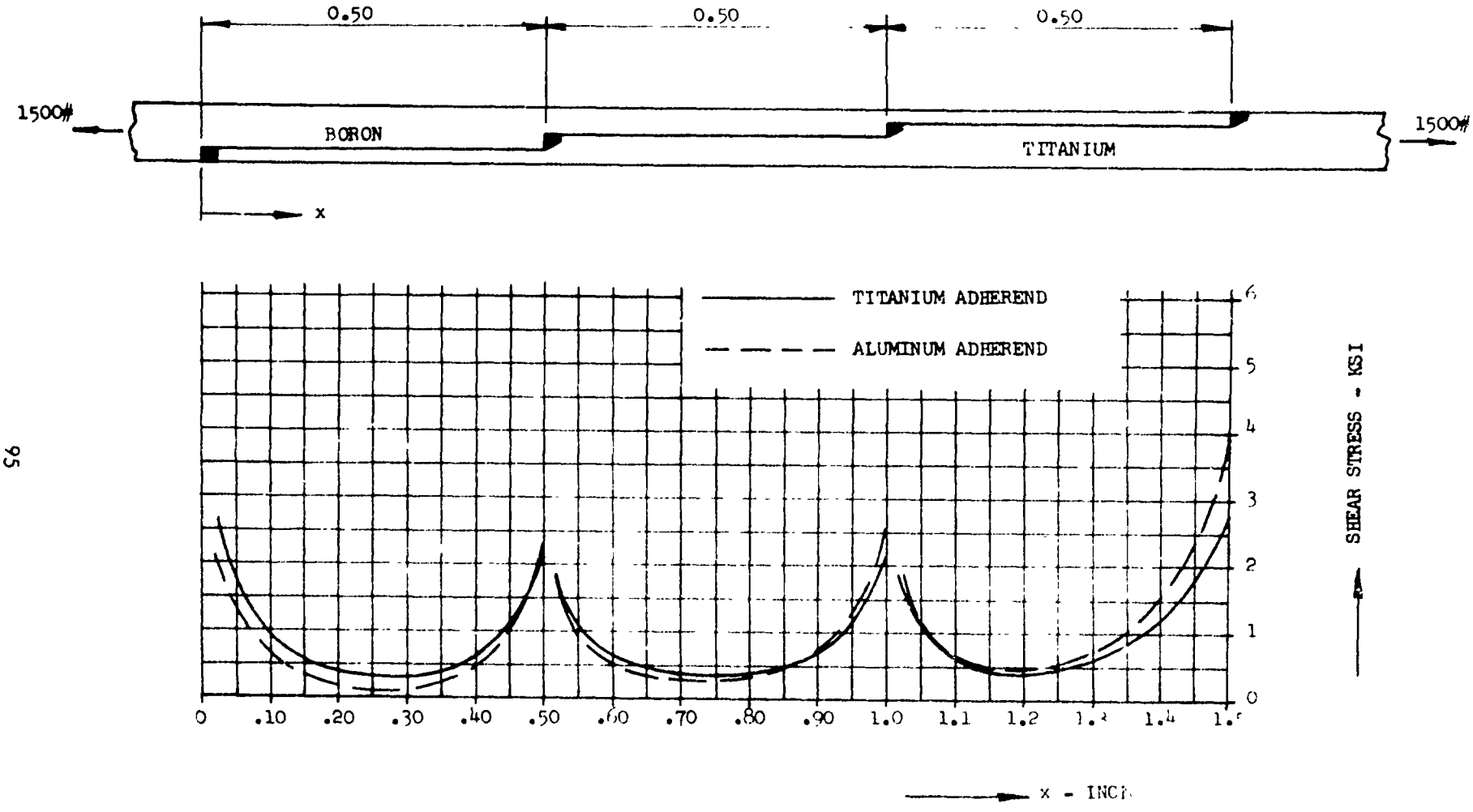

FIGURE 26 ADHESIVE SHEAR STRESS DISTRIBUTION - STEP JOINT
COMPARISON OF ALUMINUM AND TITANIUM ADHERENDS

3.0 MECHANICAL JOINT ANALYSES

Two separate finite element models were constructed in order to perform a detailed analysis of one of the Configuration 'E' small scale specimens. Dimensions and material specifications are given on Drawing No. 7226-1302IE in Appendix C of Volume II. The -1A specimen assembly consisting of an 8-ply boron laminate (-21 specimen) and a titanium splice plate was selected. Two 0.012 inch thick titanium shims were interlayered with the boron in order to provide sufficient bearing for the fasteners. The first model which is shown in Figure 27 is for the purpose of performing a detailed analysis through the thickness of the joint. Isotropic triangular plate elements are used for the titanium splice plate, titanium shims, adhesive layers, and fasteners. Anisotropic triangular plate elements are used for the boron laminae. In order to properly account for pin bending and to determine the bolt bearing loads on the individual layers of the joint, the elements of the fasteners are connected to those of the joint plates with springs that are permitted to take compression loads only.

In order to study the stress distribution around the fastener holes a second finite element model was constructed. The latter model consists of triangular plate elements in the plane of the joint and represents a layer of titanium or boron. Again, compression springs between the fastener and plate elements are used to obtain the bearing stresses caused by the bolt in the layer under consideration. This second model has been shown in Figure 28.

Average bearing stresses in the two fasteners were calculated for an applied compression load of 1000#. These stresses were obtained from the first model by dividing the final forces in the springs, between the fasteners and joint plates, by their respective areas of contact. An iterative analysis was used to assure that all final spring forces were compression by successive elimination of the tension springs. The average bearing stresses thus obtained are shown in Figure 29. Peripheral bearing stresses on the fasteners were determined with the use of the second finite element model. Figure 30 shows those transmitted by the upper titanium shim as a function of the angle θ.

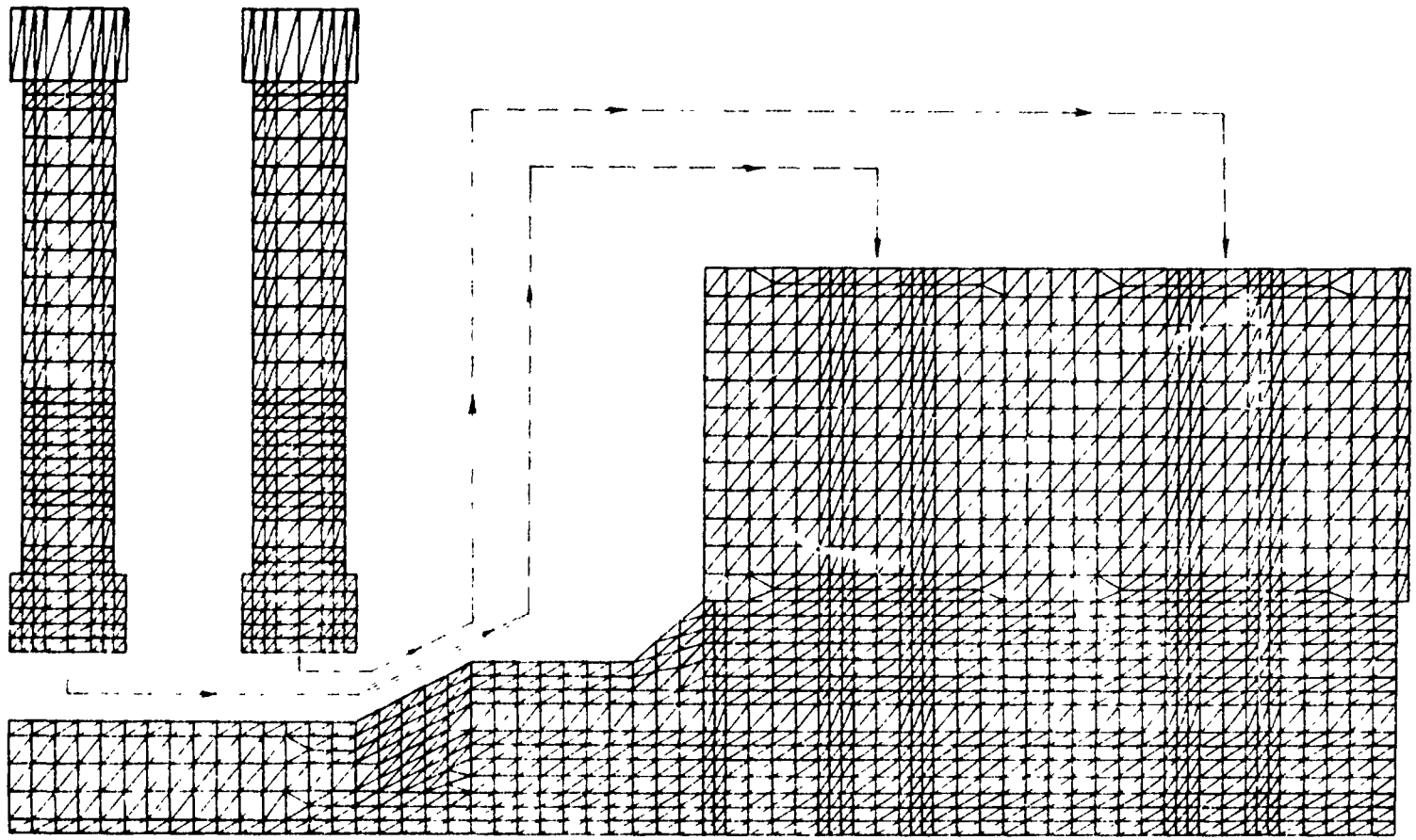

FIGURE 27 FINITE ELEMENT MODEL NO. 1 - MECHANICAL JOINT

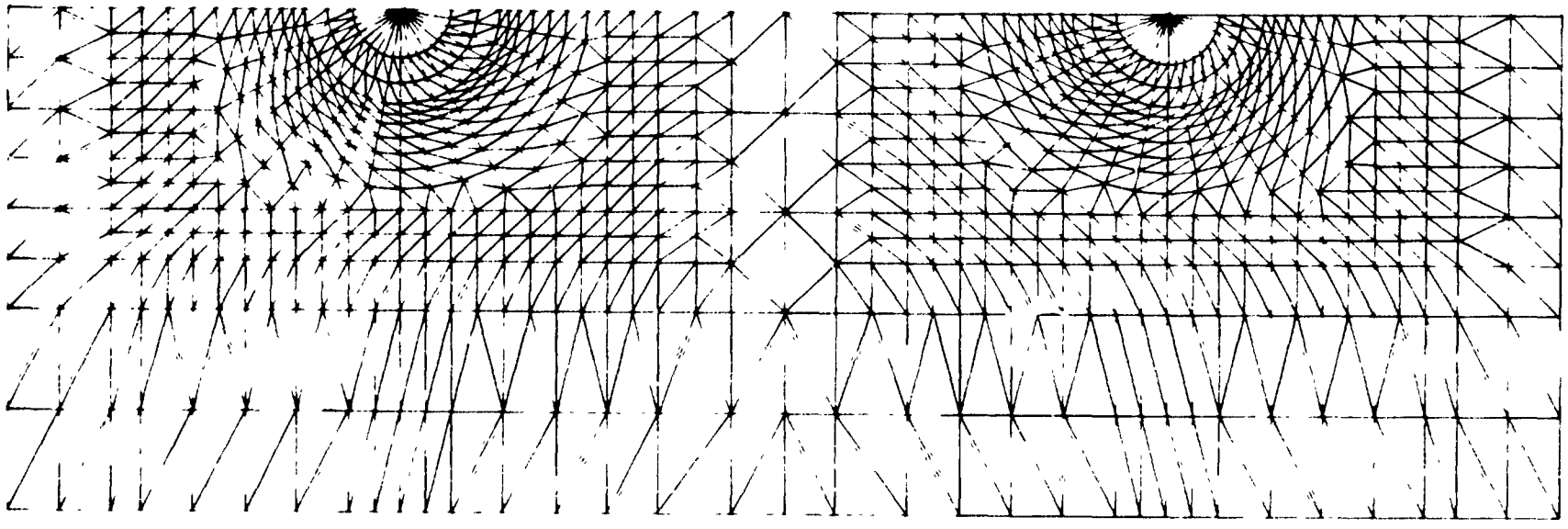

FIGURE 28 FINITE ELEMENT MODEL NO. 2 - MECHANICAL JOINT

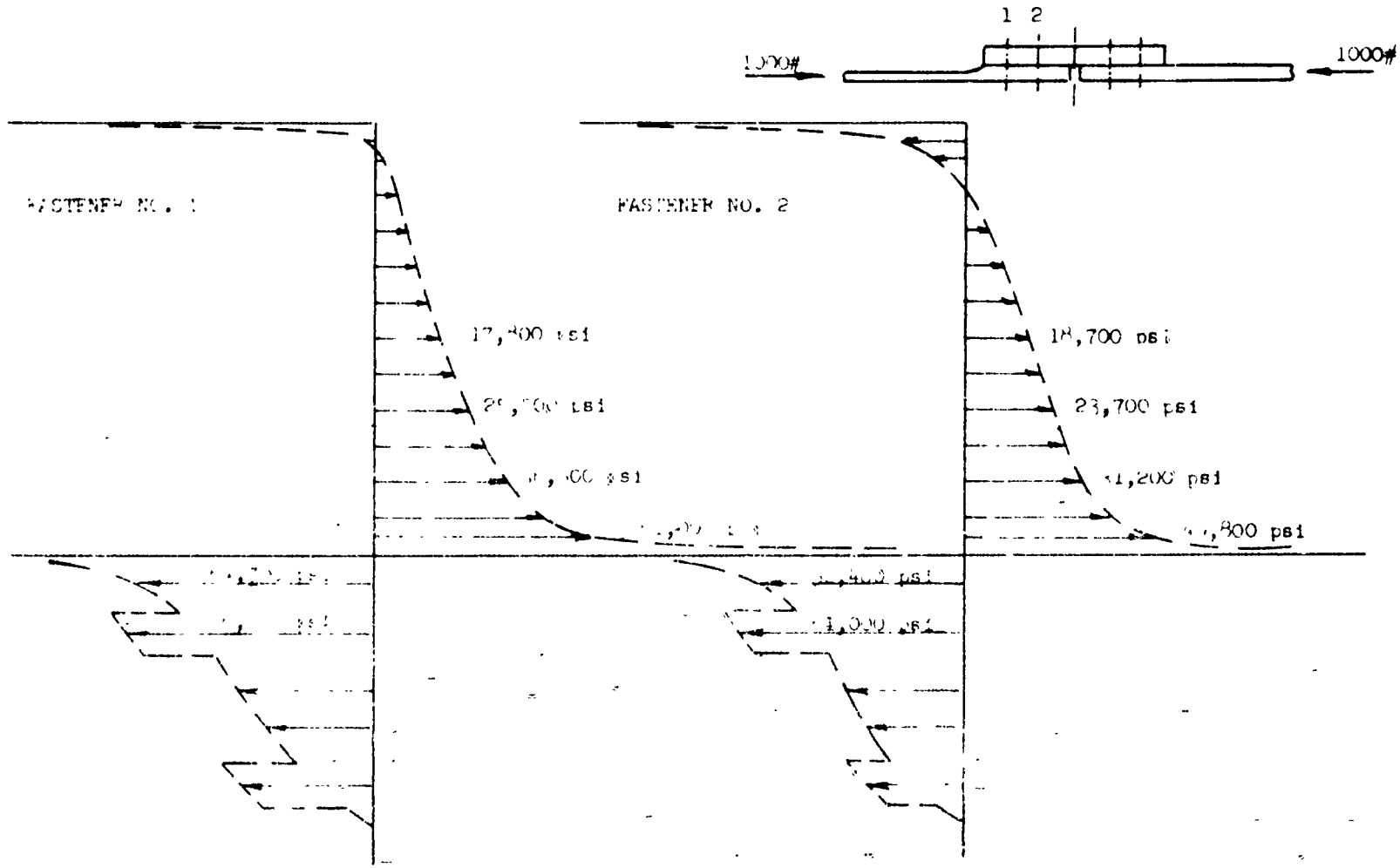

AVERAGE BEARING STRESSES - FASTENERS

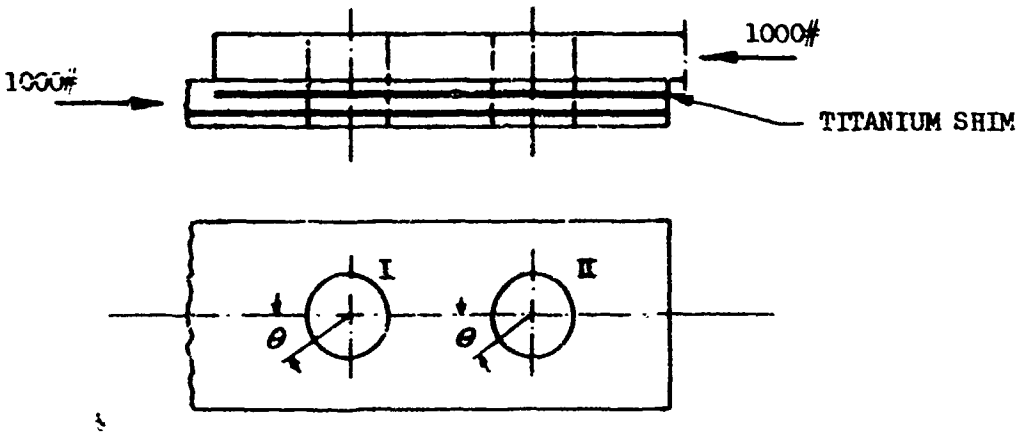

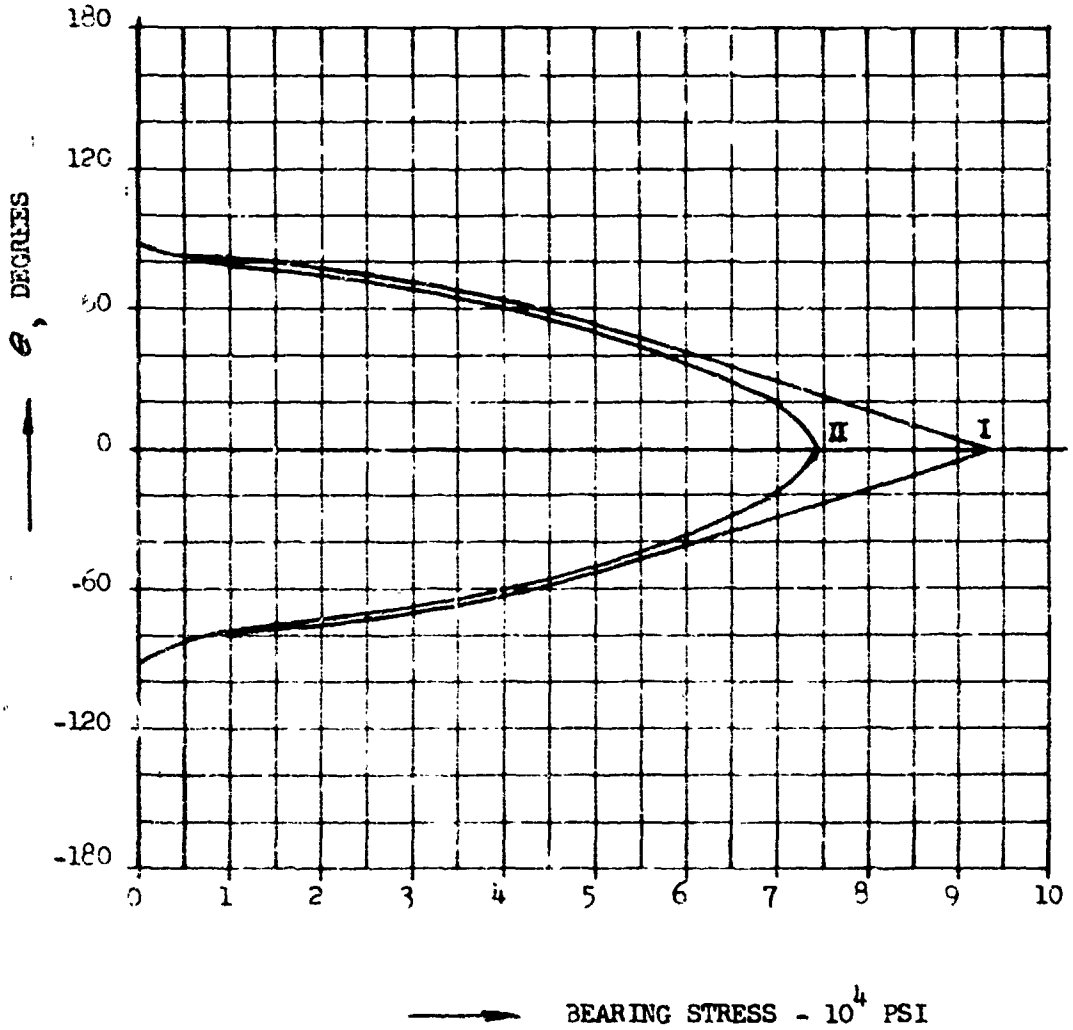

FIGURE 30 BEARING STRESSES - TITANIUM SHIM

Loading and unloading of the titanium shims has been studied. Figure 31 shows the shear stresses in the adhesive layer on both sides of the upper titanium shim resulting from an applied compression load of 1000#. Peak shear stresses, of course, occur near the fasteners where the loads are introduced into the shim. The position of the fasteners is indicated in the figure.

Net section tensile stresses for the lower titanium shim and the 0° boron layer in the center of the plate are shown in Figures 32 and 33, respectively, for a load of 1000 lbs. These stresses were determined by taking the average stresses acting on the layers, as obtained from the first finite element modle, and applying them to the second model. The stress concentration factor appears to be significantly higher for the boron.

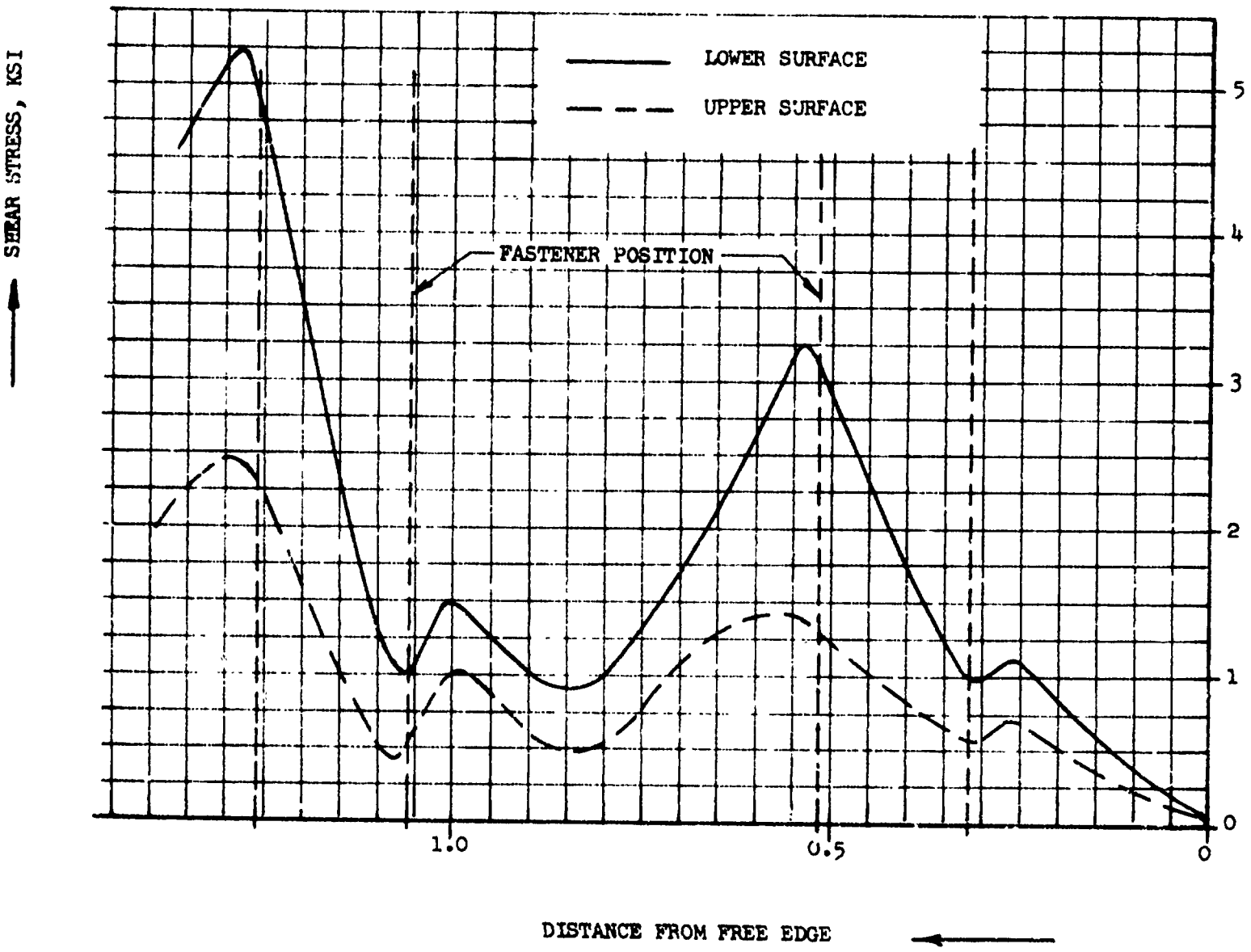

FIGURE 31 SHEAR TRANSFER - TITANIUM SHIM

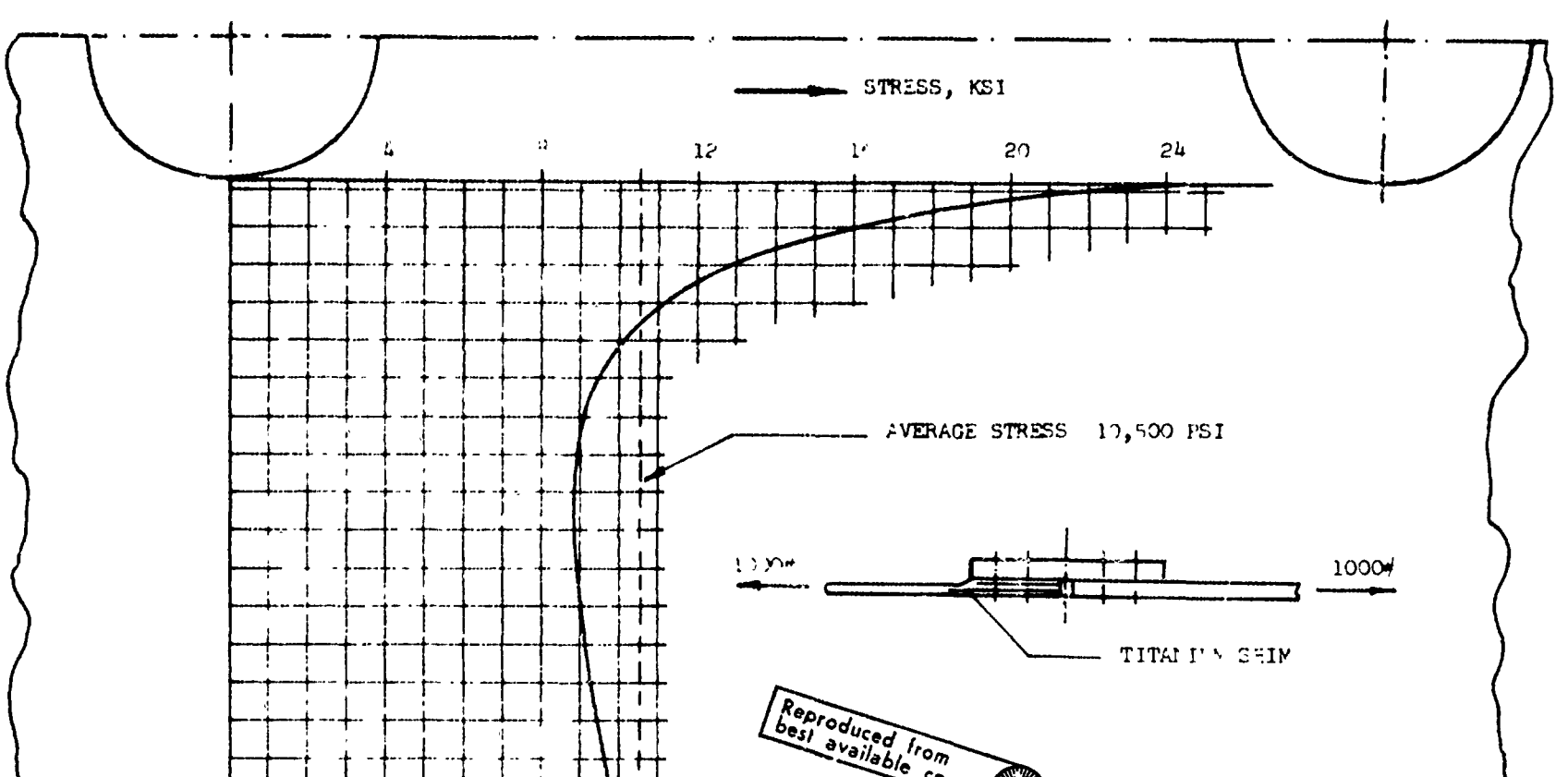

FIGURE 3 NET SECTION STRESS - TITANIUM SHIM

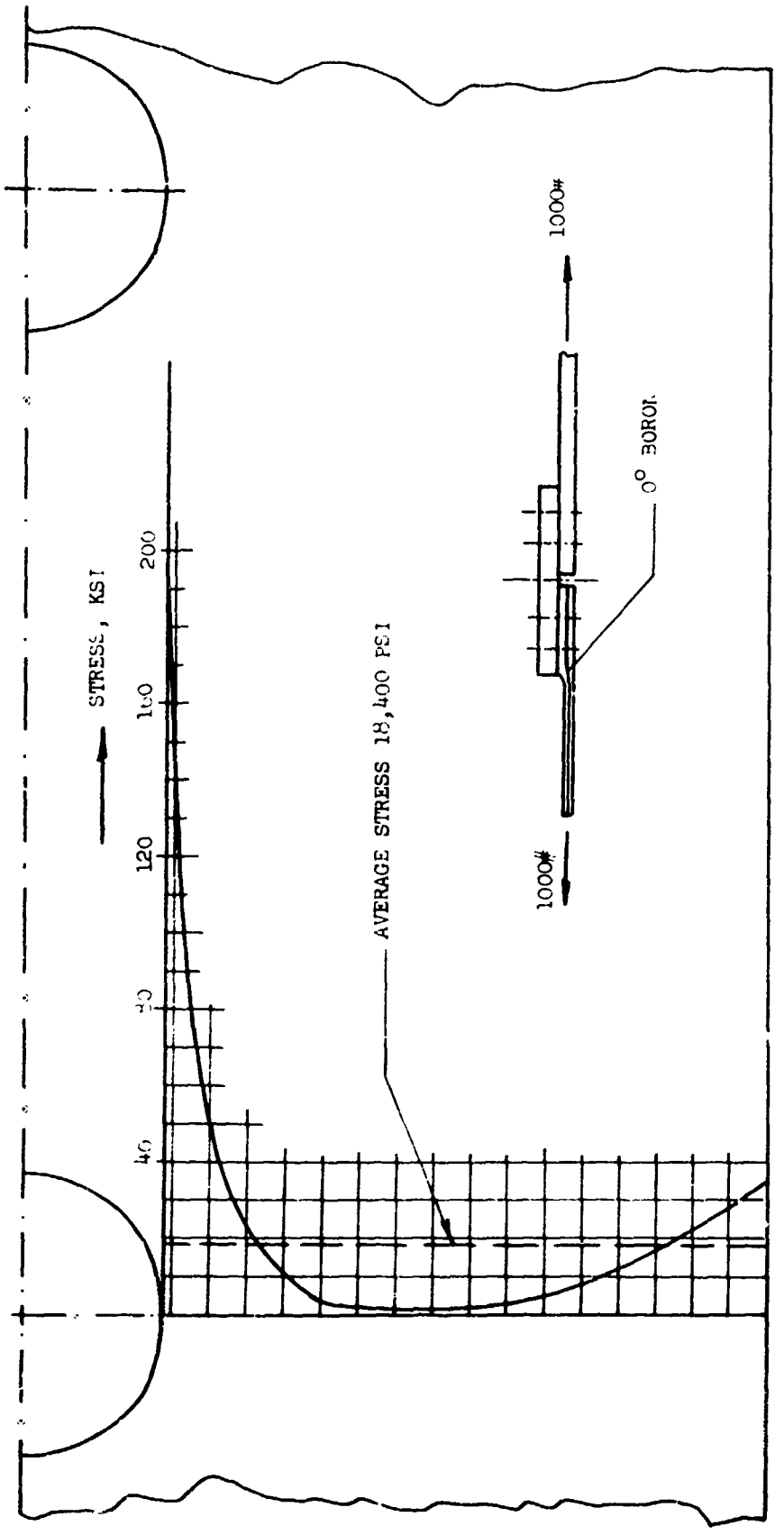

FIGURE 33 NET SECTION STRESSES - 0° BORON

V. PHOTOELASTIC STRESS ANALYSIS - BONDED JOINTS

1.0 GENERAL

An attempt was made to provide an experimental verification of the analytical stress analysis methodology developed under the program (Chapter III). This verification was limited to the linear analysis regime because of its relative importance in serving as the foundation of the subsequent non-linear analysis.

Basically, three experimental phases were accomplished during the program. The first of these involved the fabrication and photoelastic test of a Configuration D double lap joint having aluminum adherend strips and glass splice plates. This phase is described in Section 1.1. During the second experimental phase, Configuration A and D joints were tested to determine the stress distribution at the surface of its titanium splice plates. This second phase is described in Section 1.2. Finally, Section 1.3 describes the third experimental phase in which strain gage results were obtained for several configuration A and D specimens. These results were used to provide an independent check on the analytical and/or photoelastic results.

1.1 PHOTOELASTIC RESULTS - ISOTROPIC ADHEREND

This phase of the investigation was initiated in an attempt to verify an existing closed-form solution for the stress distribution in a linearly elastic, elastically isotropic joint adhesive. In order to achieve this goal, a photoelastic model of a double lap joint was constructed. The adhesive layer was simulated by a thin layer of epoxy photoelastic material. A reflective coating was painted on one side of the specimen, between the aluminum/epoxy interface, to allow determination of isochromatic lines. Although the optical sensitivity of glass is low relative to that of the adhesive layer, a reflective coating was painted between the epoxy/glass interface on the other side of the specimen to determine any contribution to the overall fringe pattern made by the glass. A schematic of this model is shown in Figure 34.

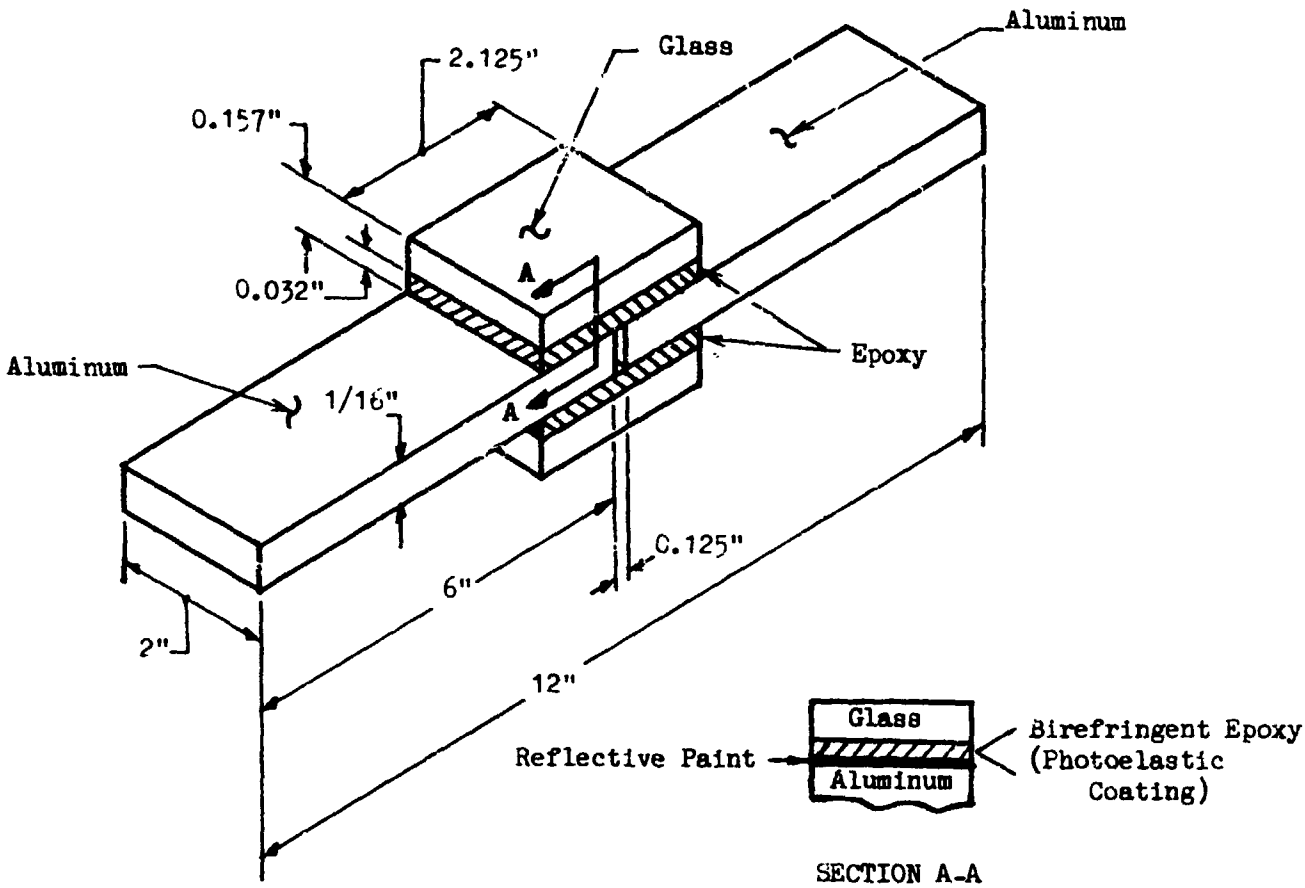

FIGURE 34 PHOTOELASTIC MODEL

The model was constructed to allow determination of the stress distribution (σ_x, σ_y, σ_{xy}), in the plane of the adhesive layer. Although the analysis of this configuration is based on the assumption that these stresses are zero (for relatively "narrow" joints), it was anticipated that at least some sort of distribution could be determined photoelastically. No such distribution could be obtained. Two models of this type were constructed and subjected to monotonically increasing sequences of static loads until the glass splice plates failed in tension (Figure 35).

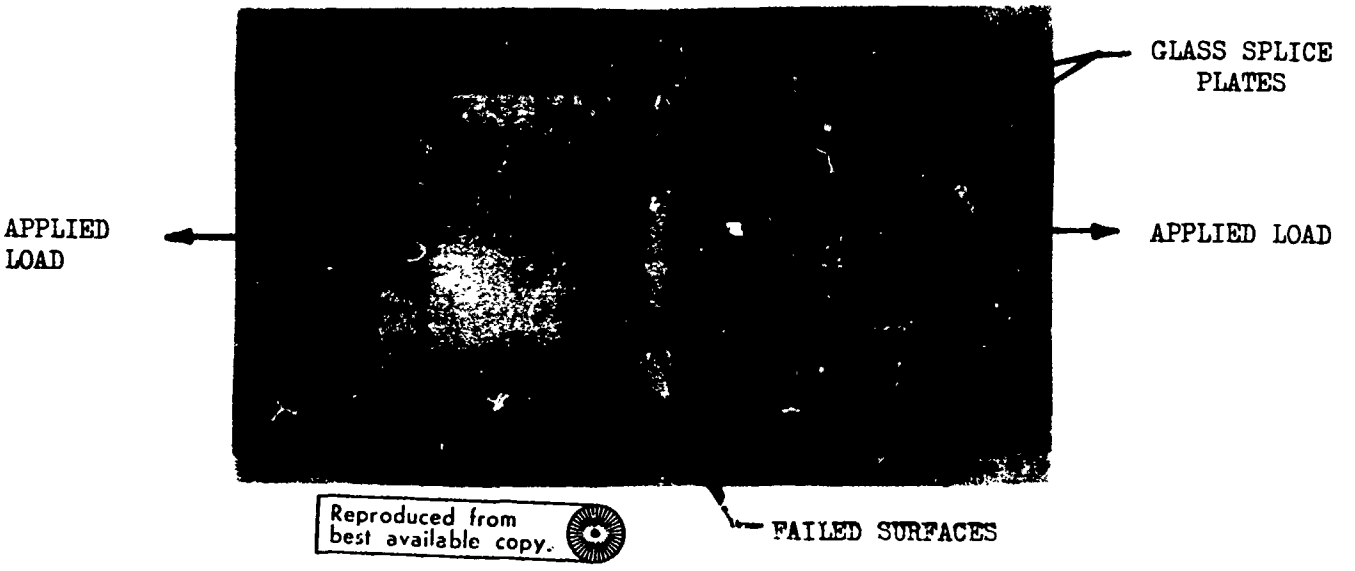

FIGURE 35 VIEW SHOWING FAILED GLASS SPLICE PLATES ON PHOTOELASTIC MODEL

In both cases, the epoxy used to model the adhesive layer was of sufficient sensitivity so that at the recorded failure load level, the shear stress, σ_{xz}, should have produced at least one full fringe in the central portion of the bonded area. The fact that no appreciable fringe pattern was observed in this area when the model was viewed normally, means simply that the stresses σ_x, σ_y, σ_{xy} were of much lower magnitudes than was σ_{xz}. This observation is, of course, in direct substantiation of the assumption made in the analysis that σ_x, σ_y, and σ_{xy} can indeed be neglected.

Although the anticipated measurement of a detailed stress distribution was not accomplished, the results which were obtained do seem to achieve the desired end goal. They substantiate the validity of the assumption that the adhesive stresses σ_x and σ_{xy} are negligible in comparison with σ_z and σ_{xz}.

1.2 PHOTOSTRESS RESULTS - COMPOSITE ADHEREND

During this phase of the program, an attempt was made to obtain a correlation between analytical joint-stress predictions and experimentally determined joint-stress. The experimental information was obtained by bonding pads of birefringent material to the splice plate surfaces of several joint specimens.

Three such specimens were considered: a 1.1"-wide specimen, a 3.0"-wide specimen, and one having a width of 9.0 inches. All three types of specimens had $0^{\circ}/\pm 45^{\circ}$ boron-epoxy adherend laminates and splice plates made of Ti-6Al-4V annealed material. The data obtained were reduced, using the shear difference method, to obtain stress and/or strain components at several desired locations.

1.2.1 1.1"-Wide Specimen

A photograph of this specimen is shown below in Figure 36. The birefringent pads used on this specimen were cut from a 0.042"-thick sheet of Photostress, Inc., S-16 material. The titanium splice plate was 0.039" thick and the base adherend was cut from an 8-ply symmetrical laminate.

Two models of the type shown in Figure 36 were tested. The second of these models was tested in an attempt to resolve difference between experimental and analytical results discovered during consideration of the first model.

The experimental investigation on the first model was conducted by loading the specimen to a 1000 lb_f load level and using a reflective polariscope to obtain isochormatic and isoclinic photoelastic data. These data were reduced to obtain the axial stress component, σ_x, plotted in Figure 37. The 1 KIP load applied to the model was not sufficient to cause appreciable yielding of any of its constituent materials. The results obtained were therefore compared with analytical predictions obtained from the linear, closed-form analysis developed under this program.

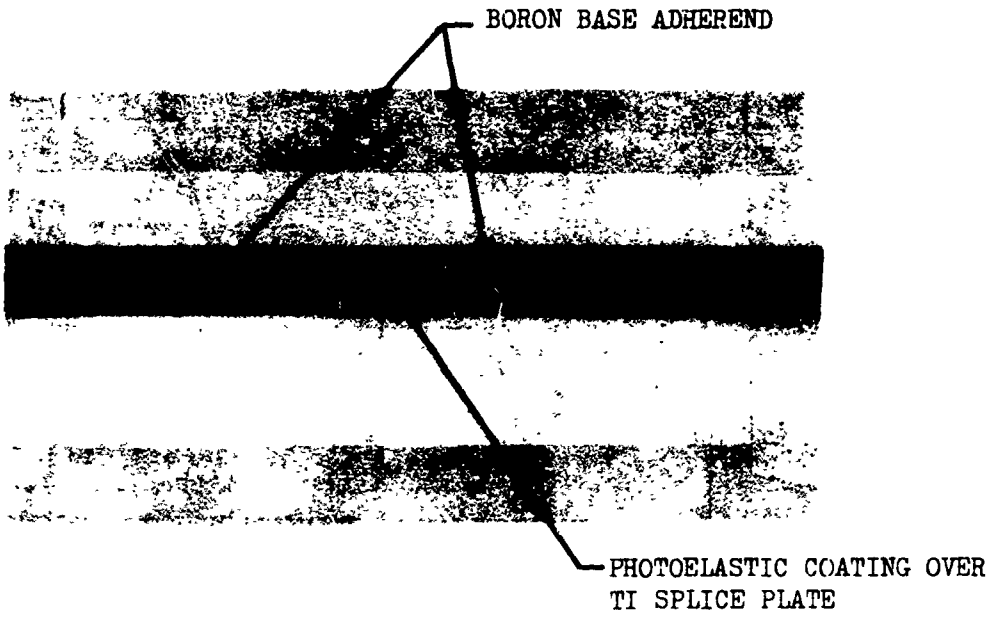

FIGURE 36 1.1"-WIDE CONFIGURATION "D" SPECIMEN WITH BIREFRINGENT PAD BONDED TO SPLICE PLATE

The analytical results obtained from the closed-torm analysis do not agree with photostress results within acceptable tolerance (Figure 37). Although the shapes of the "closed-form" and "photostress" curves are similar, the difference in stress magnitudes is thought to be too great to ignore. A complementing finite element analysis was done in an attempt to help resolve this difference. The result of this analysis is also shown in Figure 37. This latter (finite element) analysis tends to lend more credence to the "closed-form" analytical results than to the experimental results.

The experimental curve in Figure 37 was corrected for tensile reinforcing effect arising from the fact that the coating material itself carries some load. The derivation of this correction factor is based on the assumption that the coating is in a constant uniaxial state of stress. This assumption is obviously incorrect since the splice plate undergoes bending as well as longitudinal tension. A bending correction should therefore be applied to the photostress results. Since the degree of splice plate bending cannot readily be assessed, no such bending correction can be made.

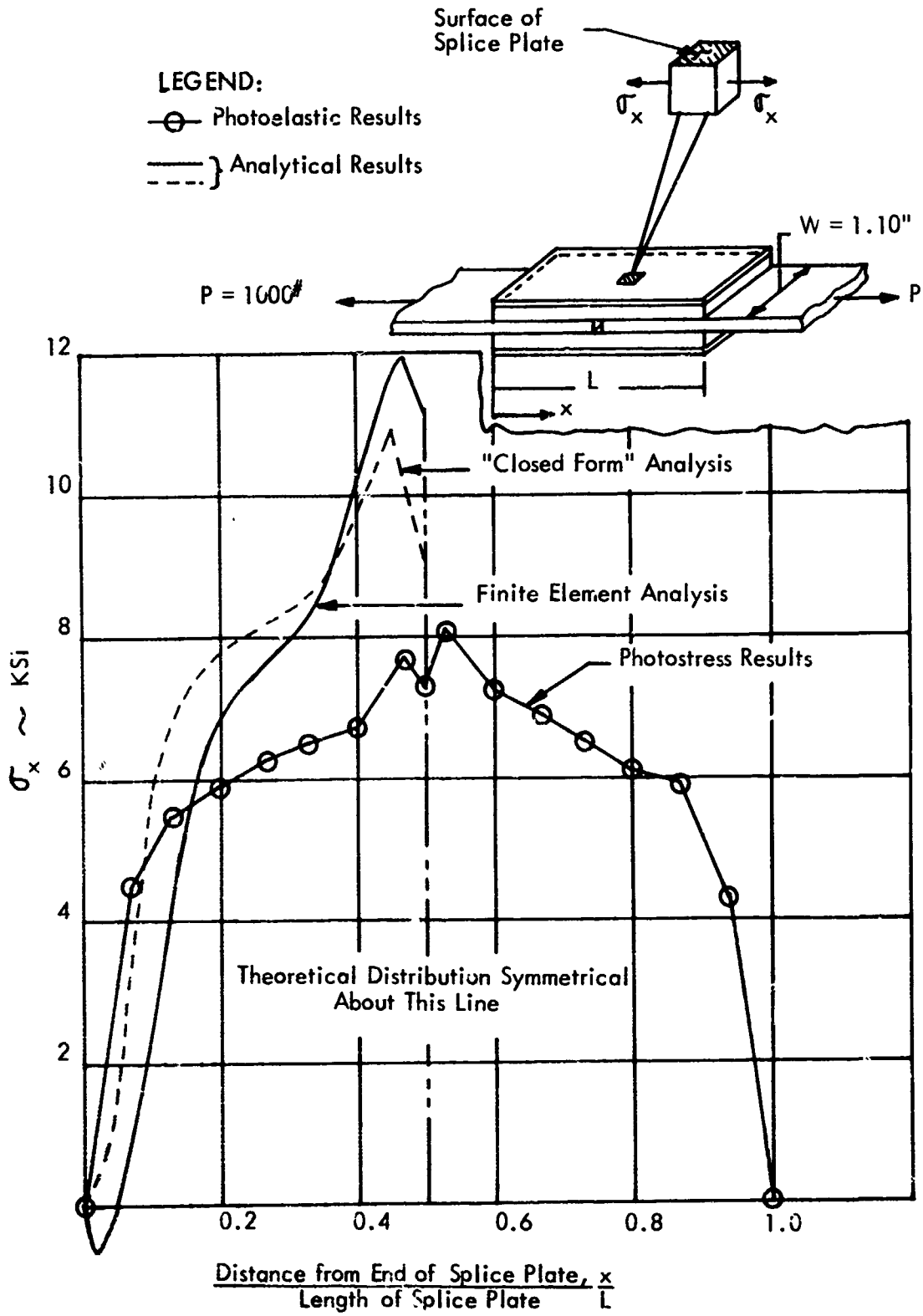

FIGURE 37 - COMPARISON OF ANALYTICAL WITH EXPERIMENTAL SPLICE PLATE SURFACE STRESS - FIRST 1.1" WIDE CONFIGURATION "D" SPECIMEN

An attempt was made to further resolve the differences between the three curves shown in Figure 37. This was done by placing strain gages at selected locations along the center-line of the surface of the splice plate of the second 1.1"-wide joint. The second joint specimen was a 16-ply thick laminate. After strain gage results were obtained, the gages were removed and photostress material bonded to the splice plate surfaces. A photostress investigation was then performed on the same model. These new strain gage and photo-stress results were compared not only with each other, but with closed form analytical results as well. The results of this comparison are presented on Figure 38. It can be seen that these three types of results correlate much better than comparable results obtained from the first specimen.

1.2.2 3.0"-Wide Specimen

Figure 39 shows a sketch of the 3.0"-wide specimen discussed in this section. The speci-men was of the 3.0"-wide, Configuration "A" variety. The $0^{\circ}/\pm45^{\circ}$ base adherend material was fabricated of Narmco 5505 boron/epoxy and was an 8-ply thick symmetrical laminate. The splice plate was cut from a sheet of Ti-6Al-4V annealed material and had a 0.0425"-thick birefringent pad bonded to a portion of its surface as shown in Figure 39.

Photostress data obtained at each of the grid nodes were used to obtain normalized plots of splice plate surface stress. Figures 40 and 41 show the longitudinal and transverse stress components, respectively. The longitudinal component displayed in Figure 40 was evaluated along line $\overline{CD}$ (Figure 39). The transverse component of Figure 41 was evaluated along line $\overline{AB}$.

The obvious anticipated symmetry about lines $\overline{AB}$ and $\overline{CD}$ is not particularly evident from the experimental results presented in Figures 40 and 41. This would seem to indicate that the data on which these results are based are somewhat questionable. The explanation for this apparent discrepancy may well be the bending undergone by the splice plate as a result of the asymmetry of the joint about its midplane. In order to properly interpret the photostress data, a correction factor must be used to account for the degree of bending caused by this asymmetry. Such a factor cannot readily be obtained for the situation

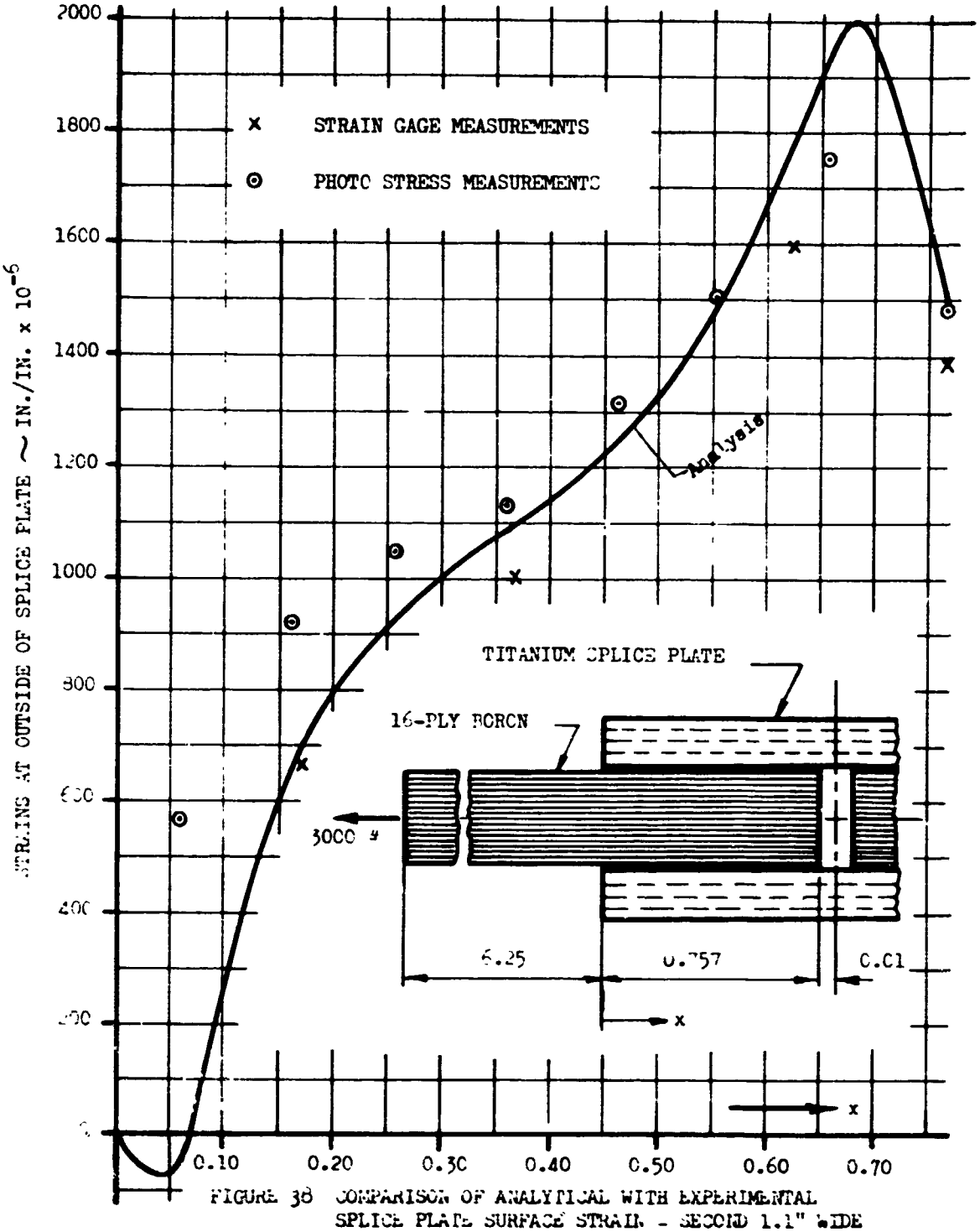

FIGURE 38 COMPARISON OF ANALYTICAL WITH EXPERIMENTAL SPLICE PLATE SURFACE STRAIN - SECOND 1.1" WIDE CONFIGURATION "D" SPECIMEN

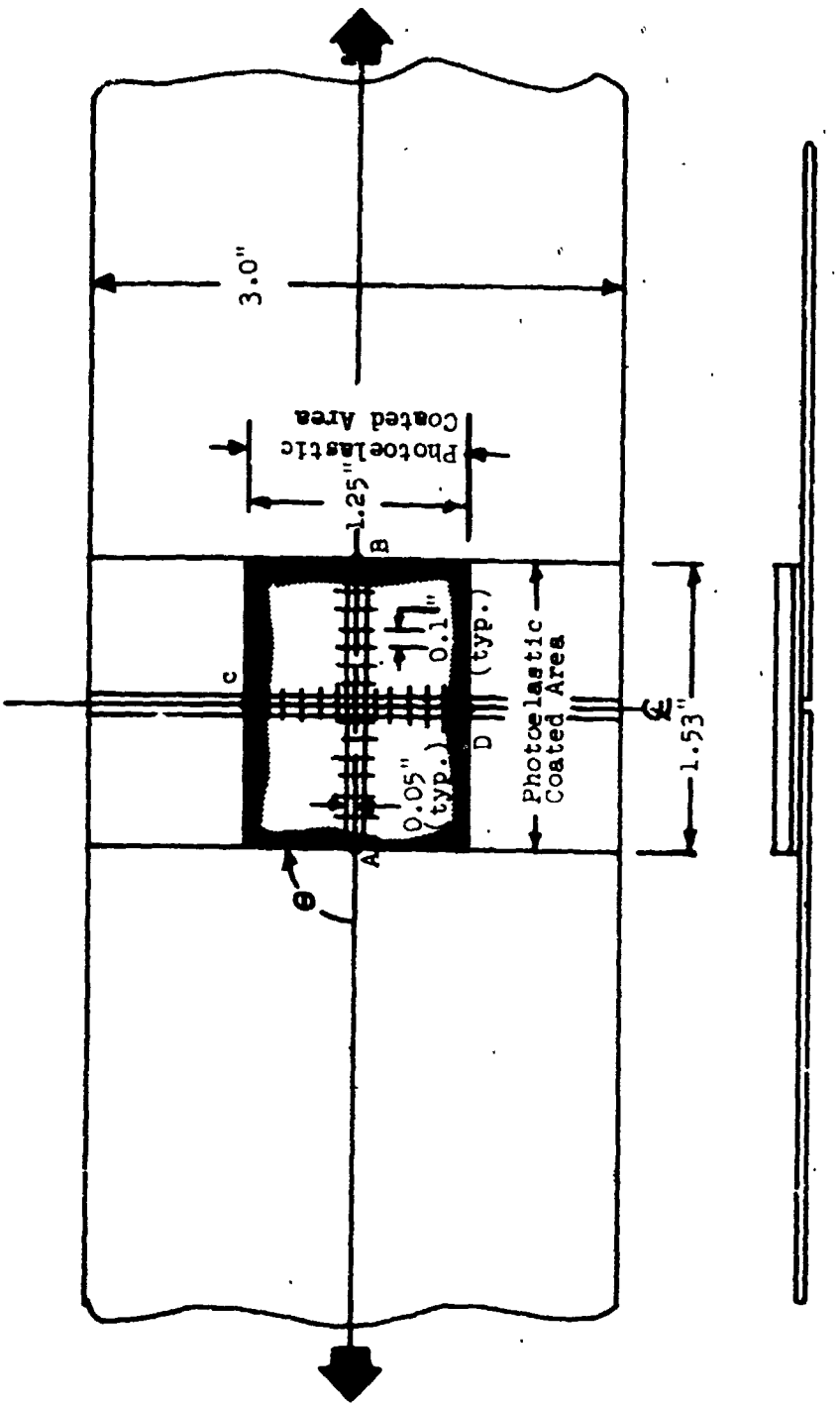

FIGURE 39 3.0"-WIDE CONFIGURATION "A" SPECIMEN USED TO OBTAIN PHOTOSTRESS DATA

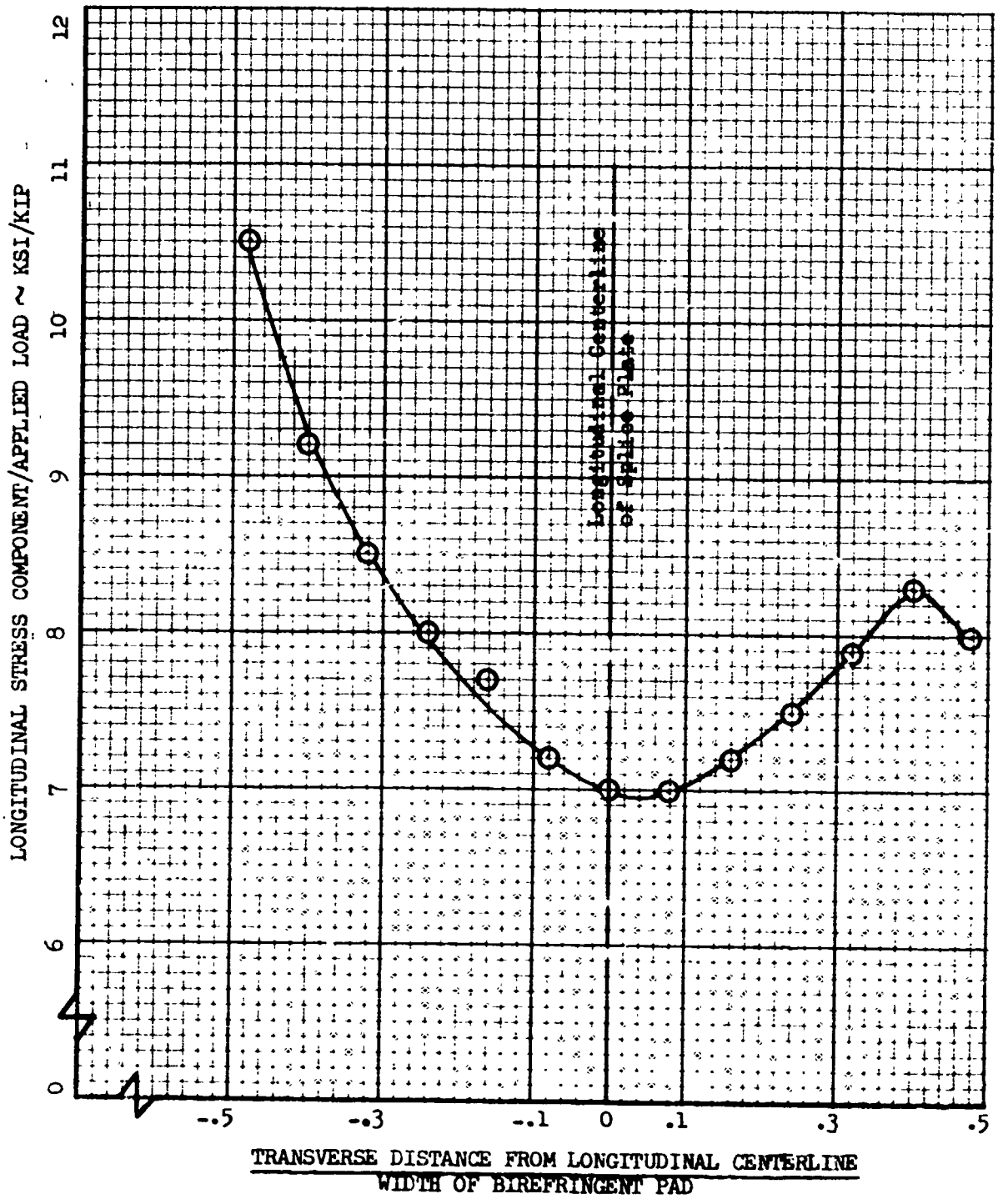

FIGURE 40 SPLICE PLATE SURFACE LONGITUDINAL STRESS COMPONENT-
3.0" WIDE CONFIGURATION "A" SPECIMEN

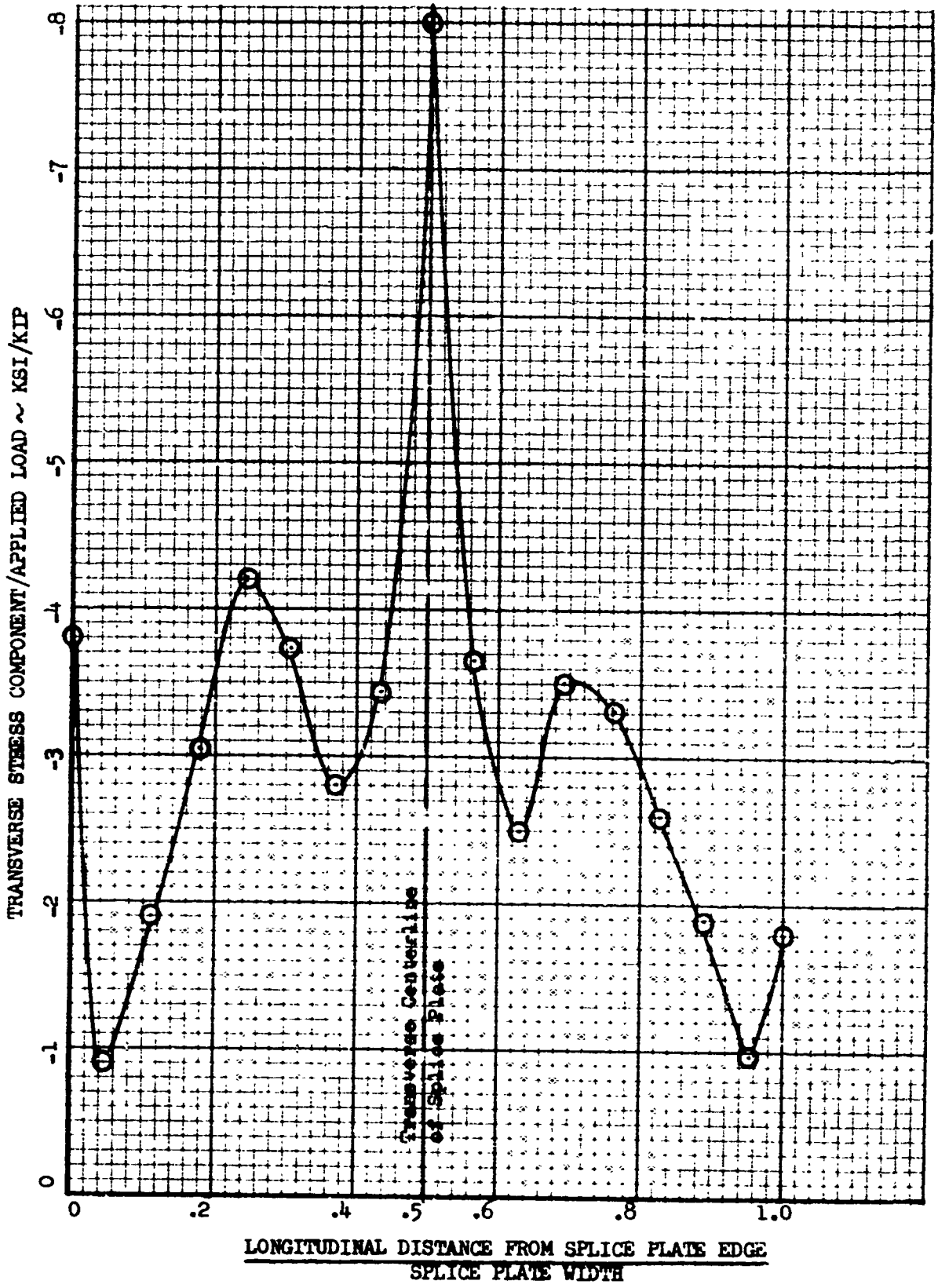

FIGURE 41 SPLICE PLATE SURFACE TRANSVERSE STRESS COMPONENT-
3 0" WIDE CONFIGURATION "A" SPECIMEN

herein discussed and, therefore, no such correction was made to the results presented on Figures 40 and 41.

1.2.3 9.0"-Wide Specimen

Figure 42 shows a sketch of the 9.0"-wide specimen discussed in this section. The specimen was of the 9.0"-wide, Configuration "A" variety, having a base adherend fabricated of Narmco 5505 boron/epoxy. The laminate was of an 8-ply thick, $(0^{\circ}/\pm 45^{\circ}/0^{\circ})_2$ configuration. Three pads of birefringent material were bonded to the splice plate at the three locations shown in Figure 42.

Photostress data obtained at each of the grid nodes were used to obtain normalized plots of splice plate surface stress. Figures 43 and 44 show the longitudinal and transverse stress components, respectively, evaluated along selected lines on each of the three photostress pads.

In similarity with results presented previously for the 3.0"-wide specimen, the symmetry about the specimen centerlines is not particularly evident from the plots of Figures 43 and 44. It is thought significant, however, that the shapes of the curves displayed on Figures 40 and 41 as compared with those displayed on Figures 43 and 44, respectively, are similar.

1.3 STRAIN GAGE RESULTS

Strain gage results were obtained on all three specimen widths. These results were obtained by placing strain gages on the surface of the titanium splice plate to obtain data along the same lines at which photostress data were obtained. Each such cluster of gages was arranged as shown in Figure 45. Gages 1 through 5 were oriented longitudinally and gages 6 and 7, transversely.

The results obtained from the second 1.1"-wide configuration "D" specimen are plotted on Figure 38. These results are compared with corresponding photostress and analytical results. The maximum joint load of 3000 lb_f was chosen to avoid yielding of either splice

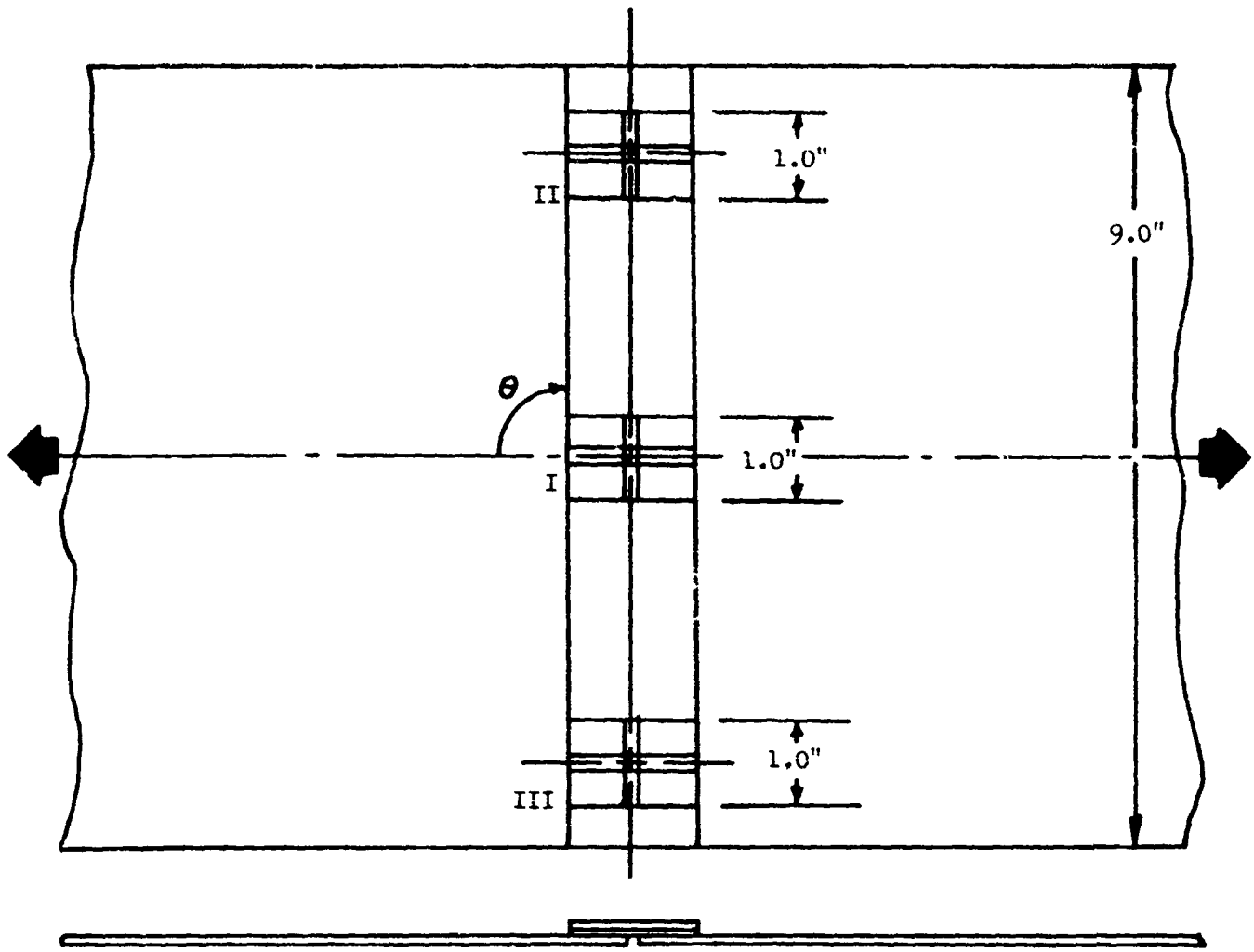

FIGURE 42 9.0"-WIDE CONFIGURATION "A" SPECIMEN USED TO OBTAIN PHOTOSTRESS DATA

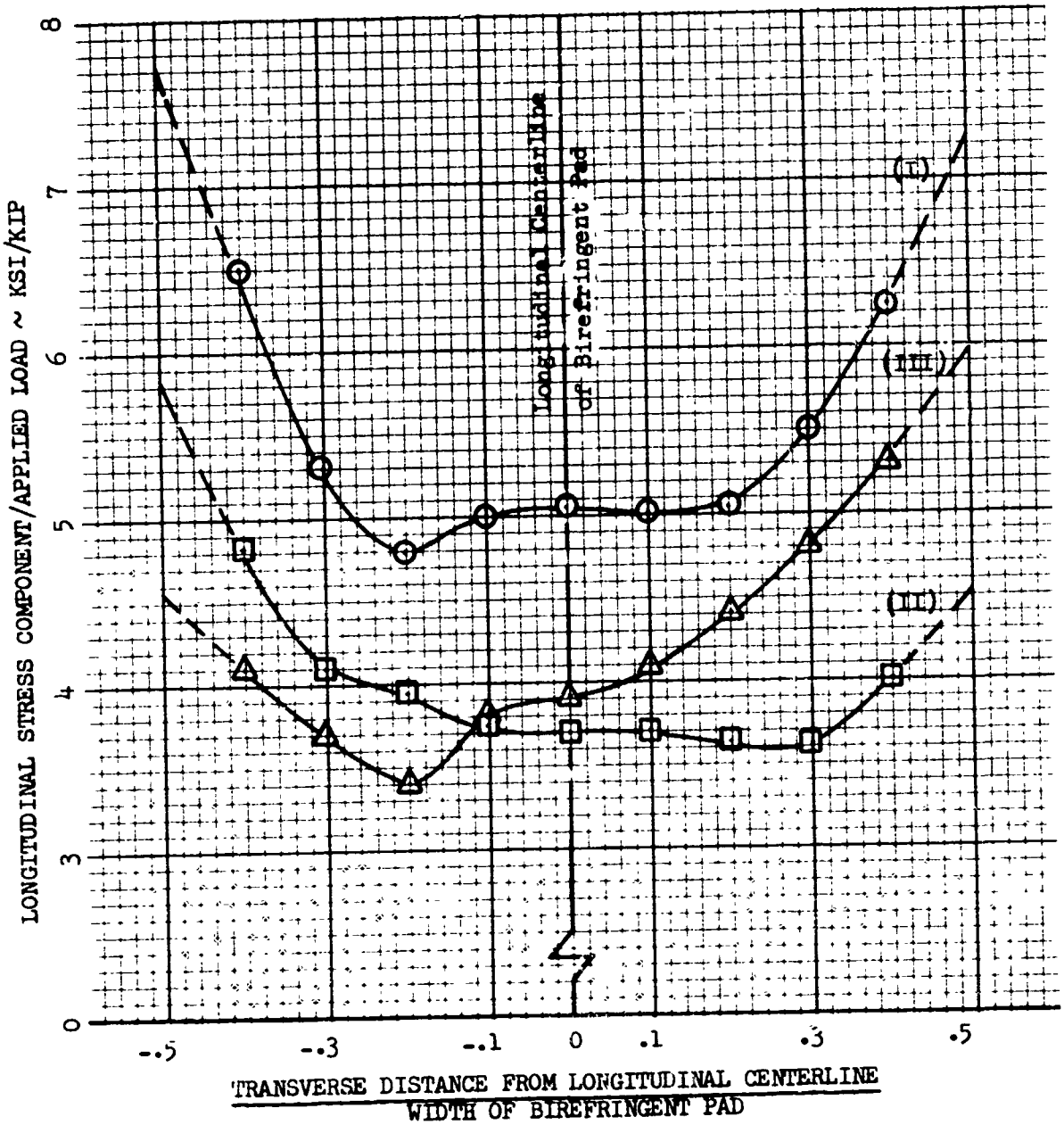

FIGURE 43 SPLICE PLATE SURFACE LONGITUDINAL STRESS COMPONENT-9.0" WIDE CONFIGURATION "A" SPECIMEN

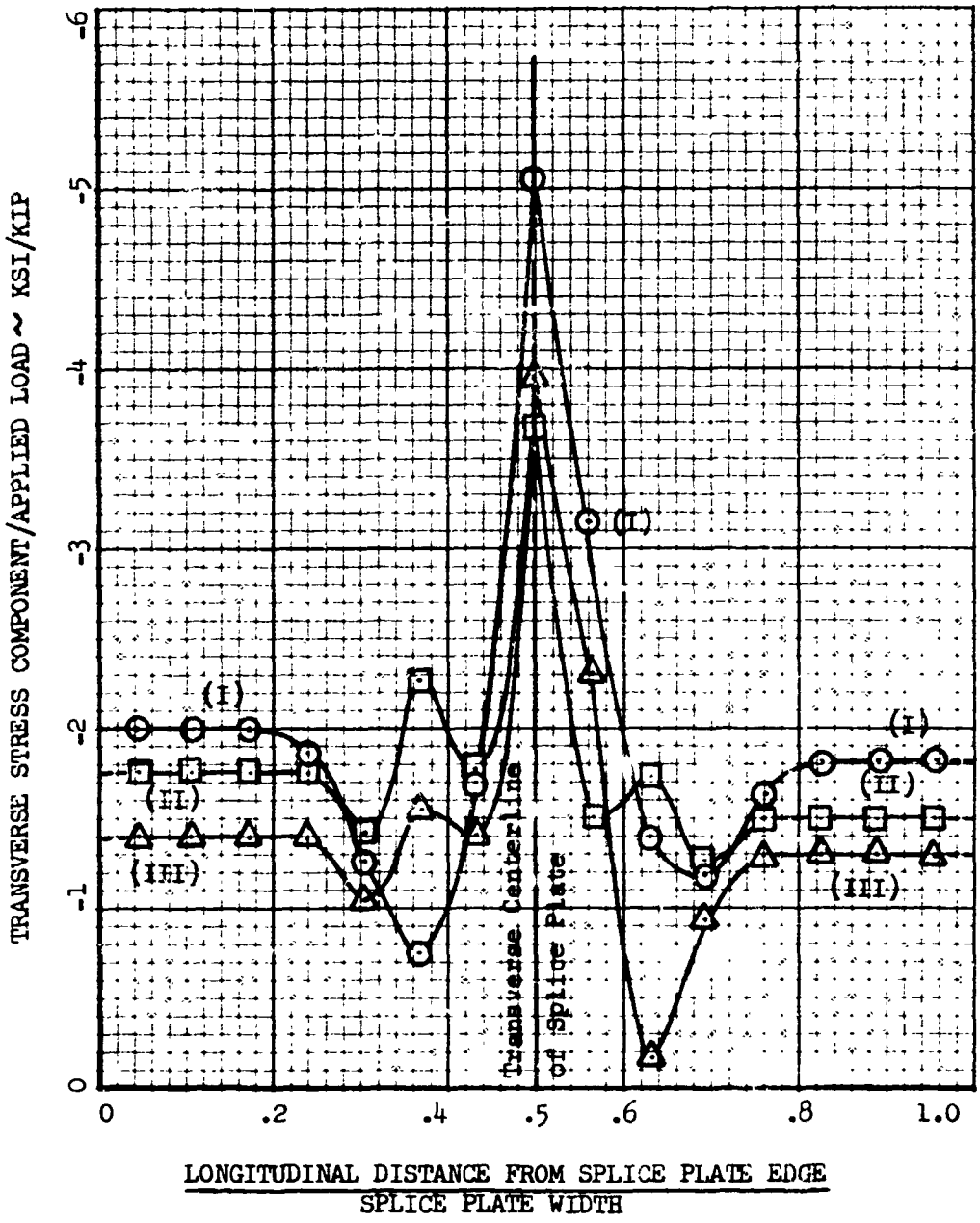

FIGURE 44 SPLICE PLATE SURFACE TRANSVERSE STRESS COMPONENT-
9.0" WIDE CONFIGURATION "A" SPECIMEN

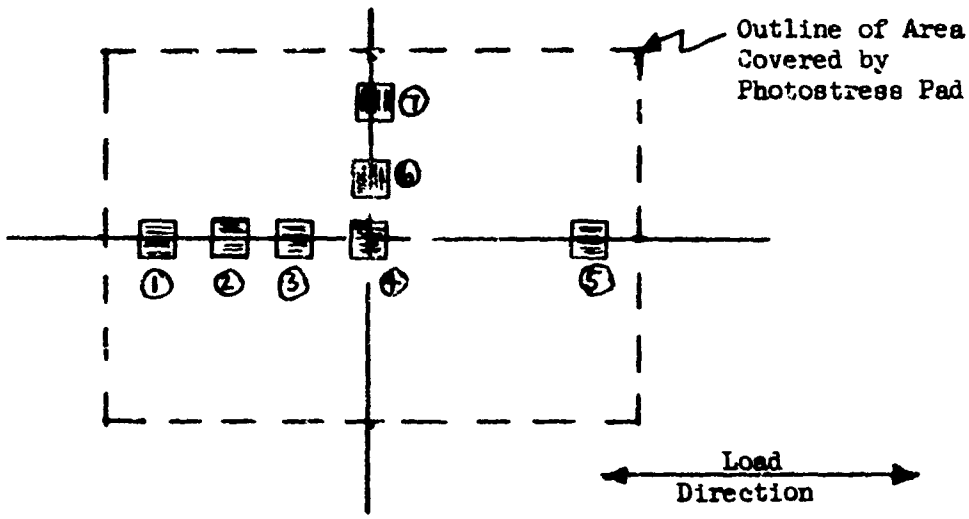

FIGURE 45 ARRANGEMENT OF STRAIN GAGES IN AREA OF PHOTOSTRESS PAD

plate or adhesive. Strain readings of all seven gages were recorded at 300 lb_f load increments up to the maximum (3000 lb_f) load level. Strain-load plots obtained from these readings were judged to be sufficiently linear to satisfy the purpose of the investigation.

Gage No. 6 exhibited the most pronounced deviation from linearity. The strain-load plot for this gage is shown in Figure 46. Figure 38 shows that the closed form linear analytical predictions compare favorably with strain gage results along the longitudinal centerline.

Strain gage results obtained from the 3.0" wide joint specimen are displayed in Figures 47 and 48. Comparable results obtained from the 9.0"-wide specimen are shown in Figures 49 and 50.

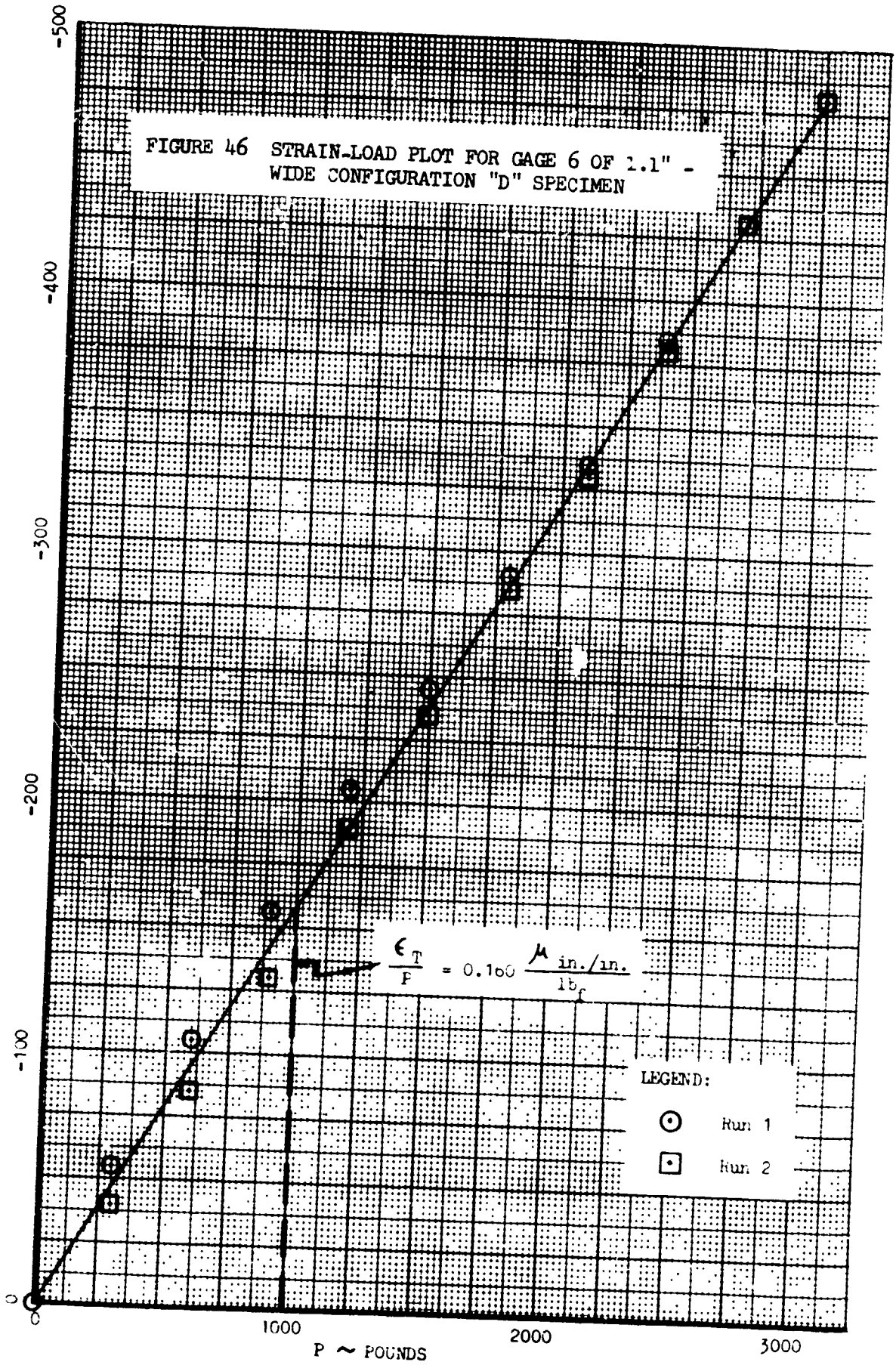
FIGURE 46 STRAIN-LOAD PLOT FOR GAGE 6 OF 2.1" - WIDE CONFIGURATION "D" SPECIMEN
ϵ_T, Transverse Strain ~ μ in./in.
-500
-400
-300
-200
-100
0
0
1000
2000
3000
P ~ POUNDS
$\frac{\epsilon_T}{P} = 0.160 \frac{\mu \text{ in./in.}}{\text{lb}_f}$
LEGEND:
Run 1
Run 2

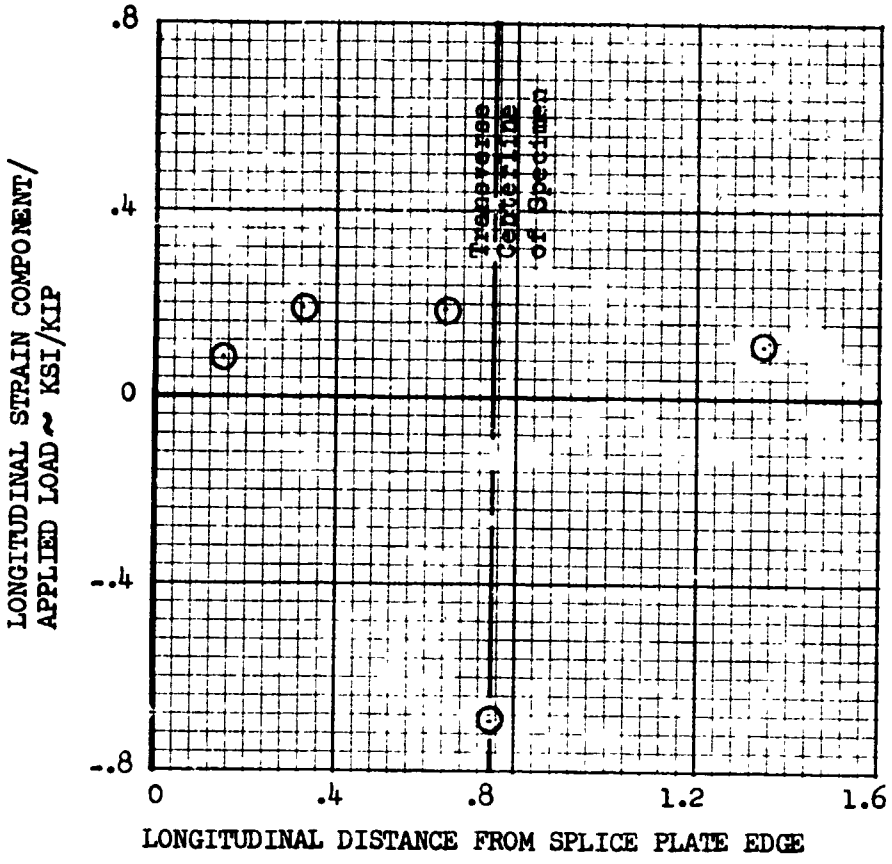

FIGURE 47 SPLICE PLATE SURFACE LONGITUDINAL STRAIN COMPONENT - 3.0" WIDE CONFIGURATION "A" SPECIMEN

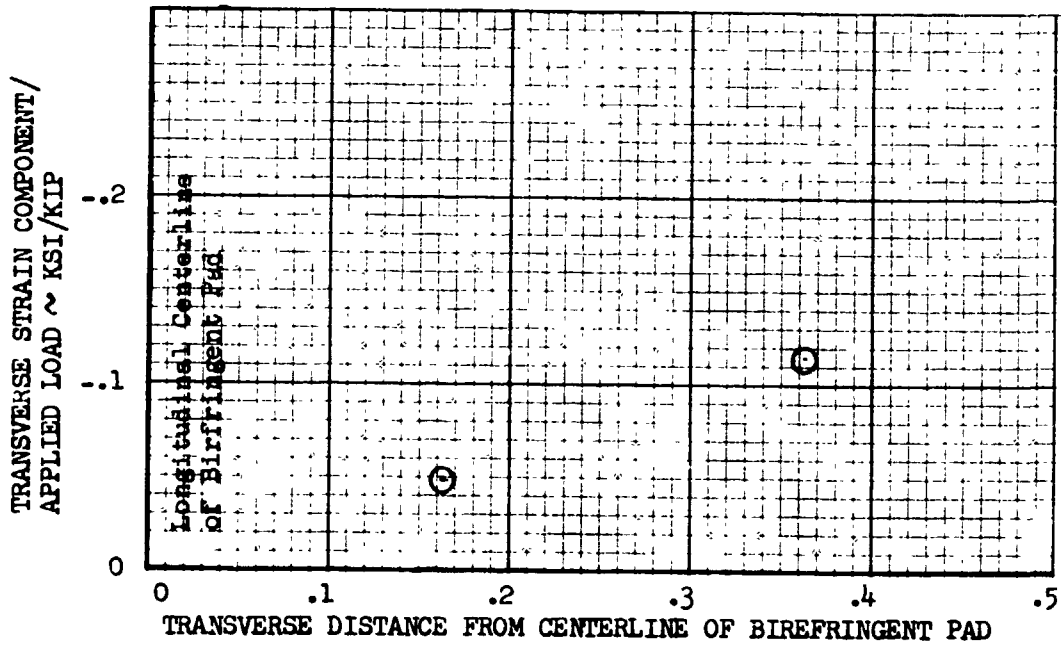

FIGURE 48 SPLICE PLATE SURFACE TRANSVERSE STRAIN COMPONENT - 3.0" WIDE CONFIGURATION "A" SPECIMEN

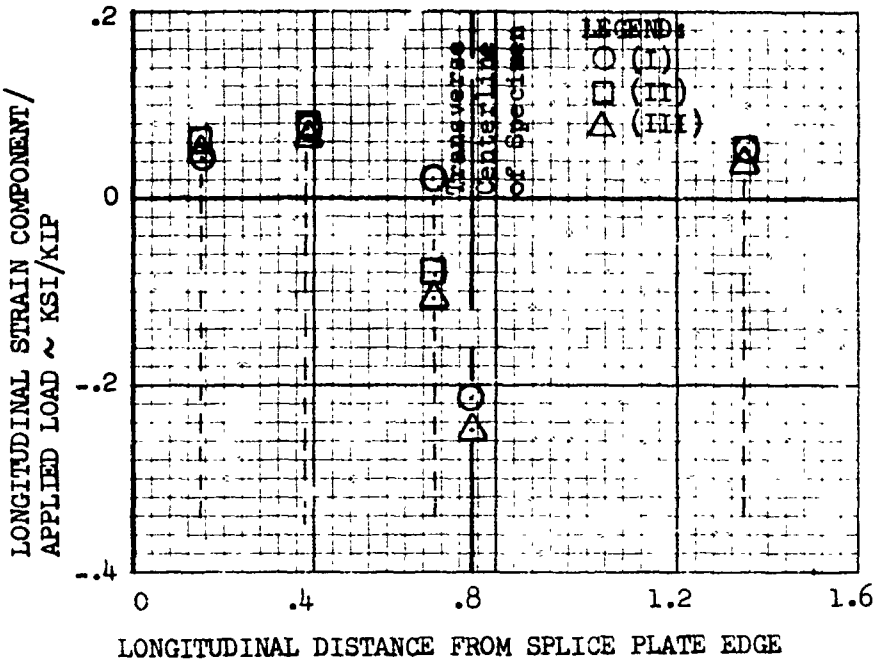

FIGURE 49 SPLICE PLATE SURFACE LONGITUDINAL STRAIN COMPONENT - 9.0" WIDE CONFIGURATION "A" SPECIMEN

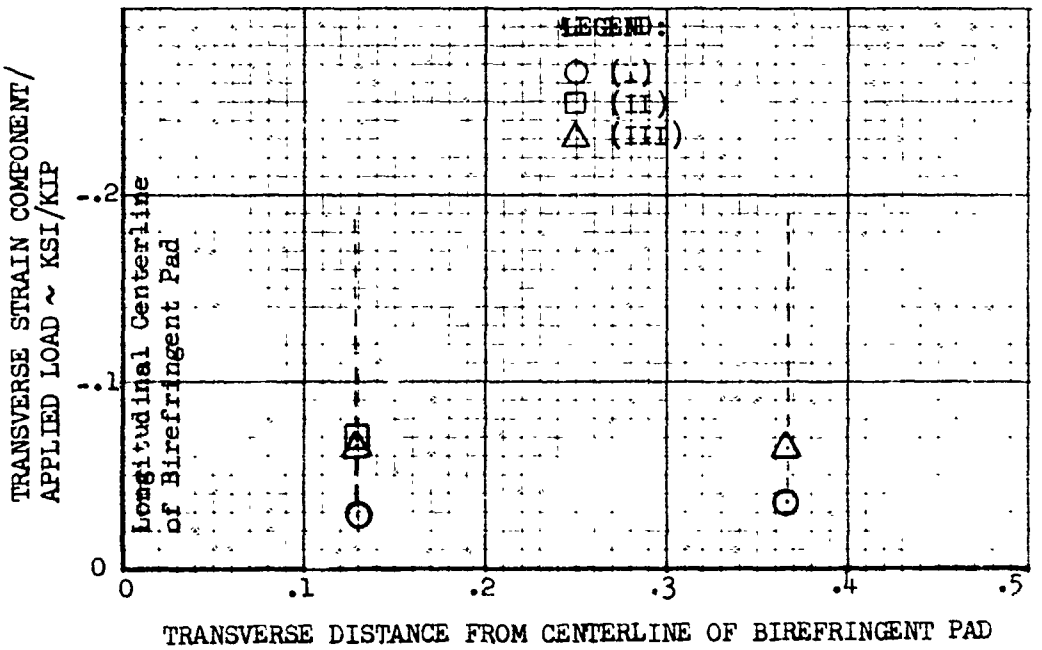

FIGURE 50 SPLICE PLATE SURFACE TRANSVERSE STRAIN COMPONENT - 9.0" WIDE CONFIGURATION "A" SPECIMEN

REFERENCES

1. Goland, M., and Reissner, E., "The Stresses in Cemented Joints," Journal of Applied Mechanics, pp. A17-A26, March 1944.

2. Volkersen, O., "Die Nietkraftverteilung in Zugbeanspruchten Nietverbindungen mit Konstanten Laschenquerschnitten," Luftfartforshung 15, pp. 4-47, 1938.

3. Szepe, F., "Strength of Adhesive-Bonded Lap Joints with Respect to Change of Temperature and Fatigue," Experimental Mechanics, pp. 280-286, May 1966.

4. Anon., "Structural Design Guide for Advanced Composite Applications," Advanced Composites Division, Air Force Materials Laboratory, Air Force Systems Command, Wright-Patterson Air Force Base, Ohio.

5. Whitney, J. M., "The Effect of Transverse Shear Deformation on the Bending of Laminated Plates," Journal of Composite Materials, Vol. 3, pp. 534-542, July 1969.

6. Technical Documentary Report No. ASD-TDR-63-447, "Research on Thermomechanical Analysis of Brazed or Bonded Structural Joints," September 1963, Air Force Flight Dynamics Laboratory, Research and Technology Division, Air Force Systems Command, Wright-Patterson Air Force Base, Ohio.